Bioprinting of Skin Equivalents for Immunotoxicity Testing

Mohammed Mahid Ahmed

A thesis submitted in partial fulfilment of the requirements for the degree of Doctor of Philosophy (Integrated)

School of Engineering

Newcastle University

April 2020

Abstract

The aim of this project was to develop bioprinted 3D full-thickness human skin equivalents (HSEs) which could be exploited for safety testing of biologics *in-vitro.* In this study, handmade 3D HSEs in a 24-well format were first optimised, and the structure of the 24-well HSEs were shown to be comparable to physiological healthy human skin. To improve the feasibility of bioprinting 3D HSEs the overall size of the equivalents was reduced by scaling the HSEs to a 96-well plate format using prototype 96-well Alvetex® inserts. Histological analysis of the optimised 96-well skin equivalents showed these to be similar to both the 24-well HSEs and physiological human skin.

To demonstrate that skin cells could be bioprinted in the high densities required to create 3D HSEs, cells were printed using a Jetlab 4 Tabletop printer and solenoid microvalves. Fibroblasts were printed at concentrations of $1x10^6$ cells/mL, $10x10^6$ cells/mL, $20x10^6$ cells/mL and $40x10^6$ cells/mL. Cell count and viability immediately post printing demonstrated that microvalves could be used to reliably dispense a high density of cells over 1 hour with minimal cell death. 96-well HSEs were then bioprinted and compared to handmade 24-well and 96-well HSEs in addition to human skin using histological techniques. Fully autologous 96-well HSEs were then bioprinted and co-cultured *in-vitro* with autologous peripheral blood mononuclear cells (PBMCs) in the presence and absence of biologics known to cause (OKT3) or not to cause (Natalizumab) immunotoxicity. Investigation of supernatants revealed significant proinflammatory cytokine responses (interferon gamma (IFN-γ)) in co-cultures treated with OKT3 when compared to negative controls.

This research developed a 96-well format bioprinted HSE and demonstrated the feasibility of using bioprinted 3D tissue equivalents for *in-vitro* immunotoxicity testing of biologics. In conclusion, microvalve based bioprinting technology can be used to fabricate HSEs suitable for application of *in-vitro* screening of biologics.

Acknowledgements

I would like to thank the Engineering and Physical Sciences Research Council, the Centre for Doctoral Training in Additive Manufacturing and 3D Printing, and Alcyomics Ltd for their financial support. Without their backing this doctorate would not have been possible.

I am ever thankful to my academic supervisory team. Thank you to Dr. David Hill whose technical knowledge and understanding of cell biology was a valuable resource throughout this PhD. Thank you to Professor Penny Lovat for providing access to clinical biopsies. Thank you to Professor Kenny Dalgarno for his guidance and support and for being a calming influence in what was a turbulent journey. I would also like to thank my industrial supervisor Professor Anne Dickinson for her contributions and for access to Alcyomics' resources.

I would like to thank the other CDT students for a memorable time in Nottingham. Thank you to the cohort 1 students, particularly Dr. Hatem Cader for his technical support. Thank you to the cohort 2 students for the many laughs and moments of levity, whether it was in Nottingham, Frankfurt, or Texas. I would also like to thank my peers in Newcastle for their support during my time here. I would like to thank Aidan Bowes for his assistance with printer repairs and modifications.

I would like to thank the Alcyomics team, past and present, for the support and assistance offered during this PhD.

Thank you to Mrs Jamie Williamson, Mrs Elizabeth Douglas, Dr. Xiao Wang, and Dr. Moyassar Al-Shaibani from the department of academic haematology who provided support during my time there.

Thank you to the department of academic dermatology for allowing me to access their facilities, equipment and for of sharing clinical samples. Thank you to the clinical teams, the medics and research nurses for sourcing the samples necessary for my work.

Thank you to Callum Squires from the School of Engineering IT team, and to Nancy Woadden and Mark Warwick of ICM IT for their assistance.

Thank you to the bio-imaging team who provided training and technical expertise during the initial stages of the PhD.

And finally, to my loving family that supported me throughout my PhD, thank you. Thank you to my father Imtiyaz, whose hard work and sacrifice laid the foundations for my success. Thank you to my mother Shaheda whose own example gave me the inspiration and courage to embark on this adventure and see it though till the end. Thank you to my beautiful wife Mariam whose support means everything to me.

Table of Contents

Table of Abbreviations

Abbreviation	Term
mAb	Monoclonal antibody
PBMC	Peripheral blood monocyte
CK1	Cytokeratin-1
CK2	Cytokeratin-2
CK4	Cytokeratin-4
CK5	Cytokeratin-5
CK10	Cytokeratin-10
CK14	Cytokeratin-14
CK15	Cytokeratin-15
ECM	Extra-cellular matrix
HSE	Human skin equivalent
DED	De-epidermised dermis
ALI	Air-liquid interface
RHE	Reconstituted human epidermis
OECD	Organisation for economic co-operation and development
MLLNA	Mouse local lymph node assay
hCAT	Human line cell activation test
IL-18	Interleukin-18
UV	Ultra-violet
ROS	Reactive oxygen species
NHP	Non-human primate
ADA	Anti-drug antibody
POS	Probability of success
2D	Two-dimensional
3D	Three-dimensional
DOD	Drop-on-demand
Hz	Frequency
P_w	Pulse width
P_a	Pulse amplitude
LABP	Laser assisted bioprinting
LIFT	Laser induced forward transfer
PLL	Poly-l-lysine

PVP	Polyvinylpyrrolidone
HLA	Human leukocyte antigen
LREC	Local research ethics committee
PBS	Phosphate buffered saline
P/S	Penicillin/streptomycin
FBS	Foetal bovine serum
DMEM	Dulbecco's modified eagles medium
DMSO	Dimethyl sulfoxide
HKGS	Human keratinocyte growth supplement
RPMI-1640	Roswell park memorial institute-1640
hEGF	Human epidermal growth factor
H&E	Haematoxylin and eosin
PCB	Printed circuit board
d	Droplet volume
W_1	Weight before printing
W_2	Weight after printing
n	Number of droplets printed
BMP	Bitmap
Vt	Total volume per print
P	Number of pixels in bitmap
D	Number of droplets in the X and Y axis of an array
OKT3	Murine anti-human CD3/MOKT3uromonab-CD3
IF	Immunofluorescent staining
AF488	Alexa Fluor-488
AF647	Alexa Fluor-647
TBS	Tris buffered saline
PAS	Periodic Acid-Schiff
MSD	Meso Scale Discovery
TGF-β1	Transforming growth factor-beta 1
miR-21	MicroRNA-21
ROCK	Rho associated kinase
IFN-ɣ	Interferon-gamma
IL-10	Interleukin-10
IL-12p70	Interleukin-12p70

IL-13	Interleukin-13
IL-1β	Interleukin-1β
IL-2	Interleukin-2
IL-4	Interleukin-4
IL-6	Interleukin-6
TNF-α	Tumour necrosis factor alpha
NK cells	Natural killer cells

List of Figures

List of Tables

List of Equations

Chapter 1 Project Aims and Literature Review

1.1 Introduction

As human tissue is not easily obtainable and in limited supply for preclinical human *in-vitro* testing, preclinical animal testing is commonly used during the drug development process. However animal models not only raise ethical concerns but the results may not be a true indication of the drugs effect on humans in clinic (Stebbings *et al.* 2007). Mostly drugs can fail when first tested in humans, even after successfully passing preclinical animal testing. This can be because the human specific immunogenic properties of the drug are not detected during animal testing and only first become apparent during clinical trials. This contributes to the high failure rate that the pharmaceutical industry experiences when taking drugs to human clinical trials (Hay *et al*. 2014). Such failures can have disastrous consequences such as the 2006 Northwick Park drug trial, which later came to be more commonly known as the "Elephant man trial". As reported by Stebbings *et al,* the CD28-specific monoclonal antibody (mAb) TGN1412 was used in the Northwick Park drug trial. Preclinical tests of TGN1412 in Cynomolgus macaques showed little lymphocyte activation in response to TGN1412 (Stebbings *et al*. 2007). The trial resulted in six of the eight healthy volunteers in clinic suffering multiple organ failure (Attarwala 2010). The remaining two volunteers had received a placebo and suffered no adverse effects. Post-trial investigations of TGN1412 demonstrated that exposure of human peripheral blood monocytes (PBMCs) to TGN1412 triggered a strong systematic immune response (Stebbings *et al*. 2007). In clinical terms this immune response is referred to as a 'cytokine storm' (Stebbings *et al*. 2007). Such adverse events highlight the need for commercially available preclinical testing of drug candidates in fully autologous human systems.

The drug development process is a lengthy and costly venture and so the general aim of early testing of biologics tends to be "fail early, fail cheap". This refers to the timely identification of inappropriate drugs that are in the early stages of the development process with an aim to minimise the loss of significant time and financial investment into a product that will likely raise safety issues during clinical trials. The use of human *in-vitro* assays which could predict human adverse events *in-vivo* would allow more accurate earlier detection of immunotoxicity in the early stages of drug development and at the pre-clinical stage before costly clinical trials (Visk 2015).

One such example of a preclinical human *in-vitro* assay is the Skimune® assay developed by Alcyomics Ltd to determine adverse responses to systemic therapies (Ahmed *et al*. 2016). As a preclinical assay that utilises immune cells combined with human tissue, Skimune® provides the pharmaceutical industry with a possible alternative to animal models, which may bridge the gap between preclinical animal studies and human clinical trials. Skimune® uses human skin biopsies for *in-vitro* explant tests along with autologous peripheral blood monocytes (PBMCs) to predict adverse events of drugs and sensitization to chemicals. Current assays are mostly single cell based, or tissue based (Stebbings *et al*. 2007), therefore the combination of using immune cells and tissue from the same donor offers an attractive proposition. The use of human immune cells with tissue could provide a more complete picture of the possible in-man response to monoclonal antibodies (mAbs), whereas animal studies would only provide a partial insight to the drug response (Stebbings *et al*. 2013). However, routinely sourcing human skin and blood from matching donors for testing is a challenge, due to both the limited size of samples that can be obtained from donors and varying availability of healthy volunteers. Samples must be taken through minimally invasive procedures and be within the size/volume guidelines outlined by ethical approval. Small samples restrict testing to a small number of drugs or chemicals and therefore are not ideal for testing panels of drug candidates on a large industrial scale.

To date there have been many advancements in the field of tissue engineering, especially when engineering (three-dimensional) 3D human skin equivalents for both clinical and research applications (Ali *et al*. 2015; Hill *et al.* 2015). Therefore, a potential solution to small sample sizes could be to isolate skin cells from donor biopsies and use the cells to engineer 3D skin equivalents allowing more tests to be performed per donor. Alcyomics have previously fabricated skin equivalents in a 6-well format referred to as Skimune3D® however this format was too large for high-throughput testing and required large cell numbers. Therefore, only a small number of skin equivalents per donor could be produced. It was recognised that this technology would greatly benefit from a reduction in format, by minimising the overall size of the 3D skin equivalents and maximising the number of equivalents per donor to develop a high-throughput platform for preclinical *in-vitro* testing.

In the years since Wilson and Boland's first cell dispensing bioprinter the field of bioprinting has very much grown beyond its infancy (Wilson and Boland 2003). The

cross-disciplinary nature of bioprinting has given rise to collaborations from the fields of cellular biology, medicine, materials science, physics and engineering to develop alternative techniques and materials to print scaffolds and cells for various functions (Murphy and Atala 2014). Regenerative medicine has inspired the bioprinting and transplantation of cartilage substitutes, vascular grafts, an airway splint and skin constructs (Cui *et al*. 2012; Marga *et al*. 2012; Michael *et al*. 2013; Zopf *et al*. 2013). While there is a large focus on developing 3D structures and tissues for *in-vivo* applications there are yet to be significant steps made in the development of bioprinted high-throughput 3D tissue equivalents for *in-vitro* applications, namely drug testing (Mazzocchi, Soker, and Skardal 2019). Reducing the size of the Skimune3D® skin equivalents could increase the feasibility of bioprinting 3D skin equivalents which are both representative of tissue *in-viv*o and can be suitable for *in-vitro* assays. The automation of bioprinting can allow for the high-throughput deposition of cells which would be ideal for the biofabrication of tissue equivalents on a large scale. Consequently, the bioprinted Skimune3D® skin equivalent could be suitable for assessing the immunotoxicity of biologics and could be adapted for other *in-vitro* applications. This would be a novel contribution to both the pharmaceutical industry and the field of biofabrication.

As with many high-throughput processes some element of automation would be advantageous, for Skimune3D® the bioprinting of skin equivalents would provide a manufacturing platform that would be scalable to industrial needs. While bioprinting and the concept of *in-vitro* therapeutic antibody testing are not novel concepts, the unique combination of the Skimune3D® platform and high-throughput bioprinting for therapeutic antibody testing would be a novel contribution to science and to the pharmaceutical industry. This novel approach to preclinical testing may provide industry with a fully autologous human system to detect immunotoxic events often related to therapeutic mAb treatments.

1.2 Literature Review

1.2.1 The Structure of Human Skin

In humans, skin is the largest organ with a range of functions such as protection, sensation, thermoregulation, excretion and absorption (Proksch, Brandner, and Jensen 2008). Skin consists of three main layers; epidermis, dermis and hypodermis (subcutaneous tissue) as is illustrated in Figure 1.1 (Kanitakis 2002).

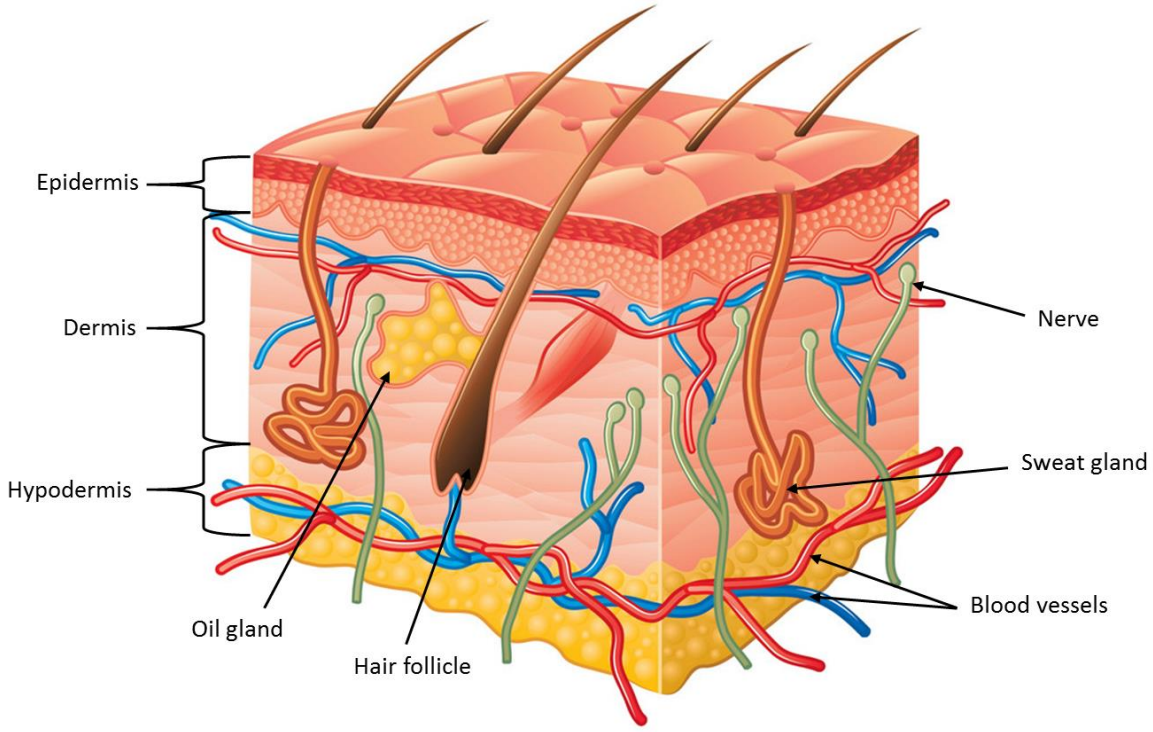

Figure 1.1. The structure of human skin. *Skin typically features three layers; epidermis, dermis and hypodermis. Human skin usually contains hair follicles, nerves, blood vessels in addition to sweat glands and oil glands. Adapted and annotated from www.VectorStock.com.*

The epidermis is the outermost layer of the skin and has a stratified structure formed by four sub layers: the basal strata, stratum spinosum, stratum granulosum and the stratum corneum (Figure 1.2). The epidermis also contains four cell types; Merkel cells, Langerhans cells, melanocytes and keratinocytes, the latter are the most abundant cells in the epidermis (Wong *et al*. 2016). Proliferative undifferentiated keratinocytes are found in the basal strata of the epidermis. These cells provide a self-renewing layer for the epidermis to replace cells lost from the upper strata. As the healthy keratinocytes begin to terminally differentiate into corneocytes they migrate from the basal layer progressing superficially through the strata towards the stratum corneum.

As the cells superficially migrate the formation of tight junction complexes aids cell-cell adhesion and allows keratinocytes to form an effective cell barrier (Kirschner and Brandner 2012). Once the keratinocytes reach the stratum granulosum cell death begins to occur as the lamellar bodies release lipids and cells become filled with keratohyalin precursors which promote the development of a cornified envelope. The keratohyalin granules become progressively more visible as the cells begin to differentiate with the granules being most noticeable in the stratum granulosum resulting in the granular appearance in histology.

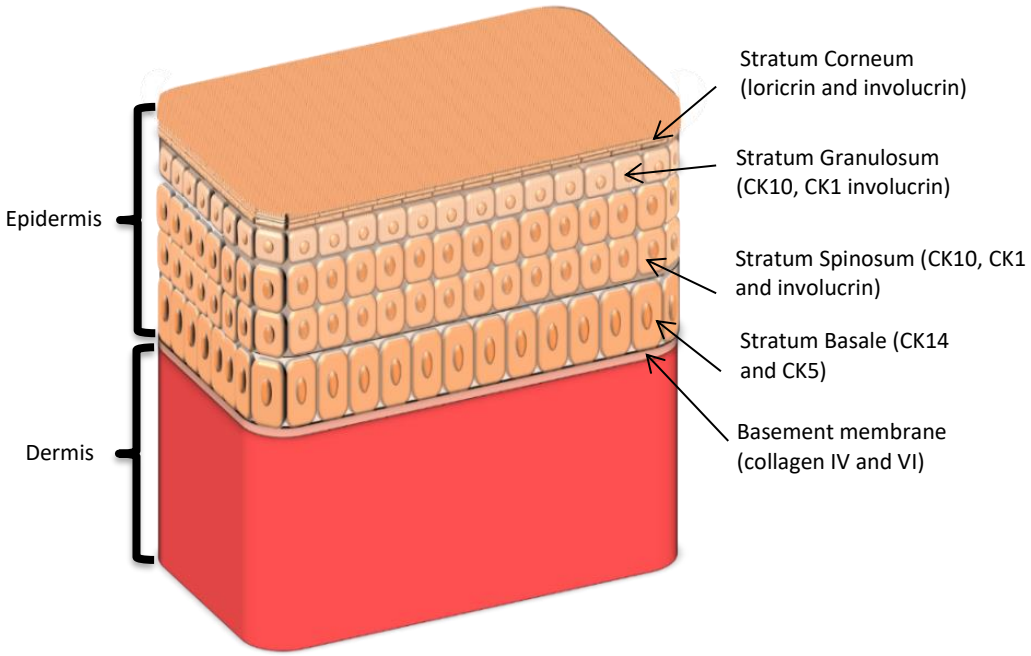

Figure 1.2. The sublayers of the epidermis and stratified markers. *The epidermis contains 4 strata each with a different range of biomarkers. The basement membrane separates the dermis and the epidermis at the dermal-epidermal junction.*

Throughout the epidermis keratinocytes express a range of cellular and cytoskeletal markers. Cytokeratin-5 (CK5), CK14 and CK15 are expressed by undifferentiated keratinocytes in the basal layer of the epidermis while CK1, CK2 and CK10 are expressed by differentiating cells which are found in the spinous and granular strata (Moll, Divo, and Langbein 2008). The stratum corneum contains structural proteins such as involucrin and loricrin (Candi, Schmidt, and Melino 2005; Nemes and Steinert 1999). These markers are routinely used to detect differentiation of keratinocytes. Beneath the epidermis lies the basement membrane which separates the dermis and the epidermis. The basement membrane mainly comprises of laminins and collagen IV in a “chicken-wire” like mesh (Breitkreutz *et al.* 2013; Behrens *et al*. 2012). Within

the basement membrane collagen VII facilitates anchoring of the basement membrane to the dermis via looping structures which interweave and adhere to dermal collagen I (Villone *et al*. 2008). This improves functional properties and structural strength of skin (McMillan, Akiyama, and Shimizu 2003).

The dermis is a thicker layer of tissue beneath the dermal-epidermal junction which supports the epidermis and has sublayers. The dermis contains connective tissues such as collagen, elastin and fibronectin (Krieg and Aumailley 2011). Such extracellular matrix proteins can define the elasticity and strength of the dermis (Bruckner 2010). The uppermost layer of the dermis is the papillary dermis located close to the basement membrane, this region contains a high population of dermal fibroblasts within a compact network of small collagen fibres (Rognoni and Watt 2018). The reticular dermis is the larger layer of dermis found beneath the papillary dermis. The reticular dermis contains thicker extracellular matrix (ECM) particularly larger reticular collagen fibres and is less densely populated by fibroblasts (Rognoni and Watt 2018). Under the reticular dermis is the subcutaneous hypodermis which contains adipocytes filled with lipid (Rognoni and Watt 2018).

1.2.2 The Historical Development of Skin Equivalents

Skin explants, also known as histocultures, are often used to replicate *in-vivo* environments. While skin explants have many uses there are also several limitations (Hoffman 1991; Li *et al*. 1992; Li, Margolis, and Hoffman 1991). Skin explants are restricted in both availability and size of the sample. Such restrictions increase the appeal of 3D human skin equivalents (HSEs). HSEs have been developed and refined over many years as an alternative to two-dimensional (2D) systems, skin explants, and animal models. However, to develop HSEs which are physiologically representative of human skin the isolation and culture of skin cells from human skin is necessary.

In 1975 Rheinwald and Green reported the successful *in-vitro* cultivation of keratinocyte colonies from a single founder keratinocyte by using lethally irradiated 3T3 mouse fibroblasts as a layer of feeder cells (Rheinwald and Green 1975). It was reported that the isolated keratinocytes could successfully form colonies and ultimately form a stratified squamous epithelium (Rheinwald and Green 1975). The addition of hydrocortisone to the culture media was reported to improve cell morphology and slightly increase proliferation, however Rheinwald and Green found the culture lifetime of keratinocytes to vary between 20-50 cell generations (Rheinwald and Green 1975).

These findings provided a foundation for future *in-vitro* studies to further improve keratinocyte culture techniques. Freeman *et al* produced a method of using decellularised and de-epidermised dermis (DED) derived from pigs to culture keratinocytes (Freeman *et al*. 1976). The DED acted as a substrate for human skin samples. Though only human keratinocytes adhered to the decellularised pig dermis, basal and granular cell layers were also reported indicating a degree of epidermal keratinocyte differentiation. As only keratinocytes adhered to the DED the resulting model was more representative of a reconstituted epidermis equivalent than a full thickness skin model. Lillie *et al* made use of culture at an air-liquid interphase (ALI) with a collagen raft to culture keratinocytes (Lillie, MacCallum, and Jepsen 1980). The ALI allowed the upper epidermis to be exposed to air, thereby replicating *in-vitro* conditions. The keratinocytes undergoing terminal differentiation were observed with pyknotic nuclei and organelle debris. The high degree of tissue organisation was attributed to the use of an ALI. Pruniéras *et al* used ALI with a human DED to culture and differentiate keratinocytes (Prunieras, Regnier, and Woodley 1983). Pruniéras *et al* identified differentiation through morphological markers however the expression of keratin precursors was limited (Prunieras, Regnier, and Woodley 1983). The limited expression of the differential keratins was attributed to the filtering qualities of the dermal substrate since the cells need to be fed from below at ALI (Prunieras, Regnier, and Woodley 1983). This study highlighted the need for an appropriate dermis to achieve a good range of keratin expression. Hull *et al* demonstrated that dermal equivalents could also be seeded with dermal fibroblasts by using a collagen lattice populated with cells (Hull *et al*. 1983). In addition to DEDs, inert acetate cellulose filters and non-biological polycarbonate films have been shown to act as acellular dermal substrates (Rosdy and Clauss 1990). Langerhan cells and melanocytes have also been integrated into the epidermis in attempts to further replicate the *in-vivo* environment of human skin resulting in more physiologically representative models (Regnier *et al.* 1998; Regnier *et al*. 1997). El-Ghalbzouri *et al* investigated the impact of fibroblasts on epidermal formation by preparing collagen matrices with increasing numbers of fibroblasts, upon which keratinocytes where seeded (el-Ghalbzouri *et al*. 2002; Hull *et al*. 1983). The findings showed that in the presence of fibroblasts, keratinocyte proliferation, differentiation and epidermal stratification improved. In the presence of fibroblasts the formation of the basement membrane at the dermal epidermal junction also improved (el-Ghalbzouri *et al.* 2002; Wong, McGrath, and Navsaria 2007). Such studies demonstrate the advantages of using a fibroblast

populated dermal equivalents when reconstructing the epidermis, however the material used for the dermal scaffold does require good consideration (Prunieras, Regnier, and Woodley 1983).

The increasing interest in 3D scaffolds has resulted in the development of both natural and synthetic biocompatible materials. There are a variety of biodegradable hydrogels and polymers such as polylactic acid and polyglycolic acid for tissue engineering (Mikos *et al.* 1993; Park *et al.* 2005; Sims *et al*. 1998; Yu, Dillon, and Bellamkonda 1999). While biodegradable scaffolds may be desirable for *in-vivo* applications, the use of biodegradable scaffolds *in-vitro* for HSEs could restrict model development as the growth of a dermal equivalent and epidermal differentiation is a lengthy process. Scaffold degradation could affect the exposure of the epidermis to the ALI which in turn can restrict maturation of the epidermis by denying optimal culture conditions. Therefore, the use of an inert scaffold would be appropriate for the fabrication of autologous HSEs for *in-vitro* early phase drug testing. Haymen *et al* developed a highly porous polystyrene scaffold which was redeveloped to be compatible with general everyday use tissue culture plastic (Bokhari *et al.* 2007; Hayman *et al*. 2004, 2005). This porous polystyrene scaffold was later used by Hill *et al* to fabricate full-thickness HSEs to model the melanoma infiltration of the dermis (Hill *et al*. 2015). Hill *et al* used primary fibroblasts and keratinocytes to develop HSEs with a fully stratified epidermis containing terminally differentiated keratinocytes and a dermal equivalent populated with fibroblast which synthesise ECM (Hill *et al*. 2015). The study by Hill *et al* was an example of the usefulness of a scaffold that could not only accommodate fibroblasts but be porous enough to allow adequate diffusion of oxygen and nutrients encouraging proliferation of cells and ECM production. The fibroblasts and ECM would then act as a dermis capable of supporting keratinocytes seeded onto the surface of the dermal equivalent. The keratinocytes were cultured at ALI to form a stratified epidermis, resulting in a full-thickness skin equivalent. Originally designed as an investigative tool to understand the early stages of melanoma invasion this fully humanised system was later patented by Alcyomics Ltd with a view to adapting the HSE into an autologous system suitable for immunotoxicity.

While there are other competitors in the market for *in-vitro* HSEs (Table 1.1) for toxicology and pharmacology testing it seems there is currently a gap in the market for autologous, full-thickness HSEs with donor matched peripheral blood monocytes (PBMCs) for *in-vitro* immunotoxicology. Commercially available HSEs are either

reconstituted human epidermis (RHE) models where human keratinocytes are cultured on a synthetic polymeric scaffold to produce a stratified epidermis or full-thickness HSEs where keratinocytes are cultured and differentiated on a fibroblast populated dermal equivalent. A RHE is developed by seeding and submerging keratinocytes on a porous transwell membrane for several days. After submerged culture the RHE is raised to ALI to allow the keratinocytes to differentiate and form a stratified epidermis. Using standard culture techniques there are now a range of commercial RHE equivalents available such as EpiDerm™ from MatTek Corporation, SkinEthic™ and EpiSkin™ from EpiSkin (which is a subsidiary of the L'Oréal group) and EpiCs® from CellSytems GmbH. Each of these RHE equivalents (shown in Figure 1.3) have been validated in assays for sensitisation and irritation using the Organisation for Economic Co-operation and Development (OECD) guidelines 439 and 432 (Andres *et al*. 2017; Cottrez *et al*. 2015; Cottrez *et al*. 2016; Gibbs *et al*. 2013; Saito *et al*. 2013). The EpiSkin™ *in-vitro* model was used by Cottrez *et al* to develop the SENS-IS assay which investigated changes in gene expression of the SENS-IS gene subset in response to sensitisation after exposure to chemicals (Cottrez *et al*. 2015; Cottrez *et al*. 2016). Cottrez *et al* showed that the use of the RHE model with the SENS-IS assay was 100% reproducible between 3 laboratories with 150 chemicals correctly predicting sensitivity with 95.8% accuracy and 96.5% specificity (Cottrez *et al*. 2016). When comparing SENS-IS assay data to literature complied by Basketter *et al* the SENS-IS assay showed 92.6%, and 90.6% compared to the mouse local lymph node assay (MLLNA) data and human data respectively (Basketter *et al*. 2014; Cottrez *et al*. 2016). MatTek EpiDerm™ was used by Saito *et al* to develop another assay named EpiSensA assay which is also a gene analysis assay (Saito *et al*. 2013). Saito *et al* used a smaller panel of 5 genes and 16 chemicals which still reported high accuracy but this was lower than what was reported by Cottrez *et al*, though the SENS-IS studies did use a much larger panel of genes and chemicals. (Cottrez *et al*. 2016; Saito *et al*. 2013). Saito *et al* later used the LabCyte EPI-MODEL from Japan tissue Engineering Co. Ltd, a subsidiary of the Fujifilm group, which was tested along with the EpiSensA assay using a total of 72 chemicals (Saito *et al*. 2017). Results showed that with the use of a RHE the sensitivity, specificity, and accuracy of lipophilic chemicals was 96, 75, and 88% respectively (Saito *et al*. 2017). According to Saito *et al* this data was more accurate than when validated using *in-vitro* 2D culture based tests for example the human line cell activation test (hCAT) and the KeratinoSens™ assay (Saito *et al*. 2017). A combination of EpiCS®, SkinEthic™, EpiDerm™ and an in house RHE equivalent were used by

Gibbs *et al* to identify an increase in production and release of interleukin-18 (IL-18) in response to exposure to sensitisers (Gibbs *et al*. 2013). The stated accuracy of the IL-18 assay was >95% (Gibbs *et al*. 2013). It is important to note that current commercial RHE equivalents only contain one cell type, keratinocytes. However, including additional cell types found within the epidermis may not be complex. The lack of a dermal compartment with fibroblasts means that there is no *in-vitro* communication between fibroblasts and keratinocytes which can influence inflammatory cytokine response in assays (Spiekstra *et al*. 2007). Additionally, the use of RHEs are currently focused on chemical sensitisation with little scope for predicting the immunotoxicity of therapeutic antibodies.

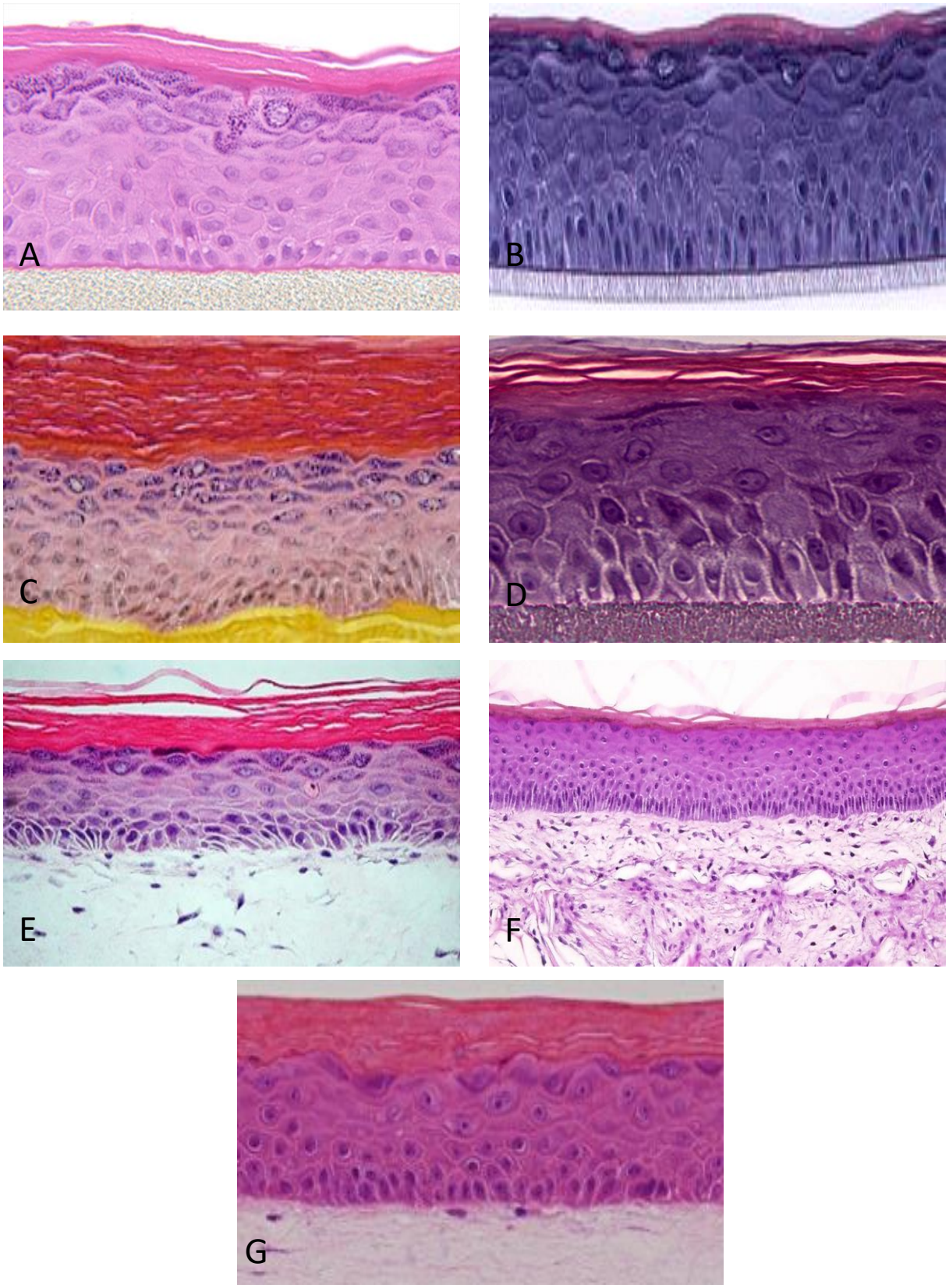

Figure 1.3. Representative histology images of commercially available reconstructed human epidermis (RHE) models *(A-D) and full-thickness skin models (E-G). (A) EpiDerm™, (B) SkinEthic™, (C) EpiSkin™, (D) EpiCs® (E) EpidermFT™, (F) Phenion® FT, (G) StrataTest®. Images adapted from www.mattek.com, https://www.phenion.com, www.episkin.com, www.reconstructed-human-epidermis.com, Rasmussen et al 2010.*

Currently there a range of commercially available skin equivalents (Table 1.1) used for various applications. However as of yet there are no 3D skin equivalents available to the pharmaceutical industry that could be exploited to assess the immunotoxicity of biologics. The main commercially available full-thickness HSEs are EpidermFT™ from the MatTek Corporation, the Phenion® FT model from Phenion of the Henkel Company and StrataTest® from the Stratatech Corporation. EpidermFT™ has been used to investigate the irritation potential of aliphatic hydrocarbons *in-vitro* (Mallampati *et al*. 2010). Mallampati *et al* incubated the EpidermFT™ equivalents with hydrocarbons of interest and measured the release of pro-inflammatory cytokines IL-1α, IL-6 and IL-8 and compared the results to murine experiments performed *in-vivo* (Mallampati *et al*. 2010). The study showed that the irritation profile and the expression of cytokines increased with heavier hydrocarbons much like the response that was seen *in-vivo* (Mallampati *et al*. 2010). The barrier property of the Phenion® full-thickness was compared with *ex-vivo* pig skin (Ackermann *et al*. 2010). The *ex-vivo* pig skin was shown to be less permeable than the Phenion® full-thickness skin equivalents, which was shown to be more permeable than RHE equivalents previously tested (Ackermann *et al*. 2010; Schafer-Korting *et al*. 2008). Rasmussen *et al* exposed the StrataTest® full-thickness skin equivalents to chemical irritants, ultra-violet (UV) irradiation and environmental stress in addition to assessing barrier function (Rasmussen *et al*. 2010). The barrier function of the HSEs were found to be comparable to physiological human skin (Rasmussen *et al*. 2010). It was shown the release of reactive oxygen species (ROS) could be detected in HSEs exposed to environmental stress but this increase in ROS could be somewhat prevented by the pre-treatment of the HSEs with the antioxidant parthenolide-depleted feverfew extract (Rasmussen *et al*. 2010). An increase in cytokines IL-1α and IL-1RA were detected in response to UV irradiation which could be prevented by the application of sunscreen prior to exposure (Rasmussen *et al*. 2010). The Vrije Universiteit Medical Centre used in-house HSEs to investigate the level of cytokines that initiate immune cell infiltration (Spiekstra *et al*. 2005). The data from this study suggested that the skin cells secreted IL-1α and Tumour necrosis factor alpha (TNF-α) in response to irritants and could trigger immune cell infiltration of the HSEs (Spiekstra *et al*. 2005). Evidently currently available commercial HSEs can serve a variety of functions however due to the use of non-human ECM the HSE are not fully human or autologous. The use of the commercially available HSEs for testing of barrier function, sensitisers and allergens, suggests that there is a gap in the market for a commercial HSE that could be used for screening of

biologics at the early stages of drug development.

Table 1.1. Currently available commercial skin equivalents, including type of equivalent, cell types used and manufacturer.

Commercial skin equivalents	Equivalent type	Manufacturer	Cell types
EpiDerm™	Epidermal	MatTek Corporation	Human neonatal foreskin keratinocytes
SkinEthic™	Epidermal	L'Oréal	Human keratinocytes
EpiSkin™	Epidermal	L'Oréal	Human keratinocytes
EpiCs®	Epidermal	CellSytems GmbH	Human keratinocytes
LabCyte EPI-MODEL	Epidermal	Japan tissue Engineering Co. Ltd	Human keratinocytes
EpidermFT™	Full-thickness	the MatTek Corporation	Human keratinocytes and dermal fibroblasts
Phenion® FT	Full-thickness	Henkel Company	Human keratinocytes and dermal fibroblasts
StrataTest®	Full-thickness	Stratatech Corporation	Human keratinocytes and dermal fibroblasts

1.2.3 Preclinical Safety Testing and the Cost of Failure

Historically regulatory preclinical safety testing has relied upon the use of various species for *in vivo* studies. Such species include rodents (mice and rats), and non-rodents (dogs, pigs and nonhuman primates (NHPs) (Prior, Sewell, and Stewart 2017). NHPs are commonly used as tools for predicting adverse events of molecules, particularly large molecules like monoclonal antibodies (mAbs) in preclinical testing

(Bode and Starck-Lantova 2018). NHPs are in high demand as they are generally considered to be the most appropriate species for safety testing of biologics, as mAbs are highly specific to human targets and the expression of targets and target function in NHPs are similar to humans (Baumann *et al*. 2014; Bode and Starck-Lantova 2018). This results in NHPs demonstrating the anticipated pharmacological effect of the mAb, more so than other species with the exception of the minipig and transgenic murine models in some cases (Baumann *et al*. 2014; Blaich *et al*. 2016). Despite this there are disadvantages to NHPs. NHP studies are costly, can take months to see through and there is also the public scrutiny associated with *in-vivo* models (Bode and Starck-Lantova 2018). When Van Meer *et al* analysed the drug registration profiles of mAbs registered in the European Union the data showed that in only 59% of cases the immunogenicity of mAbs between NHPs and humans were comparable (van Meer *et al*. 2013). Furthermore the type of antidrug antibody (ADA) response differed between NHPs and humans in 59% of the cases (van Meer *et al*. 2013). The ADAs formed were responsible for the neutralisation or clearance of the mAbs (van Meer *et al*. 2013). The disparity in responses between NHPs and human studies highlights exactly how uninformative animal studies can be when predicting adverse immune responses. In recent years there has been an increase in the use of the minipig model for preclinical safety testing (Ganderup *et al*. 2012). Minipig models can be used as cheaper short term alternatives to NHPs for investigating biologics that interact with the immune system as the immune system of minipigs are more comparable to that of humans than dog models (Baumann *et al*. 2014; Bode *et al*. 2010). Although in terms of genetic homology minipigs are not more closely related to humans than NHPs due to the closer genetic ancestry between humans and NHPs. As established the use of animal models in pre-clinical test are not fool proof, and failure to identify unsuitable drug candidates at this stage can have severe financial consequences.

Overall, the preclinical safety testing process for screening drugs using *in-vitro* and *in-vivo* studies is costly to drug developers. Such costs mandate the importance of early stage identification of adverse drug candidates to limit both the cost and chance of failure. An in depth study by Wong *et al* analysed over 406,038 entries of clinical trial data for 21,143 compounds in the US (Wong, Siah, and Lo 2018). Wong *et al* used the clinical trial data to develop an algorithm to compute the probability of success (POS). Overall Wong *et al* estimated a POS of 11.2% in 2005 which steadily declined to 5.2% in 2013, after which the estimated POS increased to 6.7% (2014) and 13.8% (2016)

(Wong, Siah, and Lo 2018). Wong *et al* proposed that the improved POS may be attributed to the use of biomarkers becoming more common allowing drug developers to target specific patients for more favourable outcomes (Wong, Siah, and Lo 2018). Another suggestion from Wong *et al* was that this period involved a wave of medical breakthroughs, citing that Nivolumab (Bristol-Myers Squibb Company) was approved on five separate occasions in multiple markets in less than one year (Wong, Siah, and Lo 2018). Another possible explanation suggested by Smietana *et al* was that pharmaceutical companies implemented changes to the research and development process for drug candidates (Smietana, Siatkowski, and Moller 2016; Wong, Siah, and Lo 2018). In the sharp decline of clinical success rates (2007-2010) many large-scale drug developers underwent changes followed by more selective development pipeline processes (Smietana, Siatkowski, and Moller 2016). Smietana *et al* suggested that the changes to research and development improved overall POS indicating that more robust early stage identification of poor drug candidates could influence the POS of a drug (Smietana, Siatkowski, and Moller 2016). Drug development is a lengthy process, failure to identify poor drug candidates early enough can be incredibly costly to pharmaceutical companies. Since 1990 there has been an increase in investment by pharmaceutical companies to investigate drug candidates, though this has not resulted in an increase in output (Pammolli, Magazzini, and Riccaboni 2011). DiMasi *et al* estimated a pre-tax, pre-approval out-of-pocket cost of $1.5 billion (2019 dollars) and a capitalised cost of $2.9 billion (2019 dollars) for new drugs (DiMasi, Grabowski, and Hansen 2016). DiMasi *et al* suggested that costs were largely influenced by the high failure rates of drug testing in humans (DiMasi, Grabowski, and Hansen 2016). Therefore, the availability of human skin equivalents for predicting adverse events *in-vitro* could potentially be beneficial to the drug development process. The use of bioprinting to scale up testing could be of use for analysis of early drug candidates. By testing immunotoxic properties of biologics early in the pipeline process drug developers can decide which molecule should not proceed to the next stage of development, thereby saving time and money.

1.2.4 Bioprinting Technology

Advances in 3D printing technology in recent years have led to the development of machines and materials which are more applicable to biomedical applications. Biomedical applications range from the printing of implants, tissue scaffolds to the deposition of cells (Murphy and Atala 2014). The addition of cells intensifies the

complexity of the printing process compared to standard 3D printing. Factors such as the printing process, cell types, printing stress on cell viability and the biocompatibility of selected materials and inks all need to be considered (Blaeser *et al*. 2016; Murphy and Atala 2014). This technology can allow the geometric and compositional complexity of tissue to be replicated through developing 3D structures with more than

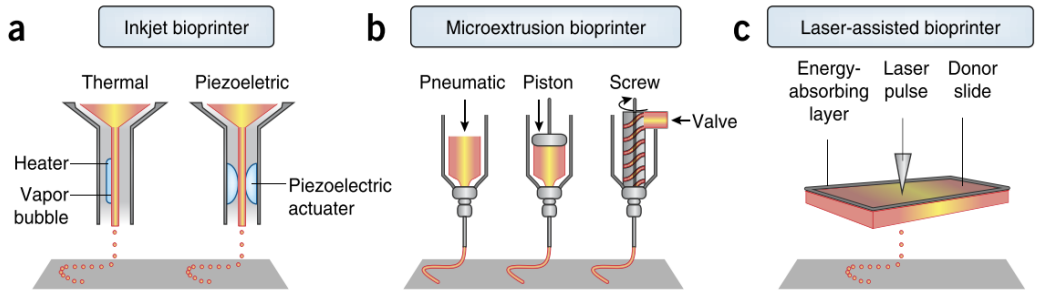

Figure 1.4. Three common bioprinting methods. (*A) Thermal inkjet systems use heat to cause shifts in pressure resulting in a droplet while piezoelectric systems depend on the sudden deflection of the actuator to trigger the formation of a droplet. (B) Extrusion processes require constant pneumatic or mechanical back pressure to extrude chains of ink. (C) Laser based printers require an absorbing substrate to generate the pressure necessary to generate a droplet. Image from Murphy and Atala 2014.*

one cell type and in a specific organisation. The three most popular printing processes are inkjet, microextrusion and laser assisted bioprinting (Figure 1.4).

Inkjet bioprinters deposit droplets on demand (DOD) to a desired location. Inkjet printers are normally driven by two different mechanisms, either a thermal actuator or a piezoelectric actuator. Thermal inkjet printers use a heating filament within the print head to quickly vaporise some ink and form a bubble. The formation of an air bubble causes changes in pressure which is enough to overcome the surface tension of the ink and force a droplet to be ejected from the nozzle. While it has been reported that the thermal process is not significantly detrimental to cell viability and functionality (Xu *et al*. 2006; Xu *et al*. 2005) the risk of thermal stress impacting cells is additional to shear forces during printing.

Piezoelectric systems use a material within the printhead which changes shape when a voltage is applied. The rapid deflection of the piezoelectric material causes an acoustic wave inside the printhead. This pulse in the printhead causes a change in pressure triggering ink to be ejected from the nozzle orifice forming a droplet (Fang *et al*. 2012). As this pulse can be manipulated by changing the voltage applied to the piezoelectric material, piezoelectric printers offer more control over droplet uniformity and directionality than thermal systems. Voltage waveforms and the vibration

frequency (Hz) are used to control the pulse. To optimise the droplet formation of inkjet printing the pulse width (P_w) and amplitude (P_a) must also be optimised (Derby 2010) (Figure 1.5). The inkjet systems are generally widely available and offer good resolution but are not without flaws. Thermal systems include the risk of exposing the inks and components to thermal stress (Murphy and Atala 2014) and the heating filaments may need to be replaced over time due to possible material deposits reducing the effectiveness of the filament. Droplet deposition and size in inkjet process are impacted by properties of the ink such as viscosity and surface tension making deposition of high viscosity ink challenging. For this reason inkjet bioprinters use low viscosity inks such as cells suspended in culture media (Blaeser et al. 2016; Murphy and Atala 2014), although it has been demonstrated that alginate based inks can also be printed using inkjet systems (Negro, Cherbuin, and Lutolf 2018). Inkjets usually have a volume range of 1-100pL (Derby 2010). Therefore, a single inkjet may not be suitable for high-throughput processing but may be ideal for the deposition of lower cell densities in low viscosity inks. The advantages and disadvantages of inkjet printing are summarised in Table 1.2, page 22.

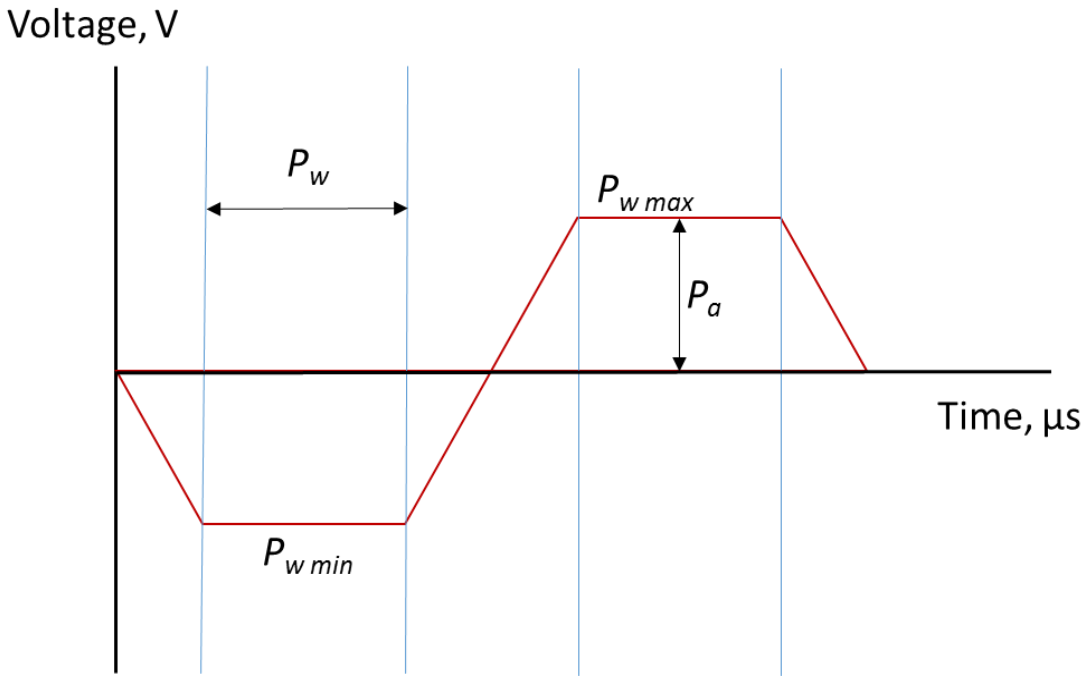

Figure 1.5. An example of jetting pulse waveform labelled with pulse width (pw) and amplitude (pa). *Trapezoid waveforms are commonly used during inkjet printing.*

Microextrusion is a similar process to many commercially available desktop 3D printers. Pneumatic and mechanical (piston and screw) mechanisms are used to

extrude material through the nozzle in microextrusion (Figure 1.4b). These printing mechanisms allow close control of the flow of material, making the process ideal for the deposition of hydrogels and high cell densities (Murphy and Atala 2014). It is worth noting that the viability of cells post printing can be lower in comparison to other printing methods due to shear forces when extruding the high viscosity inks as shown in Figure 1.6 (Panwar and Tan 2016). Larger nozzle sizes and lower pressures may be used to maintain cell viability at the cost of resolution and print speed. The advantages and disadvantages of microextrusion processes are summarised in Table 1.2, page 22.

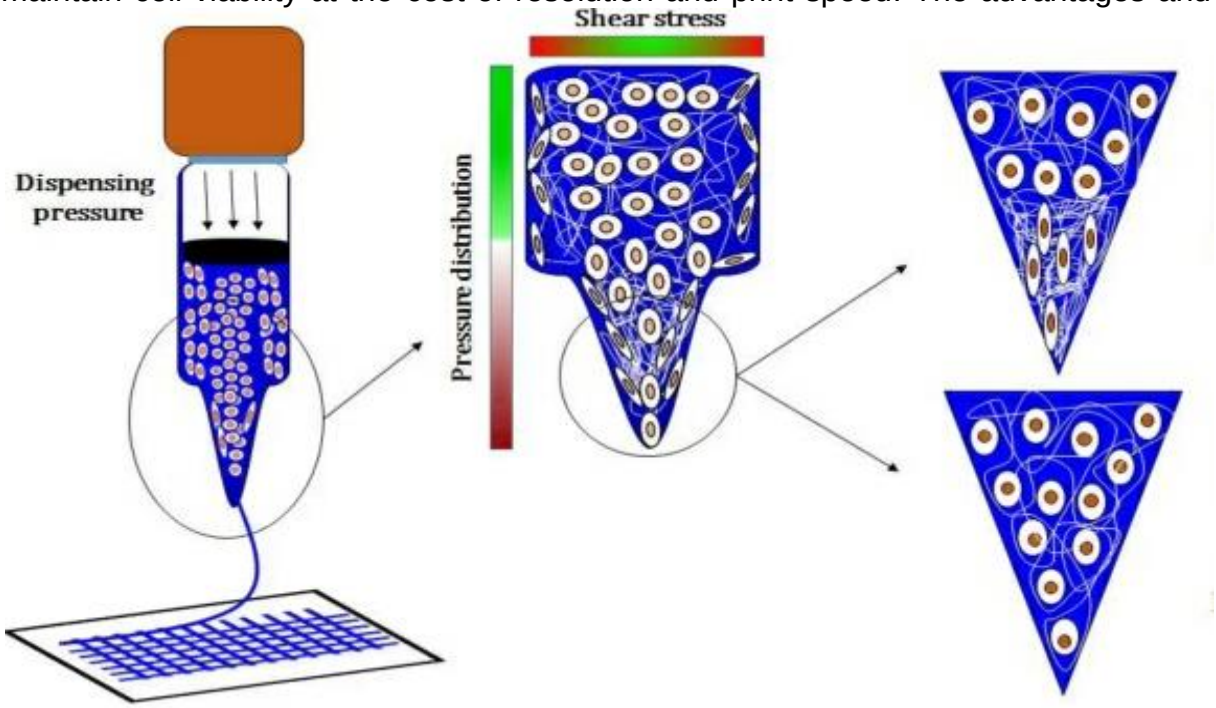

Figure 1.6. Distribution of pressure and shear stress during microextrusion. *As viscous cell laden inks are extruded there is an increase in pressure at the tip orifice. Cells close to the walls of the ink reservoir are exposed to more shear stress than those in the centre. Image from Panwar and Tan 2016.*

Laser-assisted bioprinting (LABP) was developed using the process of laser-induced forward transfer (LIFT) for DOD deposition. LIFT printing uses a laser to form a bubble between an energy absorbing layer and the bio-ink (Figure 1.4). The changes in pressure from the bubble cause a droplet of material to form. This process is also suitable for DOD deposition of bio-inks with high cells densities with cell high viability post printing (Koch *et al*. 2010). However low viscosity bio-inks with poor adhesive properties cannot be processed using LABP. As a result, LABP bioprinters are restricted to high viscosity bio-inks such as cross-linked hydrogels or gel precursors (Michael et al. 2013; Murphy and Atala 2014). The advantages and disadvantages of LABP processes are summarised in Table 1.2, page 22.

Microvalve based bioprinting is another DOD process which typically involves the use of a gas regulator which provides pneumatic pressure to the print head. Within the microvalve a solenoid coil is used to lift a plunger that blocks the nozzle orifice (Figure 1.7). When a voltage is applied to the solenoid coil a magnetic field in the coil pulls the plunger away from the nozzle, opening the nozzle orifice. Once the nozzle orifice has been opened the pneumatic pressure is used to deposit the ink. When enough pressure is applied to overcome ink surface tension and viscosity at the nozzle orifice the ink is ejected forming a droplet. At the end of the waveform there is no voltage applied to the solenoid and so the plunger drops and blocks the nozzle orifice again, this is one actuation cycle resulting in one droplet. Ink deposition is influenced by factors such as ink viscosity, ink surface tension, the applied pressure, nozzle diameter and the duration that the valve is open (Lee *et al*. 2009). Solenoid microvalves can deposit cells with high viability (Lee *et al*. 2009). The droplet size of solenoid microvalves ranges in the nanolitres allowing valves to deposit cells in high densities which would be ideal for high-throughput fabrication of tissue models (Faulkner-Jones *et al*. 2015). As microvalves can handle a wide range of pneumatic pressure, microvalve based bioprinters can dispense low viscosity inks such as cells suspended in media and high viscosity inks such as cell-laden hydrogel precursors(Faulkner-Jones et al. 2013; Lee et al. 2009; Okubo et al. 2019). The advantages and disadvantages of microvalve printing are summarised in Table 1.2, page 22.

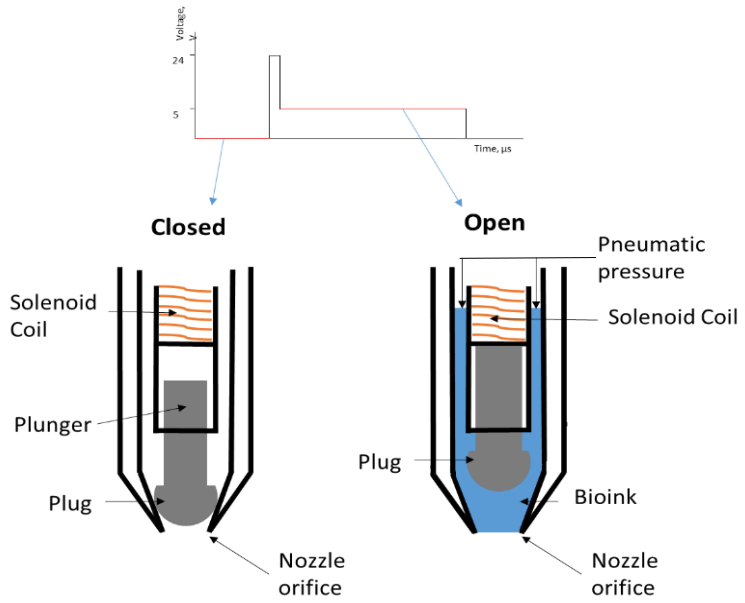

Figure 1.7. The opening a closing of a solenoid valve. *When no voltage is applied to the solenoid the valve is in a closed state. The 24v spike opens the valves as quickly as possible and the dwell voltage of 5v holds the valve open without generating too much heat. Once the valve is open a positive back pressure pushes ink through the nozzle orifice. When the voltage is no longer applied to the solenoid the plunger drops and blocks the nozzle orifice again. This is one actuation cycle triggering one droplet.*

In DOD processes cell laden bio-inks can act as unstable colloid suspensions (Figure 1.8). Cells in suspension usually form cell-cell adhesions and sediment over time, resulting in the formation of flocs. Flocs are aggregated particles in suspension. As flocs form the cells are no longer equally distributed within the bio-ink. An uneven suspension of cells within the bio-ink can impact the homogeneity of cells per droplet and block printheads therefore disrupting prints. As agitation systems for maintaining cell suspensions in bioprinters are not widely available some studies have investigated methods of preventing printing cell-cell adhesions. Ribeiro *et al* investigated the use of a temporarily speckled coating for cells using a polycation to restrict cell-cell adhesion (Ribeiro et al. 2017). Poly-L-lysine (PLL) was used to apply a speckled coating to cells to prevent cell agglomeration. Ribeiro *et al* observed that cells ingested the PLL and metabolised the polymer before returning to phenotypically normal behaviour. Ng *et al* used polyvinylpyrrolidone (PVP) macromolecules to develop bio-inks in an attempt to improve the printability of cell suspensions (Ng, Yeong, and Naing 2017). It was reported that the PVP based bio-inks were able to mitigate the cell adhesion and sedimentation over a period of 30 minutes (Ng, Yeong, and Naing 2017).

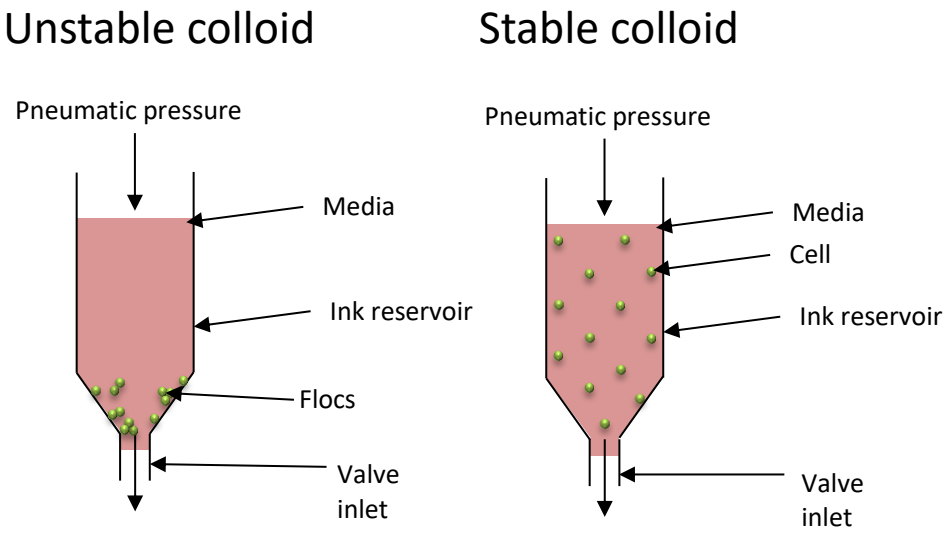

Figure 1.8. Cells in suspension act as colloidal suspensions. *In DOD systems suspensions of cells often behave as colloidal suspensions. When cells are initially suspended in even distribution they are stable colloids. The cells often form adherences to one another and naturally sediment over time. The clumps which form and sediment over time are called flocs. The formation of flocs can hinder the printing process.*

Table 1.2. Advantages, disadvantages, and available inks for bioprinting process.

Printing process	Inks used	Advantages	Disadvantages	References
Ink jet	Cell culture media	High resolution.	Low throughput. Not ideal for high viscosity inks.	Murphy and Atala 2014
Laser assisted bioprinting (LABP)	Cross-linked gels	High resolution.	Limited to viscous materials and requires treatment and coating of slides.	Koch *et al* 2012; Michael *et al* 2013
Microextrusion	Gel based inks	Can print high cell densities.	Low throughput.	Murphy and Atala 2014

Microvalve	Cell culture media and gel-based ink	High throughput. Can print low and high viscosity inks.	Lacks the resolution f other drop on demand processes	Faulkner jones *et al* 2015; Faulkner jones *et al* 2013

1.2.5 Bioprinting of Skin

While the development of 3D skin equivalents through conventional tissue engineering techniques has been well established there have been attempts to bioprint skin with varying success due to the materials and cells used. Lee *et al* used a custom built microvalve system to deposit layers of primary human dermal fibroblasts and keratinocytes within a type 1 rat tail collagen gel scaffold (Lee *et al*. 2009). Collagen gel precursors were printed and partially cross-linked using nebulised sodium bicarbonate as the crosslinking agent. Then cells were printed into the partially cross-linked gel causing the cells to be embedded within the gel. The partially cross-linked gel was further cross-linked with nebulised sodium bicarbonate to provide a foundation for the next layer. This method of embedding cells into gels showed no significant loss in cell viability and no changes in cell morphology. This work was further built upon using the same bioprinting system and crosslinking mechanism for collagen gel precursors to print HFF-1 fibroblasts and HaCaT keratinocytes (Lee *et al*. 2014). The cell laden gel constructs were printed onto a transwell membrane and cultured at ALI. Lee *et al* did not report any significant loss in cell viability, with viability decreasing to 84-89% at lower cell densities ($0.5\text{-}0.75 \times 10^6$/mL) and larger droplet spacing of 400–750 mm (Lee *et al*. 2014). These constructs were submerged in media for 4-8 days and then raised to an ALI for 14 days. The histology of the printed tissue can be seen in Figure 1.9. The dermis appeared to be sparsely populated despite the seeding of 2.3×10^5 fibroblasts in contrast to 1.4×10^5 keratinocytes. The lack of stratification is noticeable in Figure 1.9 potentially due to the use of HaCaT cells entrapped in a gel rather than primary keratinocytes printed directly onto a gel.

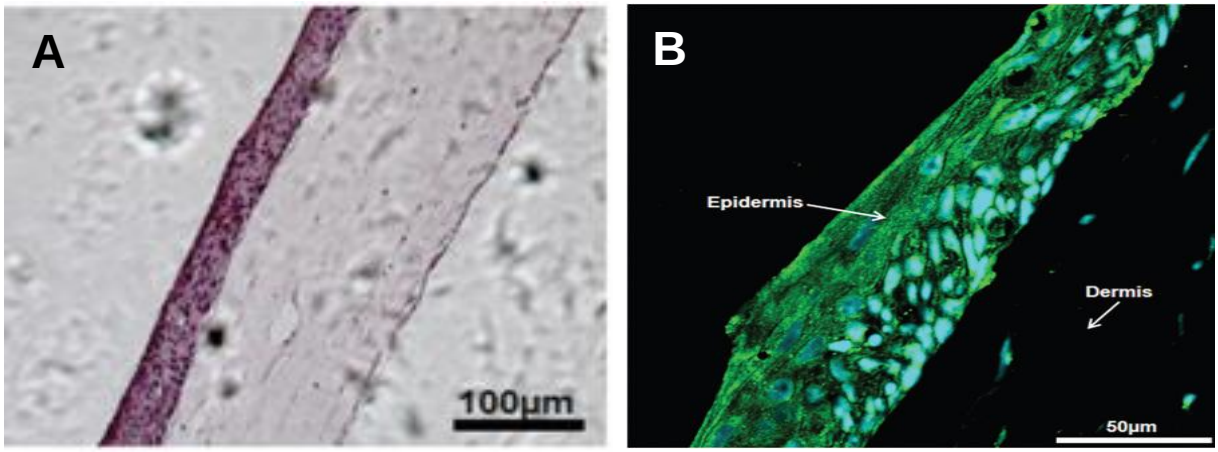

Figure 1.9. Histology of skin constructs bioprinted by Lee et al. (A*) H&E staining of tissue constructs. (B) N-cadherin staining of construct showing some degree of organisation in the epidermis. Adapted from Lee et al 2014.*

LABP technology was used by Koch *et al* to sequentially print layers of NIH-3T3 Swiss albino fibroblasts and HaCaT cells suspended in a rat tail type 1 collagen gel (Koch *et al*. 2012). An acellular dermal substitute (Matriderm^{TM}) was used as the substrate. The bioprinted gels were fabricated in two layers. The first layer (lower layer) was constructed with 20 sub-layers of fibroblasts and the upper layers were made of 20 sublayers of keratinocytes. In total $1.5x10^6$ fibrobolasts were printed in the dermal layer and $1.5x10^6$ keratincoytes were printed into the epidermal layer. The bioprinted constructs were printed and submerged in culture media for 10 days before being harvested. Figure 1.10 shows the histology of the bioprinted constructs after 10 days in culture. While it is easy to differentiate between what is referred to as the dermis and epidermis from Figure 1.10 there is little development of the epidermal layer much like the work of Lee *et al* (Lee *et al*. 2014). Later Michael *et al* used the above LABP system to sequentially print 20 layers NIH-3T3 fibroblasts and 20 layers of HaCaT keratinocytes onto Matriderm^{TM} sheets (Michael *et al*. 2013). The prints were submerged over night before being cultured at an ALI for up to 11 days. Histological sections of harvested constructs are shown in Figure 1.11. Figure 1.11 shows that the HaCaT cells do continue to proliferate but there was little evidence of a stratified epidermis.

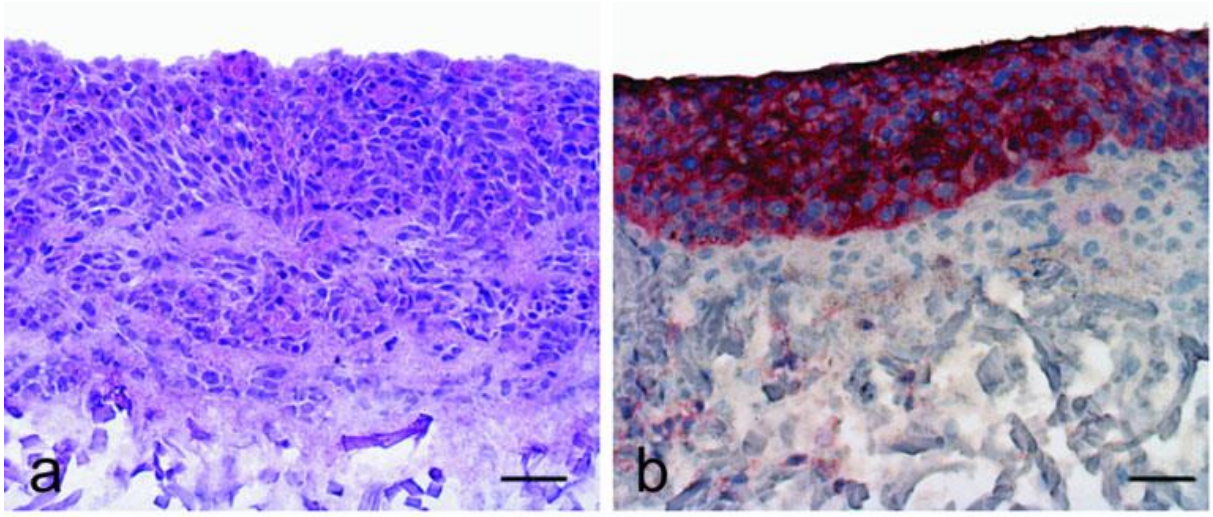

Figure 1.10. Histology of cell-gel constructs bioprinted using LABP. (A*) Sections of the bioprinted constructs 10 days after printing. Haematoxylin-eosin staining of bi-layered construct Immunoperoxidase staining of cytokeratin 14 in reddish-brown of bi-layered construct (B). Scale bars: 50µm. Adapted from Koch et al 2012.*

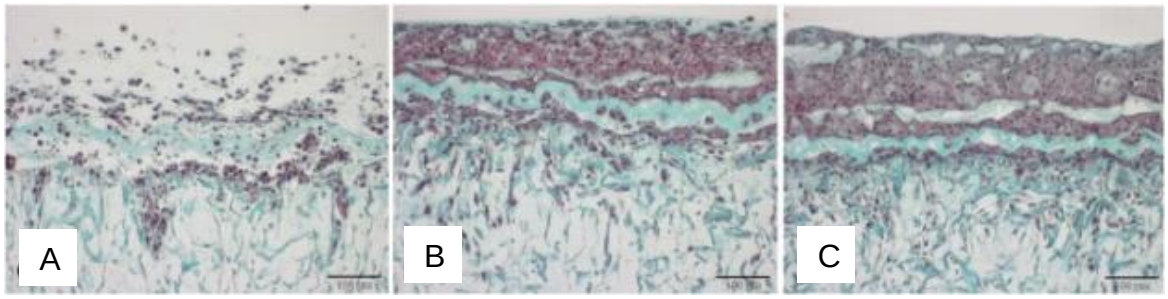

Figure 1.11 Mason trichrome staining of LABP cell-gel constructs cultured at ALI. *All constructs were incubated submerged overnight. (A) construct incubated overnight, defined as day 0. (B) Construct harvested at day 5 ALI. (C) Construct harvested at day 11 ALI. Scale bars: 100µm. Adapted from Michael et al 2013.*

The use of cell lines in the above studies do provide homogeneity between prints, however using primary human fibroblasts and human keratinocytes could help produce bioprinted skin equivalents which more accurately represent the structure of human skin *in-vivo*. A relatively simple microextrusion based system was developed by Cubo *et al* by modifying an open source Reprap Printrbot (Cubo *et al*. 2016). The Printrbot was customised to use piston based microextrusion and a mixing cartridge to extrude gels. Three separate dispensers were used to mix human fibroblasts, human plasma and $CaCl_2$ into the mixing cartridge above the nozzle prior to printing. The human fibrin-fibroblast matrix was dispensed onto transwell membranes. Following cross-linking of the dermal layer at 37^{o}c, a suspension of human keratinocytes was seeded onto the dermal layer, incubated overnight, and cultured at the ALI for 17 days. Histological staining of the *in-vitro* skin equivalents (Figure 1.12) showed some delamination of the extra-cellular matrix in the dermis, but the epidermis was well

stratified.

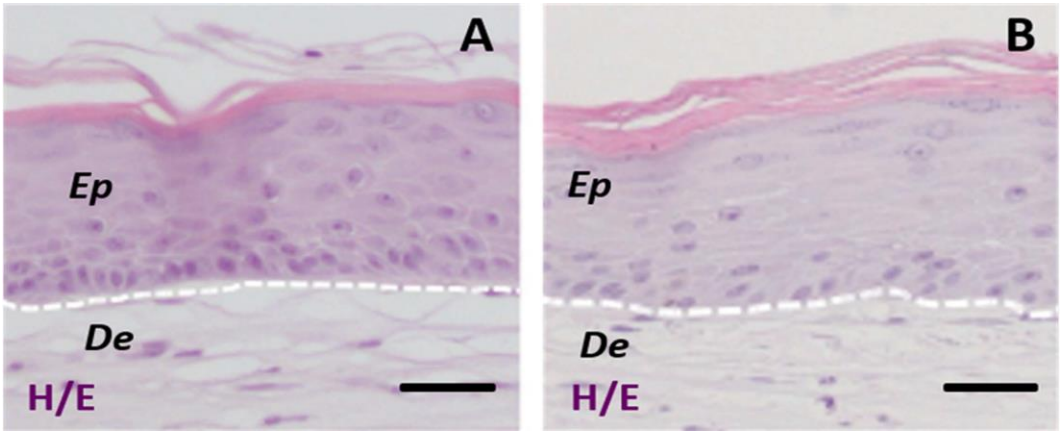

Figure 1.12. H/E staining of skin equivalents fabricated by microextrusion*. (A) 'Handmade' skin. (B) Bioprinted skin equivalent. Ep and De refers to the dermis and epidermis, respectively. The dotted line indicates the basal membrane Scale bars: 100 µm. Image from Cubo et al 2016.*

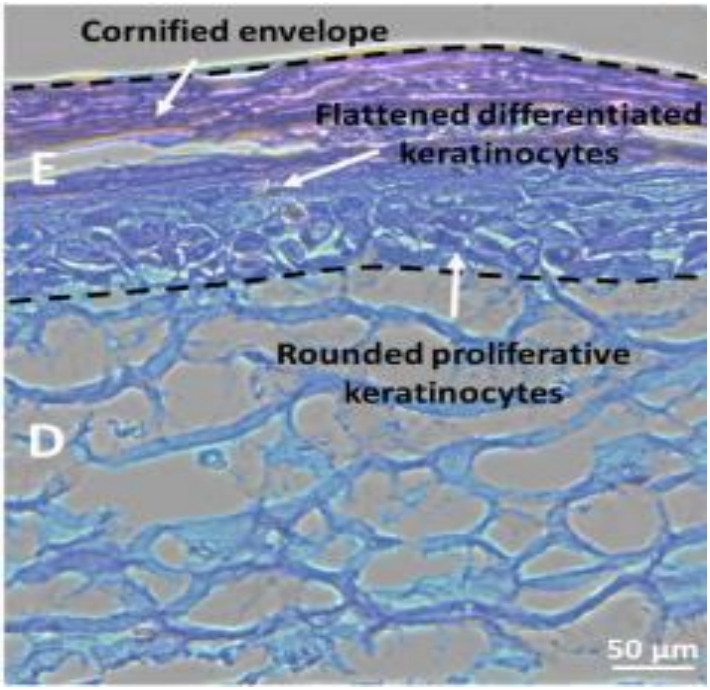

Figure 1.13. H/E stained skin equivalents fabricated with microvalves. *Representative H/E staining of a cryostat section. E represents the epidermis and D represents the dermis. Adapted from Ng et al 2016.*

Researchers from Singapore developed pigmented equivalents by using microvalves to print fibroblast-laden collagen gels which supported melanocytes and keratinocytes (Ng *et al*. 2018). Like Cubo *et al* a two-step process was used to first create a dermal construct before printing of keratinocytes and melanocytes. The fibroblast-laden collagen gels were printed into 6-well inserts and incubated submerged for 4 days. Keratinocyte and melanocyte suspensions were then printed onto the dermal construct

and incubated submerged for a further 7 days. To encourage epidermal stratification the constructs were cultured at an ALI for a further 4 weeks (Figure 1.13). Like the work of Cubo *et al*, the gel-based dermis had delaminated though in both cases this could have possibly been an artefact of the embedding or section processes. The columnar arrangement of basal keratinocytes was visible along with stratification of the epidermis.

Table 1.3. The printing techniques, scaffold type, cell types and the limitations of Studies which have bioprinted skin.

Printing process	Scaffold materials	Cell types	Limitations	Reference
Microvalve	Murine collagen gel	HFF-1 fibroblasts and HaCaT keratinocytes	• Non-human ECM • Printed layers required manual crosslinking • Gel encapsulated keratinocytes did not fully stratify	Lee *et al* 2010
Laser assisted bioprinting	Murine collagen gel	NIH-3T3 fibroblasts and HaCaT keratinocytes	• Non-human ECM (murine) • Gel encapsulated keratinocytes did not fully stratify	Koch *et al* 2012
Laser assisted bioprinting	Murine collagen gel	NIH-3T3 fibroblasts and HaCaT keratinocytes	• Non-human ECM (murine) • Gel encapsulated keratinocytes did not fully stratify	Michael *et al* 2013
Extrusion	Human fibrin gel	Primary human fibroblasts and keratinocytes	• Dermal ECM was human (fibrin) but not autologous • Visible delamination of dermis	Cubo *et al* 2016
Microvalve	Unspecified collagen gel	Primary human fibroblasts and keratinocytes	• Source of ECM not specified • Visible delamination of dermis	Ng *et al*. 2018

The preferred approach within the literature is to use hydrogels as scaffolds to manufacture a cell laden dermal substrate which then can support bio-printed keratinocytes. This approach has been used in several, the limitation of these studies are summarised in table 1.3. This use of gel based bioprinting can allow the development and maturation of both the dermal and epidermal regions simultaneously

within a co-culture rather than sequential development of the two layers. By forming both the dermis and epidermis in parallel the lead time for equivalent production can be reduced, this may be an ideal approach depending on the application of the skin equivalent. However, there are some limitations to creating gel based HSEs. Encapsulating epidermal keratinocytes within a hydrogel appears to restrict stratification of the epidermis. It is yet to be investigated if animal derived hydrogels such as non-human collagen could impact *in-vitro* immunotoxicity testing accuracy by eliciting a foreign body response. For such applications, a human fibrin-based gels may be more appropriate, though it may be necessary to source human leukocyte antigen (HLA) matched blood to prevent a background immune response and therefore false positives. The studies to date reflect the difficulty in bioprinting 3D skin equivalents and highlights that much optimisation of procedures is still required to develop 3D bioprinted skin equivalents with both a well-developed and physiologically representative dermis and epidermis. As of yet there has not been a fully autologous bioprinted full-thickness 3D skin equivalent available commercially or otherwise which is suitable for immunotoxicity testing. Therefore, there is a gap in knowledge yet to be exploited to produce skin equivalents suitable for drug testing.

1.2.6 Characterisation of Bioprinted Skin Equivalents

Currently the gold standard within the literature for analysing the formation of skin equivalents is qualitative histology. Currently there are no quantitative forms of analysis which can verify the formation of independent dermal and epidermal layers as well as stratification of the epidermis. While quantitative techniques can be used to total expression of proteins such as cytokeratins within skin equivalents, this does not necessarily indicate stratified tissue, as keratinocytes are well known to terminally differentiate even without stratification (el-Ghalbzouri et al. 2002). For these reasons the literature presented in this chapter use qualitative histology as a characterisation tool when assessing the success of human skin equivalents (Cubo et al. 2016; Koch et al. 2012; Lee et al. 2014; Lee et al. 2009; Michael et al. 2013; Ng et al. 2017). One such example of this standard approach to characterisation is the work of Koch *et al* which presented three figures of qualitative data consisting of basic histology, immunohistochemistry and immunofluorescent staining (Koch et al. 2012). Therefore, in this thesis qualitative data was used to characterise skin equivalents developed in-line with previous studies within the field of bioprinting skin.

1.3 Project Aim and objectives

This project will investigate the feasibility of bioprinting autologous human skin cells to produce human full-thickness 3D skin equivalents for immunotoxicity testing of biologics *in-vitro*.

Objectives

1. Develop robust protocols for creating handmade skin equivalents in both the 24-well and 96-well format which are representative of physiological human skin.
2. Replicate 96-well handmade skin equivalents using bioprinting and compare the structure to bioprinted skin equivalents to handmade skin equivalents and physiological human skin.
3. Use fully autologous bioprinted skin equivalents for *in-vitro* testing of monoclonal antibodies and profile the cytokine response to show proof-of-concept.

Chapter 2 Materials and Methods

2.1 Ethical Approval

This study was approved by the Local Research Ethics Committee (LREC). The primary human skin cells and blood cells used in this study were obtained from skin samples taken from donors after informed consent. For experiments which only required skin cells the cells were isolated from excess human foreskin from the urology clinic of the Freeman Hospital, The Newcastle upon Tyne Hospitals NHS Foundation Trust (REC 08/H0906/95+5). For experiments requiring autologous donor matched skin and blood cells, healthy volunteer samples were sourced by Alcyomics Ltd and used to isolate the required cells (REC 10/H0906/58, Appendix A).

2.2 Skin Processing

Skin processing and cell isolation for both cell types used a modified version of long established skin cell isolation protocol (Barlow and Pye 1990). Human skin biopsies were harvested in X-VIVO 10^{TM} medium (Lonza) following consent from donors and stored at 4°C until processing. Biopsies were washed in phosphate buffered saline (PBS, Sigma-Aldrich) and carefully trimmed using sterile scissors and a scalpel to remove subcutaneous tissue. The underside of the dermis was lightly scored with a scalpel to facilitate enzymatic digestion of the basal membrane using dispase (Sigma-Aldrich). The samples were then incubated overnight at 4^{o}C in 4 mLs of a dispase solution to separate the epidermal and dermal layers. The dispase solution contained 1.0 U/mL of dispase, 1% penicillin/streptomycin solution (P/S, Sigma-Aldrich) and 1% amphotericin B solution (Sigma-Aldrich). After dispase treatment samples were washed and gently agitated in PBS to remove any excess dispase and to help loosen the epidermis from the dermis. The epidermis was then peeled from the dermis with ethanol sterilised forceps (Figure 2.1). The epidermis and the dermis were further processed separately.

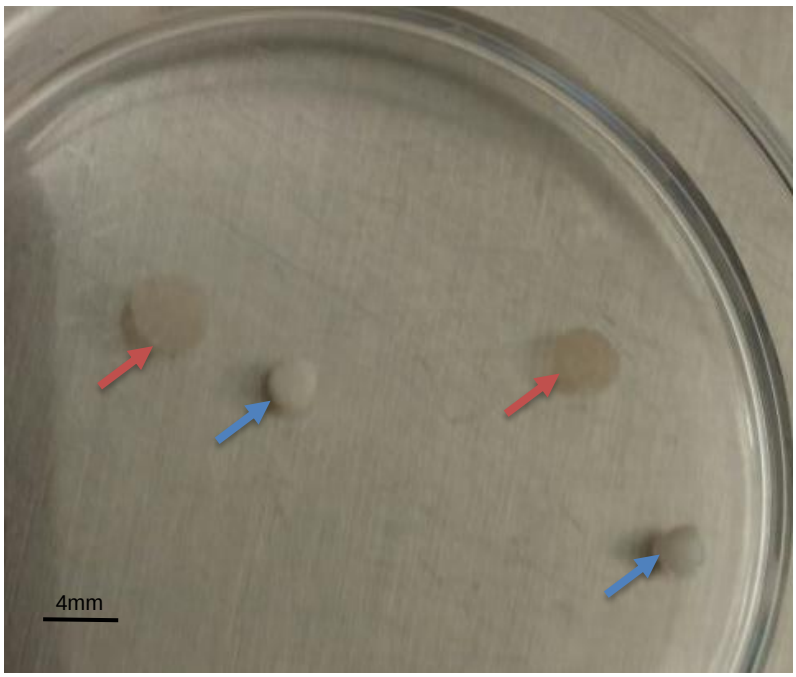

Figure 2.1. Enzymatically separated dermis and epidermis of a 4mm skin punch biopsy. *The floating epidermis is indicated by the red arrow, while the thicker dermis is shown by the blue arrows.*

2.3 Isolation and Culture of Primary Dermal Fibroblasts

Once separated the dermal samples were further dissected into six smaller pieces which varied in size. Dermal samples were placed into 6-well plates (Greiner CELLSTAR®, Sigma-Aldrich). The bottom of each well was scored with a scalpel to improve adhesion of the sample to the well. Any excess PBS from each dermal sample was aspirated and 100 µL of foetal bovine serum (FBS, Thermo Fisher Scientific) was used to cover each dermal sample. The dermal samples were incubated at 37°C with 5% CO_2 for 24 hours. The following day the wells were topped up with 5 mLs of complete Dulbecco's Modified Eagle Medium (DMEM, Sigma-Aldrich) supplemented with 20% FBS, 1% penicillin/streptomycin solution (P/S, Sigma-Aldrich), 1% l-glutamine solution (Sigma-Aldrich) and 1% amphotericin B solution (Sigma-Aldrich) was added. After 3 days the media was replaced with complete DMEM with 10% FBS. Beyond this stage DMEM supplemented with 10% FBS, 1% P/S and 1% amphotericin B was used as fibroblast growth medium. The dermal samples were fed twice weekly with 5 mLs of fibroblast growth medium until sufficient fibroblast outgrowth from the dermis was observed. This was considered as passage 0. Once enough outgrowth was observed the dermis was then removed with ethanol sterilised forceps and discarded. The fibroblast growth medium was aspirated, and wells were washed twice

with PBS. The fibroblasts were enzymatically dissociated by incubation with trypsin-EDTA (Sigma-Aldrich) for 5 minutes at 37^{o}C with 5% CO2. Once the fibroblasts were detached fibroblast growth medium equal to the volume of trypsin-EDTA was added to each well and the cell suspension was aspirated and pelleted by centrifuging (Megafuge 8, Thermo Fisher) at 400g for 5 minutes. Cells were resuspended in fibroblast growth medium and counted using a haemocytometer (Hawksley). Fibroblasts were further cultured in tissue culture flasks (Greiner, Sigma-Aldrich) with the media changed twice weekly. Cells which were not intended for immediate use in experiments were stored at -140^{o}C at passage 2 for future use. Fibroblasts used for experiments were not cultured beyond passage 7. To cryopreserve the fibroblasts the cells were dissociated from flasks using trypsin-EDTA and pelleted by centrifugation at 400g for 5 minutes. The supernatant was discarded, and the cells were resuspended at 1 x 10^{6} cell/mL with fibroblast freezing solution consisting of 9 parts fibroblast growth media and 1 part dimethyl sulfoxide (DMSO, Fisher Scientific). The DMSO prevented the formation of ice crystals when freezing which could cause cell death. The cells were transferred to cryovials (Nunc, Sigma-Aldridge) and frozen at -80^{o}C overnight to achieve a freezing rate of -1^{o}C/min. The following day cryovials were transferred to a -140^{o}C freezer for long term storage.

2.4 Isolation and Culture of Primary Keratinocytes

Following the separation of the dermis from the epidermis, the epidermis was not further dissected into smaller pieces. Rather the epidermis was incubated with trypsin-EDTA at 37^{o}C with 5% CO2 for 5 minutes. After 5 minutes an equal volume of fibroblast growth media was added to the epidermis to neutralise the trypsin-EDTA. The suspension containing the epidermis was centrifuged for 5 minutes at 400g. After centrifugation, the trypsin-EDTA/fibroblast growth media solution was decanted and the epidermis along with the cell pellet, was resuspended in keratinocyte growth media and seeded into a tissue culture flask. This was considered passage 0. The keratinocyte growth media was EpiLife® Medium (Thermo Fisher Scientific) supplemented with 1% human keratinocyte growth supplement (HKGS, Thermo Fisher Scientific), 1% P/S, and 1% amphotericin B solution. The following day the floating epidermis was removed, and the media changed to remove any non-adherent cells. The remaining adherent keratinocytes within the flask where fed thrice weekly and split using trypsin-EDTA once reaching 70% confluency. Keratinocytes were not cultured beyond passage 4. Keratinocytes which were not intended for immediate use were

cryopreserved at passage 1 or 2 using the process described for freezing of fibroblasts, but with the keratinocytes frozen in a keratinocyte freezing solution consisting of 9 parts keratinocyte growth media and 1 part DMSO.

2.5 Peripheral Blood Monocytes Isolation from Whole Blood

Cell isolation from whole blood was conducted using a modified method described by (Yeo et al. 2009). For experiments which required donor matched autologous peripheral blood monocytes (PBMCs) 60 mL of whole blood from healthy human volunteers was provided by Alcyomics Ltd. Whole blood was provided in sodium heparin blood tubes (BD, Fisher Scientific) to prevent coagulation of blood, additionally approximately 8 mL of whole blood was provided in a serum tube (BD, Fisher Scientific) which contained clot activators. The serum tube was centrifuged at 400g for 5 minutes to separate serum from blood cells. After centrifugation, 1 mL of serum was aspirated from the serum tube without disturbing the blood clot and aliquoted into an Eppendorf tube. The serum was heat inactivated at 56^{o}C for 1 hour then stored at -80^{o}C for future use. The blood from the sodium heparin tubes was diluted 1:1 with Earle's Balanced Salt Solution (Sigma-Aldrich) and carefully layered onto 6 mL of Lymphoprep™ density gradient medium (STEMCELL Technologies) so as not to mix the diluted blood and the Lymphoprep™ (Figure 2.2). The tubes containing layered blood and lymphoprep were centrifuged at 800g for 15mins (FisherScientific Accuspin). During centrifugation, the granulocytes, and erythrocytes sedimented through the Lymphoprep™ solution due to a higher density at the osmotic pressure of the density gradient medium. The less dense monocytes remained at the plasma-Lymphoprep™ interface (Figure 2.2). The plasma directly above the PBMC layer was discarded and the PBMC layer at the plasma- Lymphoprep™ interface was harvested. PBMCs were washed in PBS, centrifuged, and resuspended in RF10 media and counted. RF10 was comprised of Roswell Park Memorial Institute-1640 (RPMI-1640, Sigma-Aldrich) media supplemented with 10% FBS, 1% P/S, 1% amphotericin B solution, and 1% l-glutamine solution. The PBMCs were frozen in a freezing solution containing 9 parts RF10 and 1 part DMSO. PBMCs were stored at -140^{o}C for further experiments.

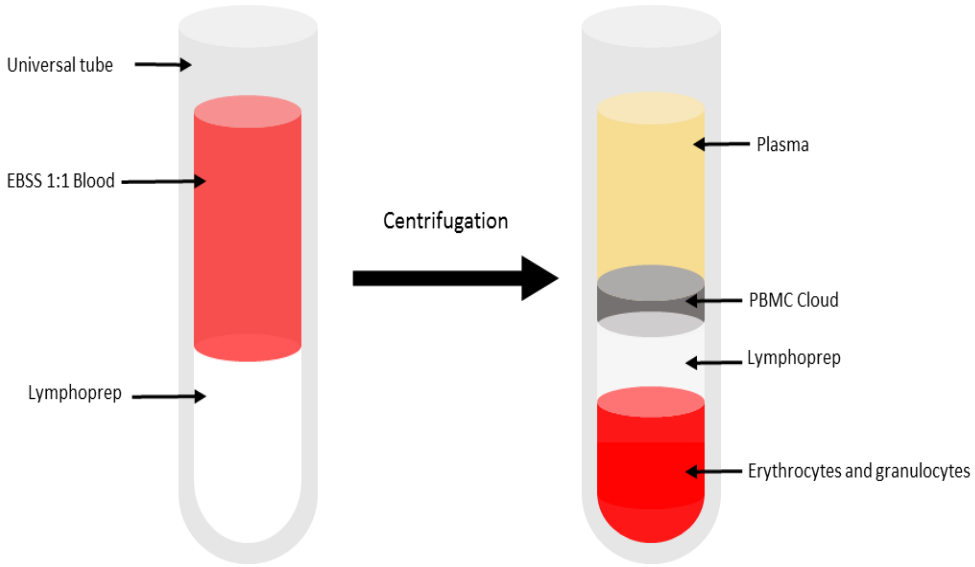

Figure 2.2. Density gradient separation of monocytes from whole blood. *Diluted whole blood was layered onto lymphoprep and centrifuged to separate cells by density gradient. The PBMCs of interest were located at the plasma-Lymphoprep™ interface.*

2.6 Producing Handmade Skin Equivalents Using Transwell Inserts

To develop consistent three-dimensional (3D) models, smaller prototypes of Alvetex® transwell inserts initially used in 6-well format by used by Hill *et al (Hill et al. 2015)* were used. The smaller prototypes were used in the 24-well format and the 96-well format inserts and were provided by Reprocell Europe Ltd (Figure2.3). The transwell system was used to ensure that the resulting human skin equivalents (HSEs) would be fully human and not contain animal extra-cellular matrix (ECM). The general protocol for constructing handmade and bioprinted HSEs between 24-well and 96-well formats was largely unchanged from the original 6-well format first described by Hill *et al (Hill et al. 2015)*. This process is summarised in Figure 2.4.

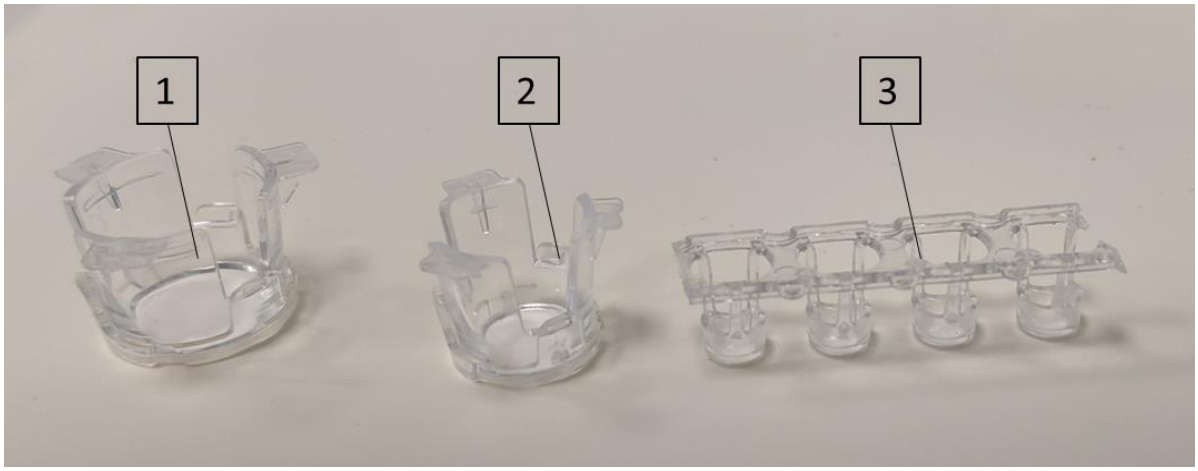

Figure 2.3. Alvetex® transwell inserts*. 1) 6 well insert used by Hill et al (Hill et al 2015)). 2) Prototype 24-well transwell inserts. 3) Prototype 96-well transwell inserts.*

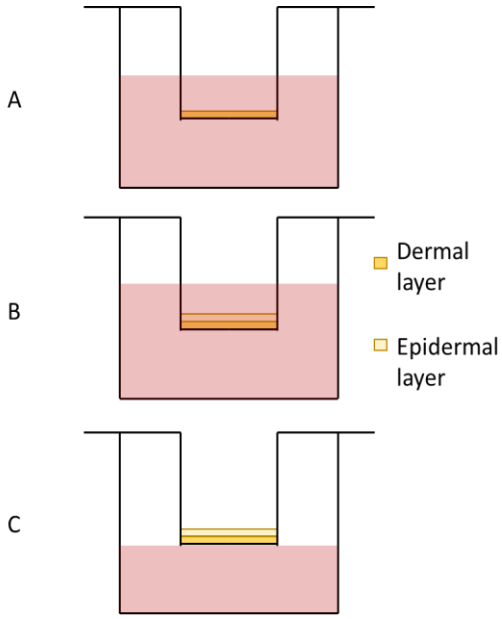

***Figure 2.4. Diagram of 3D skin equivalent culture method**. (A) Dermal incubation of fibroblasts only for up to 28 days. (B) Basal incubation of keratinocytes for 3 days. (C) Incubation of model at air-liquid interface for 14 days.*

Before use, the prototype transwell Alvetex® inserts were soaked in 70% ethanol for 60 seconds. The ethanol both sterilised the scaffold and rendered the material hydrophilic, allowing media and cells to penetrate the scaffolds. Excess ethanol was fully removed by washing the inserts in several changes of PBS followed by washes in three changes of fibroblast growth media. The primed inserts were transferred to a new sterile tissue culture plate (Greiner CELLSTAR®, Sigma-Aldrich), and excess fibroblast growth media was carefully aspirated from the outer well and from within the transwell insert without damaging the scaffold. To form a dermal equivalent, primary dermal fibroblasts were seeded onto the top of the scaffold first. The primary fibroblasts were used up to passage 7. Prior to seeding fibroblasts, fibroblast growth media was added to the outside of each well to ensure that the bottom of the scaffold was in contact with media. The cell suspension containing the dermal fibroblasts was carefully pipetted directly onto the centre of the scaffold. The plates containing the dermal fibroblasts were carefully transferred to an incubator and incubated for 90 minutes at 37°C with 5% CO_2. After this time, fibroblast growth media was carefully pipetted to the outside of each well, gently flooding the chamber of the transwell inserts and submerging the scaffold containing the fibroblasts. Dermal equivalents were fed daily with fibroblast growth media supplemented with 100µg/mL of ascorbic acid (Sigma-

Aldrich). Fibroblasts were left to grown in the scaffold and produce extracellular matrix (ECM) and develop a dermal equivalent for at least 18 days. The production of dermal ECM by the fibroblasts was needed to prevent any infiltration of keratinocytes into the scaffold and to allow the formation of an epidermal layer. To form the epidermal layer, the dermal equivalents which had already been growing for at least 18 days were first prepared for seeding with keratinocytes. The fibroblast growth media was aspirated, and the dermal equivalents were rinsed with PBS to remove any residual fibroblast growth media present within the outer well. Once the PBS was aspirated from the outer well basal media was pipetted to the outside of each insert to ensure that the bottom of the dermal equivalent was in contact with media. The basal media consisted of a 3:1 ratio of DMEM and Ham's F12 nutrient mixture (Sigma-Aldrich) supplemented with 5% chelex-treated FBS, 1% P/S, 1% amphotericin B, 8.5 ng/mL of cholera toxin (Sigma-Aldrich) 0.4 µg/mL hydrocortisone (Sigma-Aldrich), 5 µg/mL of human insulin (Sigma-Aldrich), 24 µg/mL of adenine (Sigma-Aldrich), and 20 ng/mL of human epidermal growth factor (hEGF, Peprotech). Chelex-treated FBS was prepared by adding 100g of Chelex-100 resin (BioRad) to 500 mL of FBS and stirring overnight at 4^{o}C. The resin slurry was then removed by filtering the treated FBS with Whatman filter paper (Thermo Fisher Scientific). Before use, the Chelex-treated FBS was sterile filtered using a 0.2µm syringe filter (Thermo Fisher Scientific). Keratinocytes were used up to passage 4 and were resuspended in basal media. The keratinocyte suspension was seeded onto each respective dermal equivalent and then incubated for 3 hours at 37 °C with 5% CO_2. After the 3 hour incubation basal media was slowly added to the outside of each well to gently submerge the keratinocytes with minimal disturbance. The keratinocytes were cultured sumberged for 3 days to allow the cells to proliferate and form a basal monolayer on the dermis. The basal media was changed daily.

To encourage the formation of a stratified epidermis, the skin equivalents were raised to the air-liquid interface (ALI) after 3 days of submersion in basal media. To raise the model to ALI, the basal media was aspirated from each well and replaced with ALI media added to the outside of the insert ensuring the media was in contact with the underside of the dermal equivalent. The ALI media consisted of a 3:1 ratio of DMEM and Ham's F12 nutrient mixture supplemented with 10% FBS, 1% P/S, 1% amphotericin B, 8.5 ng/mL of cholera toxin, 0.4 µg/mL hydrocortisone, 20 ng/mL of EGF, 5 µg/mL human transferrin (PeproTech) and 100 µg/mL ascorbic acid. Enough ALI media was added to each well making sure the bottom of the equivalent was in

contact with ALI media while the keratinocytes were exposed to air. Skin equivalents were cultured for 14 days at the ALI, media was changed every 24 hours. After 14 days of incubation at ALI the media was aspirated, and the equivalents were carefully washed with PBS to remove any excess media and then harvested.

2.6.1 Optimisation of Handmade 24-well Skin Equivalents

Initially a protocol developed by Alcyomics was used to construct 24-well based HSEs by adapting the work of Hill *et al* (Hill *et al*. 2015), this protocol was later optimised. The prototype 24-well inserts were manufactured with the aim of reducing the overall number of cells necessary to create 3D skin equivalents from the original work (Hill *et al*. 2015). The rationale for decreasing the number of cells per HSE was to potentially increase the number of skin equivalents that could be constructed per donor.

In the 24-well format fibroblasts were suspended at a concentration of 20 x 10^6 cells/mL. 50 µL of this cell suspension was seeded onto each scaffold. 1 mL of fibroblast growth media was added to the outside of each well to ensure that the bottom of each scaffold was in contact with media. After the 90-minute incubation a further 600µl of fibroblast growth media was carefully pipetted to the outside of each well. For the epidermal layer, keratinocytes resuspended in basal media at 20 x 10^6 cells/mL. 50 µL of the keratinocyte suspension containing 1 x 10^6 keratinocytes were seeded onto each dermal equivalent. To raise the HSEs to the ALI in the 24-well format the basal media was aspirated and 1 mL of ALI media was added to the outer well. Once mature 24-well HSEs were washed in PBS. The HSEs were carefully unclipped from the transwell inserts, cut in half using a scalpel (Thermo Fisher), covered in tissue wrap (Fisher scientific) and placed into tissue cassettes (Fisher scientific). The tissue cassettes were submerged in 10% neutral buffered formalin for at least 24 hours. The formalin fixed samples were processed, paraffin embedded, sectioned, and stained with haematoxylin and eosin (H&E) by the Department of Cellular Pathology, Royal Victoria Infirmary, Newcastle upon Tyne. Further analysis of the structure of the 24-well skin equivalents were observed through histological staining techniques as described in section 2.11.

2.6.2 Development of Handmade 96-well based model

As there was no established protocol for the fabrication of handmade 96-well skin equivalents using the 96-well prototype Alvetex® inserts (provided by Reprocell Europe Ltd), it was necessary to investigate the number of fibroblasts and dermal

incubation period required for the development of the dermal layer prior to optimising the formation of an epidermal layer. The fabrication protocol was optimised by hand prior to being replicated with bioprinting. The processing, embedding, and sectioning of models made with 96-well Alvetex® inserts are detailed in section 2.11.

2.6.2.1 96-well Dermal Equivalent Optimisation

To form a dermis there needs to be enough fibroblasts to both adequately populate the scaffold and produce enough ECM to support an epidermis and prevent infiltration of keratinocytes into the scaffold. Varying numbers of fibroblasts (1×10^5, 3×10^5, 5×10^5 and 7×10^5) were suspended in fibroblast growth media and seeded onto 96-well scaffolds. These numbers were chosen as the 96-well scaffold was approximately one quarter the size of the 24-well scaffold. Cells were seeded in a final volume of 20 µL of per scaffold. To prevent the underside of the dermis from drying 150 µL of fibroblast growth media was added to the outside of the wells. After the 90-minute incubation 50 µL of fibroblast growth media was added to each well to fully submerge the scaffolds. The dermal equivalents were fed daily with fibroblast growth media supplemented with 100 µg/mL ascorbic acid and harvested after 10, 14 and 18 days of culture. Harvested equivalents were washed in PBS and submerged in 10% neutral buffered formalin for 24 hours. Dermal equivalents were processed, embedded, sectioned and structurally validated by haematoxylin and eosin (H&E) staining and Picro-Sirius red staining as described in section 2.11.3.

2.6.2.2 96-well Full-thickness Equivalent Optimisation

Different numbers of keratinocytes (1×10^5, 3×10^5, 5×10^5 and 7×10^5 cells) were seeded onto 96-well dermal equivalents to investigate how many cells were required to form an epidermis. Dermal equivalents were made with both 3×10^5 and 5×10^5 fibroblasts and incubated for 18 days. Keratinocytes resuspended in 20 µL of basal media were seeded onto the surface of each dermal equivalent. 150 µL of basal media was added to the outer well. After the 3 hours incubation an additional 50 µL of basal media was added to the outside of each well, fully submerging the equivalents. To raise HSEs to ALI culture the basal media was aspirated and adding 150 µL of ALI media added to the outer well. Equivalents were cultured at ALI for 14 days with media changed twice daily. On day 14 equivalents were harvested, washed once in PBS, and fixed in 10% neutral buffered formalin for 24 hours.

2.7 Bioprinting of Skin Cells to Fabricate Skin Equivalents

Before bioprinting skin equivalents variables such as the jetting parameters, the number of cells in suspension, and the deposition volume, required thorough optimisation to ensure that prepared scripts were robust and reproducible for model development. The methods described in following bioprinting subsections were developed and optimised within this thesis.

2.7.1 Bioprinter Apparatus

For this study, a Microfab Jetlab 4 XL (Microfab Technologies Inc.) printer, shown in Figure 2.5, was retrofitted to accommodate solenoid micro dispensing valves (INKX0514300AA, Lee Products Ltd) to create a high throughput bioprinting platform. The inkjet printhead of the Jetlab 4 printer was replaced with a microvalve printhead (Figure 2.6) that could accommodate four individual custom-built ink reservoirs each with an ink capacity of 2.5 mL. The outlets of the reservoirs were threaded to contain a male-male 062 MINSTAC threaded connector (Lee Products Ltd) one side of which was fixed into the reservoir (Figure 2.7). The other end of the male-male connector was used to attach the solenoid VHS series micro dispensing valve (Figure 2.7). The valve configuration used in this study had female 062 MINSTAC threaded inlets and outlets allowing the design of a modular printhead which could be used with various 062 MINSTAC threaded valves and nozzle types. 062 MINSTAC jewelled orifice nozzles (Lee Products Ltd) with orifice diameters of 190.5μm were used with the VHS series valves as they could be removed and sonicated to remove biological debris without causing any damage to the nozzle. To convert device waveforms to be compatible with the solenoid valves it was necessary for spike and hold electrical drivers (Lee Products Ltd) to be connected to both the Jetlab 4 device signal output channels and the signal connections of the individual valves. This allowed signals produced by the waveform printed circuit board (PCB) of the Jetlab to be converted to a 24V spike voltage to open a valve as quickly as possible and a 5V dwell voltage to keep the valve open for the duration of one actuation cycle.

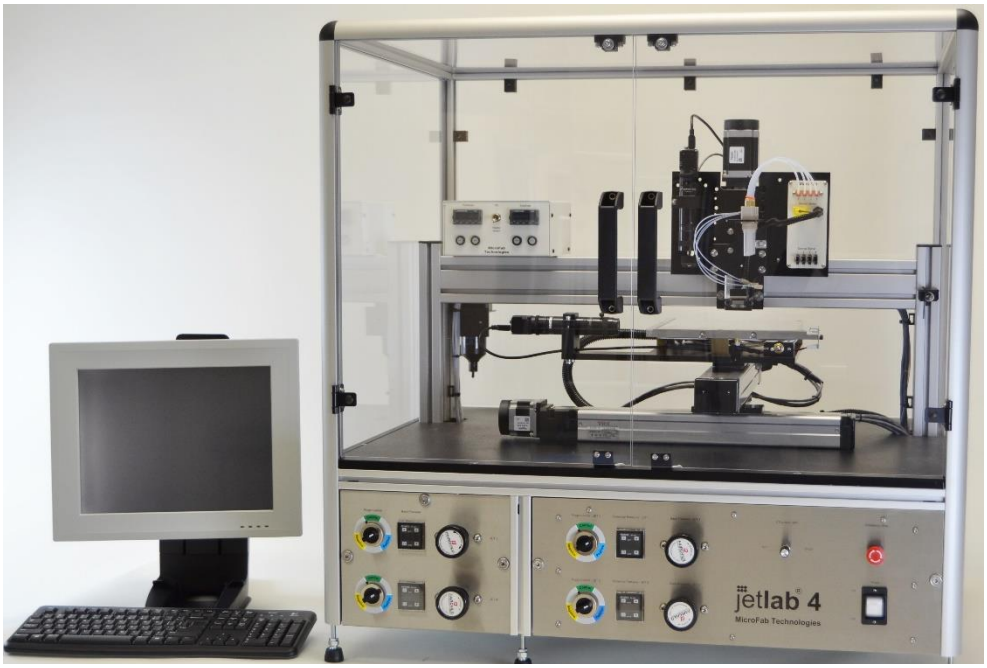

Figure 2.5. Unmodified Jetlab 4 XL. *Image from www.microfab.com.*

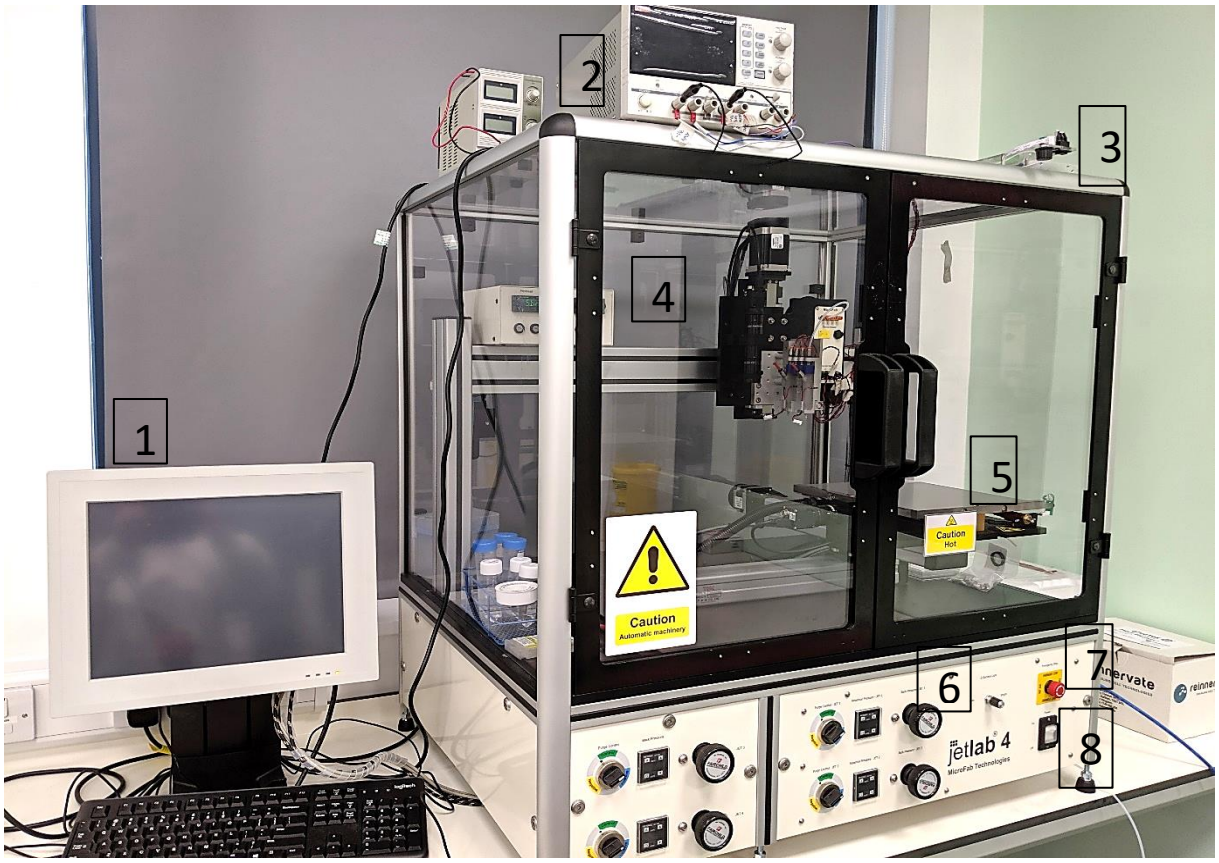

Figure 2.6. Modified Jetlab 4 Tabletop. (1). PC used to run Jetlab software. (2) DC power supply unit. (3) Potentiometer controlling agitation speed. (4) Z axis print head. (5) XY printing platform. (6) Pneumatic pressure controllers. (7) Emergency stop. (8) On/off switch.

To operate the bioprinter, jetting parameters and xyz coordinates were defined by user input via Jetlab software provided with the Jetlab 4 system. The two key variables which influenced volume dispensed per drop were dwell time (duration of dwell voltage, see Figure 1.7) and pneumatic back pressure. Dwell time was adjusted via the Jetlab software while the backpressure was manually adjusted by the pressure controllers located on the front of the Jetlab (Figure 2.5). To reduce cell sedimentation within the reservoir, an agitation system (designed by Dr Matthew Benning, Newcastle University) was used to agitate the cells within the reservior. A gold-plated magnet (First4magnets) was added directly into the reservoir with the bio-ink to agitate the cells. The magnet in the reservoir was rotated by rotating a metal shaft located perpendicular to the reservoir. The shaft was connected by a drive belt to a DC 24V motor (RS Components). The voltage supplied to the motor determined the agitation speed of the magnet within the reservoir. For printing of cells this motor was operated at 18 volts.

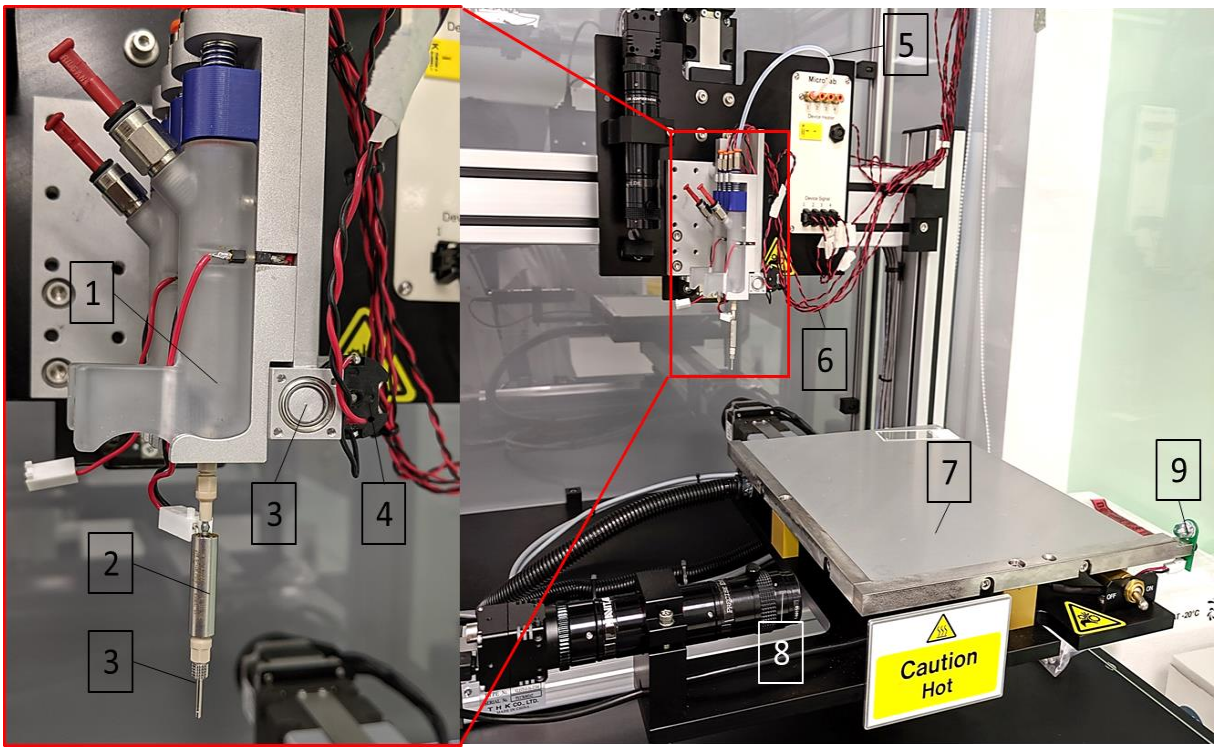

Figure 2.7. Components within the bioprinter cabinet. *(1) Ink reservoir. (2) Solenoid valve. (3) Removable nozzle. (3) Metal agitation rod. (4) 24V motor. (5) Backpressure tubing. (6) Valve actuation signal wiring. (7) XY printing platform. (8) Drop analysis camera. (9) Stroboscopic LED.*

2.7.2 Investigating the Influence of Dwell Time and Back Pressure on Droplet Volume

To select the printing parameters to bioprint human skin cells a study was conducted to investigate the range of volumes per droplet that could be dispensed by the bioprinter. This study involved investigating the relationship between valve dwell time and pneumatic back pressure on the volume of bio-ink dispensed. To quantify the volume dispensed, 200 droplets of fibroblasts growth media was dispensed into a 1.5 mL Eppendorf tube. The Eppendorf tubes were weighed with a microbalance before and after printing. Dwell times of 100-1000µs were investigated with measurements taken at increments of 50µs. These experimental limits were chosen as dwell times of less than 100µs did not produce droplets whereas dwell times larger than 1000µs resulted in the formation of droplet ligaments and satellite droplets which could affect printing accuracy. Backpressures of 50-500mmHg were investigated with measurements taken at increments of 50mmHg. Backpressures of less than 50mmHg did not consistently generate droplets and so were not investigated. The backpressure was limited to 500mmHg as backpressures greater than 500mmHg caused splashing on printing substrate which adversely affected printing accuracy. The volume per droplet (*d)* was calculated using Equation 1. Prints were conducted in triplicate to account for variability when measuring the volume of cell culture media dispensed.

$$d = \frac{(W2 - W1)x1000}{n}$$

Equation 1. Calculation for volume per droplet (µL). *d denotes the volume per droplet. W1 and W2 represent weight of collection tube in grams before and after printing, respectively. The number of droplets printed is represented by n.*

2.7.3 Bioprinting of Skin Cells

To investigate the relationship between the number of cells within the bio-ink and the number of cells dispensed, a range of cell numbers were loaded into reservoirs and printed into a 24-well plate over 1 hour. The cells printed in this experiment were primary dermal fibroblasts which were suspended into fibroblast growth media at 1 x 10^6 cells/mL, 10 x 10^6 cells/mL, 20 x 10^6 cells/mL, and 40 x 10^6 cells/mL. This experiment was carried out using biological triplicates to account for donor to donor variation in cell viability. Cells were loaded into the printer and 100 µL of the ink containing the cell suspension was printed at 0 minutes, 15 minutes, 30 minutes, 45

minutes, and 60 minutes. To print 100 µL of ink directly into a 24-well plate a circular monochromatic bitmap (BMP) scaled to a 24-well plate was created to dispense cells directly into the centre of each well (Figure 2.7). Each pixel was recognised by the software as a droplet and BMPs were printed into each well with user defined parameters. The BMPs were printed with a back pressure of 150mmHg, a droplet spacing of 0.15mm, a dwell time of 900µs and a fly rate of 35mm/s. 150mmHg was selected to reduce potential shear stress to cells during the printing process. The 900µs dwell time allowed a large volume per droplet while limiting the formation of satellite droplets. The fly rate was this speed at which the printhead moved across the x-axis. As the volume per droplet (*d*) at these parameters was previously calculated it was possible to calculate the total number of pixels/droplets in a bitmap (*P*) required to print a total volume (*Vt*) of 100 µL. The number of pixels required per BMP (*P*) was calculated using Equation 2. Prior to printing cells, the total volume dispensed (*Vt*) when printing BMPs was confirm by weighing media printed directly onto glass slides. Slides were weighed using a microbalance. Once printed the number of cells were manually counted and cell viability was recorded using a trypan blue exclusion assay (section 2.8).

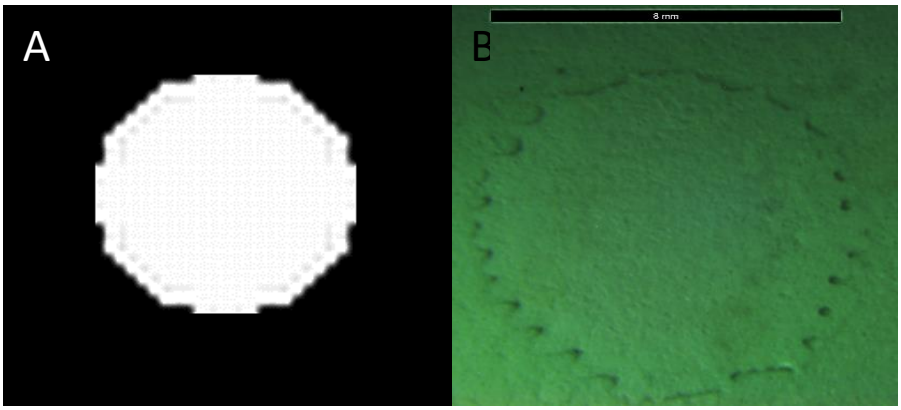

Figure 2.8.Well shaped monochromatic bitmap (bmp). *A) An example of a well-shaped bmp which is recognised by the Jetlab software as a printing pattern. B) A well-shaped bmp printed onto a glass slide and imaged with a Leica M205 C Stereo microscope. Scale bar: 8mm.*

$$P = \frac{Vt}{d}$$

Equation 2. Calculation for the number of pixels required per bitmap. *P represents to number of pixels within a bitmap. Vt represents the total volume to be dispensed. The volume per droplet is represented by d.*

2.7.4 Bioprinting of Full-Thickness 96-well based Skin Equivalents

To bioprint cells directly onto the prototype 96-well Alvetex® scaffold, printing scripts were adjusted to deposit a *Vt* of 20 µL per well. Due to the unique shape of the transwell insert a small but simple square array was scripted to replace the bitmaps used previously. The backpressure was 150mmHg and the dwell time was 900µs used. A backpressure of 150mmHg was used to minimise potential shear stress on cells during the printing process. The dwell time of 900µs was selected increase the volume per droplet without forming large droplet ligaments and satellite droplets. The number of droplets required within both x and y axis of the scripted array (*D*) were calculated using Equation 3. To ensure the printed array would fit into the transwell cradle, the spacing between droplets was reduced to 0.02mm. To confirm that 20 µL would be dispensed per well, media was dispensed onto glass slides using the above parameters and the weight of the dispensed media was measured using a microbalance. This was done in triplicate to account for variability in measurements. Before printing full-thickness skin equivalents the number of printed cells per well was confirmed by manually counting the dispensed cells, and cell viability was assessed by trypan blue exclusion assay (section 2.8). This was carried out using both primary dermal fibroblasts and keratinocytes in biological triplicates to account for donor to donor variation in cell viability. Dermal equivalents were bioprinted first by suspending fibroblasts at 25 x 10^6 cells/mL in fibroblast growth media and dispensing the cells onto scaffolds using the optimised parameters. Dermal equivalents were cultured for 18 days as detailed in section 2.6.2. After day 18 the dermal equivalents were washed with PBS in preparation for bioprinting of keratinocytes. Keratinocytes were suspended in basal media at 20 x 10^6 cells/mL and printed onto dermal equivalents. Equivalents were then cultured and harvested as outlined in section 2.6.2.

$$D = \sqrt{\frac{Vt}{d}}$$

Equation 3. Calculation for the number of droplets required in the X and Y axis of an array of droplet. *D represents the number of droplets in X and Y axis of array. Vt represents the total volume to be dispensed. The volume per droplet is represented by d.*

2.8 Trypan Blue Exclusion Assay

To distinguish between viable and non-viable cells in cell suspensions post printing trypan blue (Sigma-Aldrich) was used. This methodology was a modified protocol described by W Strober (Strober 2015). Trypan blue is negatively charged and so interacts with cells that have compromised membranes. Therefore, viable cells were not stained while cells with damaged membranes (non-viable cells) were stained blue. 30 µL of a cell suspension was mixed 1:1 with 30 µL of 0.2% trypan blue. The mixture was loaded into a Neubauer haemocytometer and both live and dead cells were counted using an upright Zeiss Jenamed 2 microscope (Carl Zeiss Ltd). The percentage of viable cells was calculated using Equation 4.

$$\%\ viable\ cells\ = (live\ count\ \div total\ count) \times 100$$

Equation 4. Equation used to calculate cell viability of trypan blue exclusion assay.

2.9 In-vitro Testing of Biologics with Bioprinted Skin Equivalents

In-vitro testing of biologics using skin equivalents was carried out with fully autologous skin equivalents in biological triplicates. Autologous skin equivalents were bioprinted as outlined in section 2.7.4. The matured skin equivalents were washed twice with PBS before co-culture with autologous PBMCs. Autologous media was used for the skin equivalent-PBMC co-culture which consisted of RPMI, 10% heat-inactivated autologous serum, 1% P/S solution and 1% l-glutamine solution. The autologous skin equivalents were co-cultured in 96- well plates with 1 x 10^6 PBMCs per well. Two biologics were tested alongside two negative controls. The first biologic, Natalizumab (pharmaceutical name Tysabri) is used in clinic to treat relapsing multiple sclerosis and has been shown to cause little immunotoxicity in human settings (Fletcher *et al*. 2018). The second biologic was a murine anti-human CD3 antibody, also known as OKT3 (marketed under muromonab), which was the first monoclonal antibody (mAb) to be approved for use in humans (Kuhn and Weiner 2016). Both mAbs were provided by Alcyomics Ltd and were tested at a final concentration of 1 µg/mL. The negative controls were autologous skin equivalents incubated with autologous media only (media control) and autologous skin equivalents incubated with PBMCs without mAbs (PBMC control). The co-cultures were incubated at 37^{o}C with 5% CO_2 for 3 days. After 3 days 100 µL of supernatant was aspirated to analyse proinflammatory cytokine release from each co-culture and stored at -20^{o}C until used.

2.10 Embedding and Sectioning of 96-well Skin equivalents

Due to the small size and unique design of the prototype inserts, the Alvetex® scaffold could not be easily removed from the transwell insert without heavily damaging the full-thickness skin equivalents. Therefore, rather than removing the scaffold which was heat welded to the insert, the insert was trimmed after processing and paraffin embedded with the Alvetex® still attached.

2.10.1 Manual Processing and Embedding of Skin Equivalents

Following fixation, skin equivalents were manually dehydrated to remove water present within the equivalent. This was necessary as the hydrophobic paraffin wax would not be able to permeate the tissue in the presence of water. To dehydrate the skin equivalents the tissues were immersed in a series of ethanol solutions increasing in concentration with a final immersion in 100% ethanol at room temperature (table 2.1). The increasing concentration of ethanol allowed the water present in the skin equivalents to gradually be replaced with ethanol. Histoclear II (National Diagnostics) was used to remove ethanol from the skin equivalents at room temperature followed by immersion in a solution containing an even mixture of histoclear II and molten paraffin wax (Thermo Fisher Scientific) at 60^{o}C. Skin equivalents were then incubated in 100% molten paraffin wax, allowing the wax to fully penetrate the skin equivalent. Once fully immersed in wax samples were embedded into paraffin blocks using a histostar embedding station (Thermo Scientific).

Table 2.1. 96-well skin equivalent processing procedure. *Skin equivalents were dehydrated with ethanol to gradually remove water. Ethanol was replaced with histoclear II which is miscible with paraffin wax.*

Reagent	Incubation time (minutes)	Incubation temperature (°C)
30% ethanol	10	18-26
50% ethanol	10	18-26
70% ethanol	10	18-26
80% ethanol	10	18-26
90% ethanol	10	18-26
95% ethanol	10	18-26
100% ethanol	20	18-26
100% Histoclear II	30	18-26
50:50 histoclear II: paraffin mixture	30	60
100% paraffin	30	60

2.10.2 Sectioning of Skin Equivalents

To section paraffin blocks, a HM 325 microtome (Thermo Fisher Scientific) with XM35 microtome blades (Thermo Scientific) was used to cut 4µm thick sections. Embedded biopsies and 24-well equivalents were cooled for several minutes using the cold plate of the embedding station before sectioning on the microtome. Sections were transferred to a paraffin section flotation bath (Cole-Parmer), mounted onto superfrost slides (Thermo Fisher Scientific) and baked in an oven overnight (dry-line, VWR). Blocks containing 96-well skin equivalents were cooled in a fridge for 10 minutes before sectioning (Figure 2.8). 96-well skin equivalent blocks required trimming to cut through the plastic cradle and section the skin equivalent.

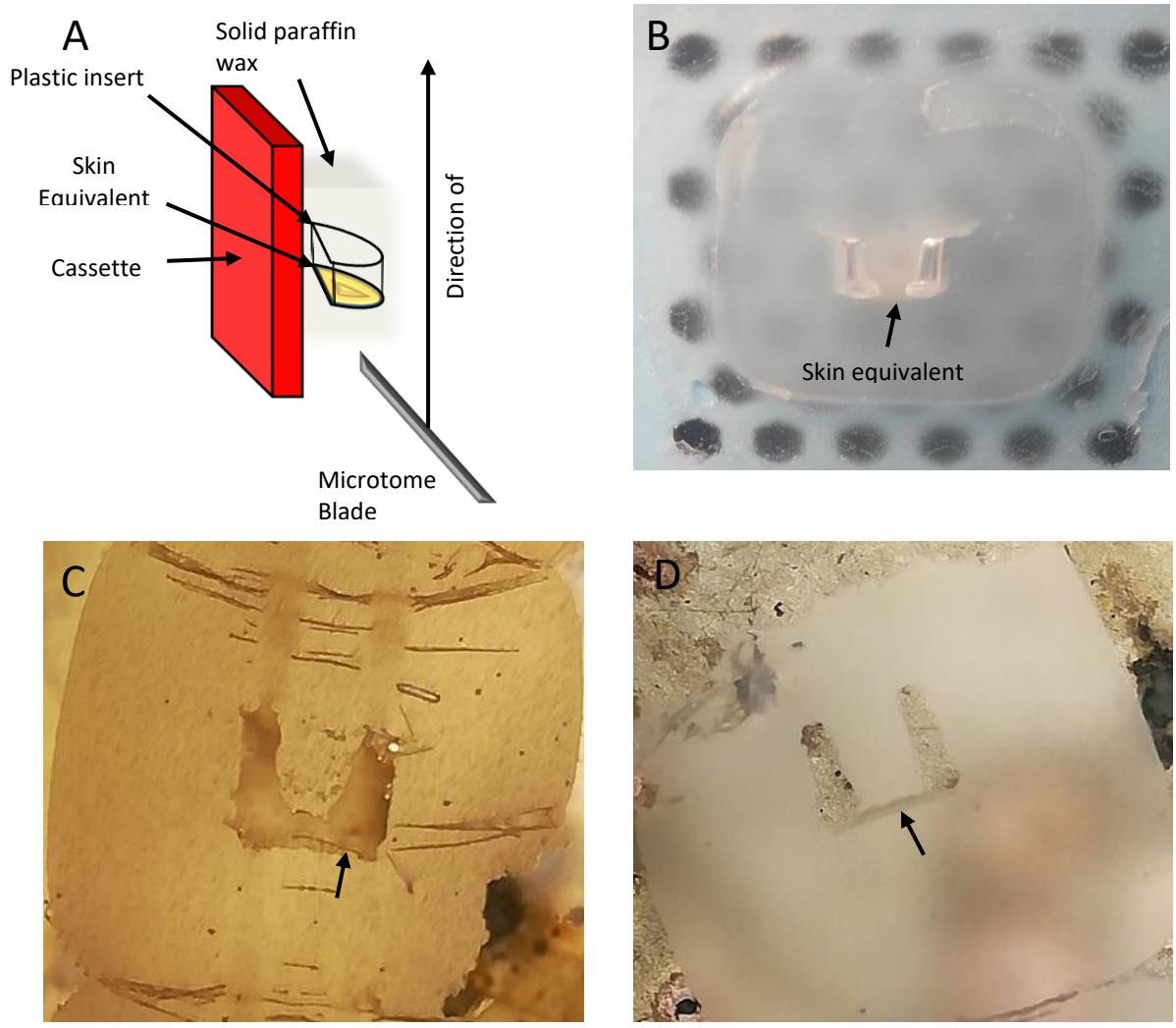

Figure 2.9. Embedding orientation and sectioning of 96-well skin equivalents. *A) Orientation of skin equivalents embedded in paraffin blocks. B) An embedded 96-well skin equivalent which was trimmed to cut through the cradle and reveal the skin equivalent. C) Floating section of a 96-well block cooled on a histostar cooling plate. The damaged skin equivalent is indicated by the black arrow. D) Section of a 96-well skin equivalent that was cooled in a fridge before cutting. Intact skin equivalent is indicated by the black arrow.*

2.11 Histological Techniques

To image skin equivalents a range of histological techniques were used to highlight the general structure of tissue or specific markers located within the dermis or epidermis.

2.11.1 Haematoxylin and Eosin Staining

Haematoxylin and eosin (H&E, Thermo Fisher Scientific) were used to stain the general structure of physiological human skin and skin equivalents using a protocol developed and optimised by Alcyomics. Haematoxylin stains the basophilic structures (nuclei) blue/purple while eosin stains acidophilic structures (cytoplasm) pink. 4µm sections were deparaffinised through two washes in xylene (Fisher Scientific) followed by rehydration through a decreasing gradient of alcohols (100%, 70% and 30% ethanol) ending with rehydration in tap water. Rehydrated sections were immersed with haematoxylin for 5 minutes then rinsed in tap water to remove excess dye. Slides were then placed in Scott's tap water for 30 seconds before being rinsed under running tap water. Scott's tap water was used as a blueing agent to improve the contrast between haematoxylin and eosin. Sections were then stained with eosin for 2 minutes and again rinsed in tap water. Stained sections were dehydrated through graded alcohols (30%, 70%, and 100% ethanol) cleared in two changes of xylene and mounted using DPX mountant (Sigma-Aldrich). Images were captured using an Axioimager microscope (Carl Zeiss Ltd).

2.11.2 Immunofluorescent Staining

Immunofluorescent (IF) staining was used to stain for specific dermal and epidermal components. A modified version of the IF procedure described by Hill *et al* was used (Hill et al. 2015). To optimise the IF staining procedure primary antibodies specific for human epitopes were titrated using the procedures described in this section. All primary antibodies were purchased from Abcam. Sections of human skin provided by healthy donors were used as positive controls to optimise the IF protocol and antibody concentrations. For staining of dermal components mouse anti-collagen III was titrated to detect dermal ECM. To detect the presence of the basement membrane mouse anti-collagen IV, mouse anti-collagen VII and rabbit anti-laminin-5 were also titrated. The optimised protocols were then used to validate the structure of the 3D skin equivalents by locating epidermal markers. The primary antibodies used for staining of epidermal markers were mouse anti-cytokeratin 14 1:250, rabbit anti-involucrin 1:400, rabbit anti-

cytokeratin 10 1:500, and rabbit anti-loricrin 1:125 all of which were purchased from Abcam. The secondary antibodies were goat anti-mouse Alexa Fluor-488 (AF-488) (Thermo Fisher Scientific) and goat anti-rabbit Alexa Fluor-647 (AF-647) (Thermo Fisher Scientific), both used at 1:200. Sections were baked and taken to water and then submerged in pH 6.0 citrate buffer for heat mediated antigen retrieval for up to 10 minutes. Antigen retrieval was necessary as methylene bridges which form during fixation with formalin, could have potentially masked target epitopes, preventing the primary antibody from binding to the target. After this step, the sections were washed with 5mM tris buffered saline (TBS) pH 7.6 for 5 minutes. 0.2% Triton-X was then used to permeabilise sections for 10 minutes at room temperature followed by a TBS wash. The sections were then blocked with 10% goat serum (Sigma-Aldrich) for up to one hour at room temperature to limit non-specific binding of the primary antibodies. The residual goat serum was removed by washing twice with TBS. The primary antibodies were applied to the sections for 1 hour at room temperature. For each primary antibody used a null primary slide was also prepared. The null primary slides were used as negative controls and were incubated with blocking solution rather than a primary antibody. The null primary slides were used to establish microscope parameters before imaging other sections. After 1-hour primary antibodies were removed and slides were washed in TBS. The fluorophore conjugated secondary antibodies were then applied to all slides including the null primaries for 2 hours at room temperature protected from light. Slides were washed again in TBS to remove the secondary antibody. Cell nuclei were counterstained with 5 µg/mL of Hoechst 33342 (Sigma-Aldrich) for 10 minutes protected from light at room temperature. Sections were again washed with TBS before dehydration through graded alcohols and were washed twice in xylene. Coverslips were mounted with DPX mountant. Fluorescent images were captured using an Axioimager microscope (Carl Zeiss Ltd) with Hoechst 33342, Alexa Fluor 488, and Alexa Fluor 647 filters.

2.11.3 Picro-Sirius Red Staining

A Picro-Sirius Red kit (Abcam) was used to detect the development of dermal ECM (collagen I and III) generated by dermal fibroblasts in the skin equivalents. Picro-Sirius Red stains collagen type I and type III red while staining cell cytoplasm and nuclei yellow. Staining was conducted as per manufacturer instructions. 4µm sections were washed twice in xylene and rehydrated through graded alcohols. Rehydrated sections

were covered with neat Picro-Sirius Red solution and incubated in a humidified chamber at room temperature for 1 hour. The sections were then rinsed twice in two quick changes of acetic acid (Abcam) and rinsed once in absolute ethanol (Sigma-Aldrich). Sections were then dehydrated through graded alcohols and mounted in DPX mountant (Sigma-Aldrich). The speed of the dehydration in 100% ethanol influenced the strength of the yellow cytoplasm and nuclei staining. Slides dehydrated quickly resulted in clear contrast between collagen and cell nuclei/cytoplasm, whereas slides that were overexposed to 100% alcohol had orange nuclei/cytoplasm. Images were captured using an Axioimager microscope (Carl Zeiss Ltd) with unpolarised light.

2.11.4 Periodic Acid-Schiff Staining

Periodic Acid-Schiff (PAS) stains tissues rich in polysaccharides such as glycogen (Tabatabaei Shafiei *et al.* 2014). PAS (Sigma-Aldrich) was used to detect mucopolysaccharides, specifically glycoproteins present within the basement membrane, which is located at the dermal-epidermal junction in healthy human skin. Staining was conducted as per manufacturer instructions. Deparaffinised sections were rehydrated and immersed in periodic acid solution for 5 minutes. Periodic acid solution oxidises glycols in tissue to aldehydes. Excess periodic acidic solution was removed by rinsing slides in several changes of distilled water. Slides were then immersed in Schiff's reagent for 15 minutes. Schiff's reagent reacts with aldehydes to form a magenta stain. Slides were washed under running water for 5 minutes followed by counter staining of nuclei with haematoxylin. Excess haematoxylin was removed by rinsing slides in tap water and then slides were dehydrated and mounted in DPX mounting resin. Images were captured using an Axioimager microscope (Carl Zeiss Ltd).

2.12 Multiplex Proinflammatory Cytokine Detection Assay

To quantify cytokine secretion in supernatants of autologous skin equivalent-PBMC co-cultures, a multiplex human proinflammatory cytokine panel kit (Meso Scale Diagnostics (MSD) was used as per manufacturer instructions. The assay uses an MSD MULTI-SPOT® 96-well plate with each well containing 10 separate electrodes covered with immobilised capture antibodies for specific cytokines (Figure 2.9). As per supplier instructions the MULTI-SPOT® plate was washed thrice with a wash buffer (PBS + Tween-20). Samples and calibration controls were added to respective wells and incubated on a plate shaker (Cole-Parmer) for 2 hours to allow cytokines to bind with immobilised antibodies. Plates were washed thrice again with wash buffer and

detection antibodies (with the exception of IL-8) were added to each well. Plates were incubated for a further 2 hours. Excess detection antibodies were removed by washing the plates thrice with wash buffer. Wells were topped up with a read buffer (MSD) and the plates were analysed using a QuickPlex multiplex plate reader (MSD). The plate reader applies a voltage to each electrode which, when combined with the read buffer results in electrochemiluminescence. The instrument used the intensity of transmitted light to calculate a quantitative measure of each cytokine. Supernatants were analysed in biological triplicates.

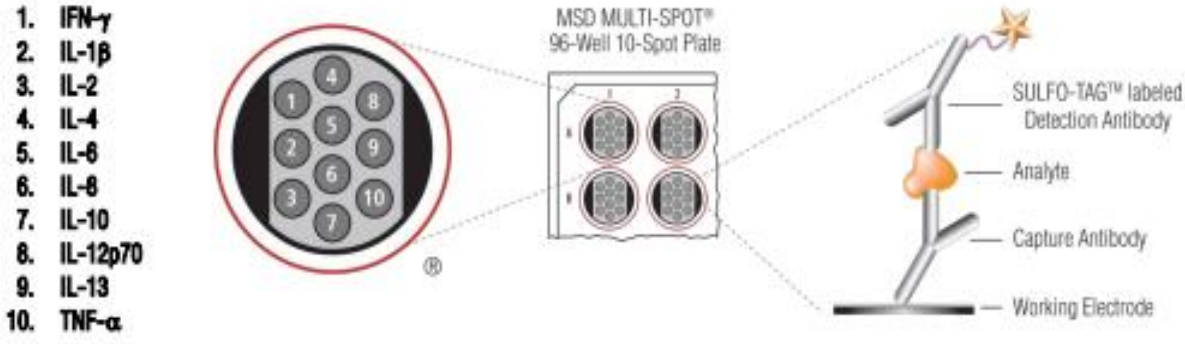

Figure 2.10. MSD MULTI-SPOT® electrode arrangement. *Each electrode surface contains immobilised capture antibodies for specific cytokines. The cytokines bind to the capture antibodies and in turn bind detection antibodies which are conjugated to electroluminescent SULFO-TAG™ labels.*

2.13 Statistical Analysis

Statistical analysis was carried out using GraphPad Prism version 8. Analysis of the quantified cytokine levels were conducted in biological triplicate (N=3) using repeated measures one-way ANOVA with Bonferroni correction. P values of <0.05 were considered statistically significant.

Chapter 3 Optimisation of a Handmade 24-well Skin Equivalent

3.1 Introduction

In this chapter the 24-well based full-thickness Skimune3D® human skin equivalent (HSE) was optimised using primary human skin cells and compared to human skin. The Skimune3D® HSE was originally developed in a 6-well format by Hill *et al* and adapted for use with 24-well transwell inserts by Alcyomics (Hill *et al*. 2015). The format of the Skimune3D® HSE was reduced further to decrease the number of cells required per HSE and to increase the number of HSEs that could be developed per donor. This chapter explores the reproducibility of the established 24-well HSE. The 24-well HSEs were then optimised by investigating the impact of fibroblast numbers to improve the development of both the dermal and the epidermal layers. The structure of the optimised HSEs were stained using basic histological and immunohistological techniques to visualise dermal extra-cellular matrix (ECM) and epidermal differentiation markers. Finally, the HSEs were compared to human skin biopsies to determine if Skimune3D® was physiologically representative of human skin.

3.2 Aims

1. Reproduce and optimise the 24-well Skimune3D® HSE using primary cells isolated from human skin.
2. Analyse the structure of the handmade HSEs to detect dermal and epidermal markers.
3. Compare the physiology of the HSEs to that of physiological human skin.

3.3 Results

3.3.1 Skin equivalents made with the 24-well Skimune3D® protocol

As initially established by protocol provided by Alcyomics, the 24-well based HSEs were first produced with a 1:1 ratio of fibroblasts and keratinocytes. Haematoxylin and eosin (H&E) staining provided an insight into the extent of HSE development and variation from donor to donor. The HSEs were made with the established protocol using $1x10^6$ fibroblasts and $1x10^6$ keratinocytes from several donors (n=6). The resulting HSEs developed did not form successfully with a similar issue occurring in each HSE to various degrees.

It was observed in some donors that the dermal compartment had completely failed to form and was sparsely populated with fibroblasts (Figure 3.1). Donor 1 produced a layer of fibroblasts which lined the underside of the Alvetex® scaffold, however no

fibroblast layer was observed at the top of the scaffold. The poorly formed dermis formed by donor 1 resulted in the infiltration of keratinocytes into the Alvetex® scaffold and therefore no epidermal layer was observed. Donor 2 also failed to form a dermis with no fibroblast layer visible above or beneath the scaffold and subsequently no epidermal layer. Few fibroblasts were seen within the scaffold which mostly appeared to contain differentiating keratinocytes. Additionally, donor 3 did not form a complete dermis, or an epidermis and few fibroblasts were visible in the scaffold. Once again, the scaffold was populated with differentiating keratinocytes. Donor to donor variation resulted in some HSE's which had partially formed (Figure 3.2). Both donors 4 and 5 partially developed a dermis and an epidermis. However, the incomplete dermis resulted in some fall through of keratinocytes into the scaffolds. No basal strata could be seen in donors 4 and 5 although spinous and granular strata were visible. Donor 6 also partially formed a dermis however epidermal development was poor, only a partial corneal envelope was present. Overall, the data showed that the use of one million fibroblasts largely resulted in complete or partial failure of the fibroblasts to form a dermis. This was possibly due to a lack of dermal ECM.

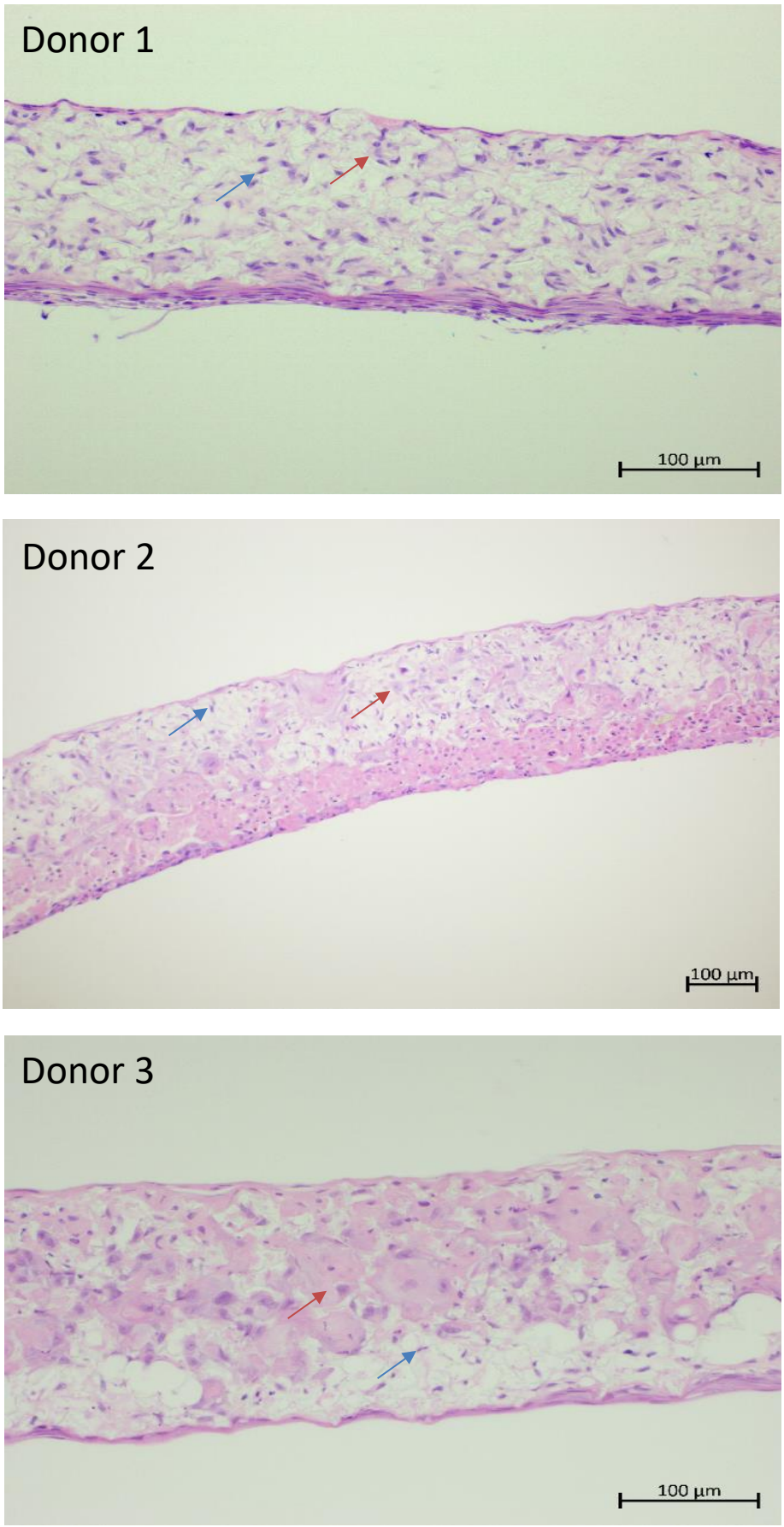

Figure 3.1 H&E staining of HSEs produced with the original protocol using cells from donor 1-3. *Blue arrows show fibroblasts within the Alvetex® while red arrows show the keratinocytes which are infiltrating dermal equivalent.*

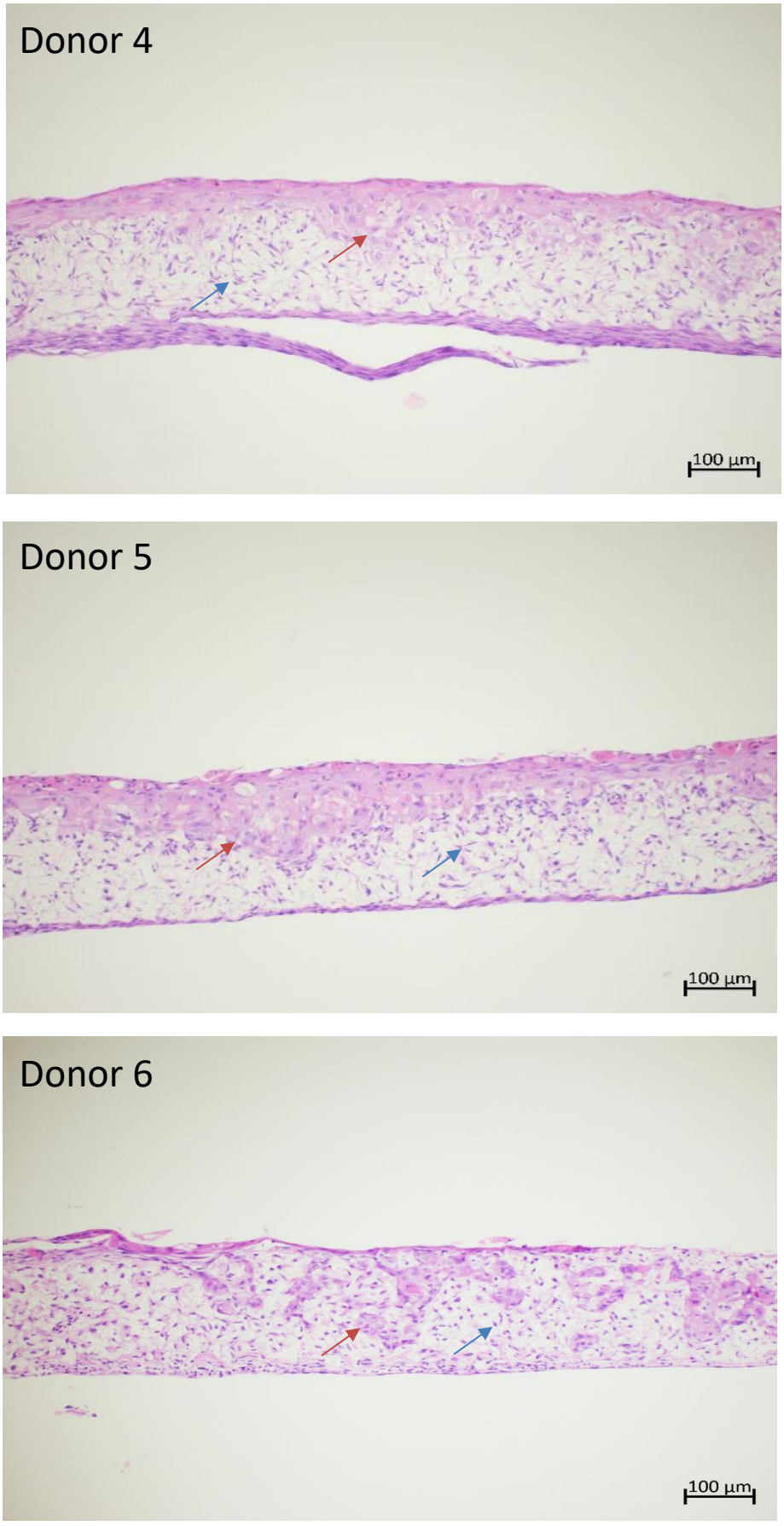

Figure 3.2 H&E staining of HSEs produced with the original protocol using cells from donor 4-6. *Blue arrows show fibroblasts within the Alvetex® while red arrows show the keratinocytes which are infiltrating dermal equivalent.*

3.3.2 Optimisation of dermal development

It was hypothesised that an increase in the number of dermal fibroblasts would increase the amount of ECM produced and improve the formation of the dermal equivalent. The numbers of fibroblasts seeded per model were investigated using $0.5x10^6$, $1x10^6$, $1.5x10^6$ and $2x10^6$ fibroblasts. The dermal equivalents were developed for up to 28 days. $1x10^6$ keratinocytes were added on to the dermal equivalents to allow epidermal formation and cultured as per the previous protocol. Three independent experiments were performed.

To observe the overall structure of the HSEs, sections of 3 additional donors (7, 8 and 9) were stained with H&E. Figure 3.3A shows the H&E staining of the full thickness model for donor 7, which contained $0.5x10^6$ fibroblasts and $1x10^6$ keratinocytes. This model showed similar issues to the initial protocol, where the dermal development was poor, and some keratinocyte infiltration was apparent. As expected, a similar issue was observed with the full thickness model which contained $1x10^6$ fibroblasts and $1x10^6$ keratinocytes (Figure 3.3B). The full thickness model which contained $1.5x10^6$ fibroblasts and $1x10^6$ keratinocytes shown in Figure 3.3C showed a noticeable improvement in the formation of a dermis, however some infiltration of keratinocytes was noticeable. Due to the improved dermis development in this model, an improved, more organised, and thicker epidermis was visible. This resulted in a more defined dermal-epidermal junction. The epidermis showed spinous, granular and cornified strata. While there were undifferentiated keratinocytes at the bottom of the epidermis, the columnar organisation of typical basal keratinocytes was not visible. The full thickness model which contained $2x10^6$ fibroblasts and $1x10^6$ keratinocytes (Figure 3.3D) showed a complete dermis with no visible keratinocyte infiltration into the dermal compartment. The fibroblasts adequately covered the surface of the scaffold and produced sufficient ECM to the support keratinocytes allowing improved epidermal formation. As a result, a more densely populated epidermal layer was observed which was more clearly defined. More undifferentiated keratinocytes were visible resulting in a slightly better formation of the basal strata indicated immediately above the black dashed line. The epidermis of this model also featured a thicker spinous layer with the presence of granular keratinocytes and a thin cornified envelope.

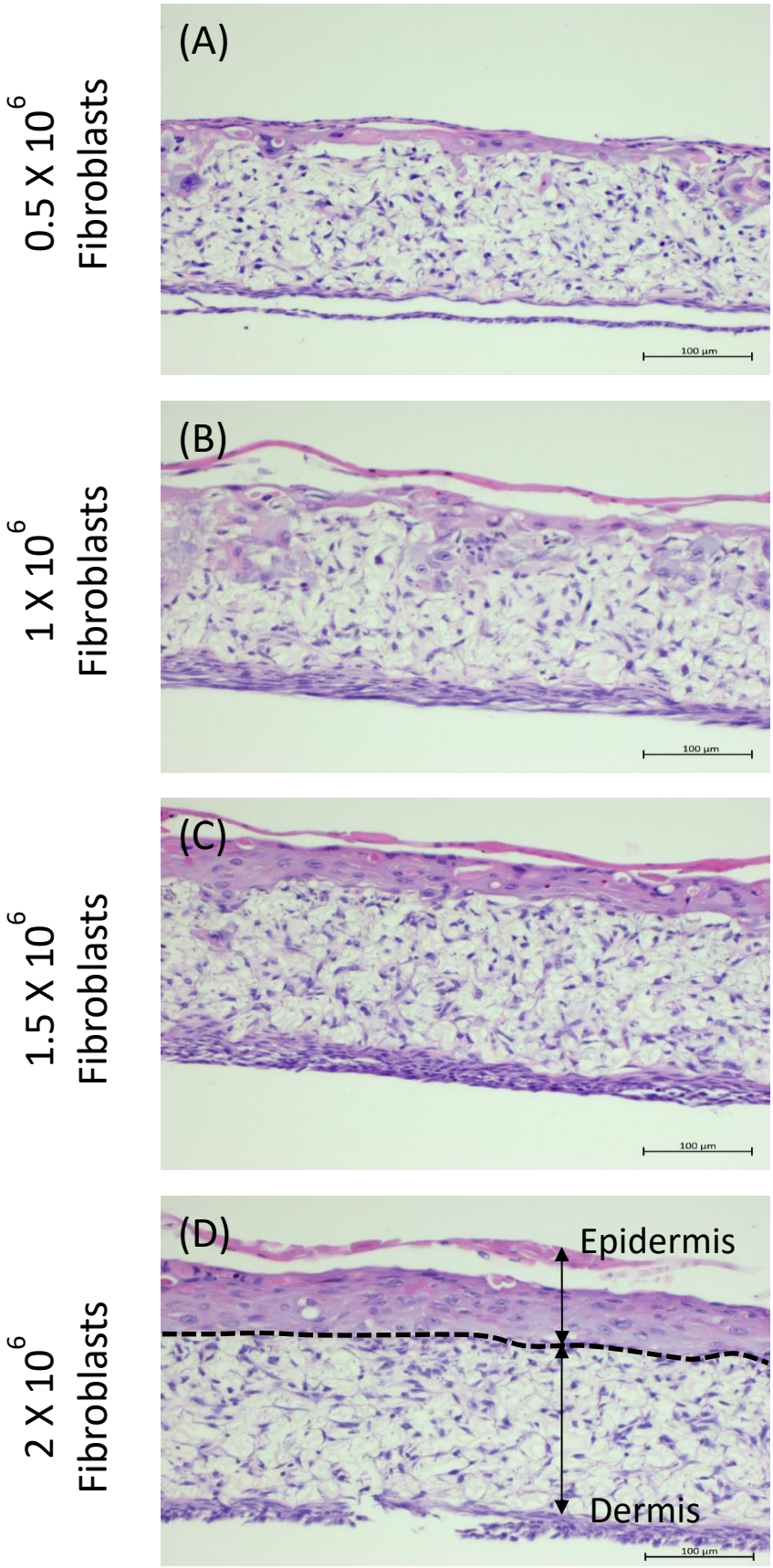

Figure 3.3 H&E staining of HSEs made with cells from donor 7. (A) *HSE made with 0.5x10^6 fibroblasts and 1x10^6 keratinocytes. (B) HSE made with 1x10^6 and 1x10^6 keratinocytes. (C) HSE made with 1.5x10^6 fibroblasts and 1x10^6 keratinocytes. (D) HSE made with 2x10^6 fibroblasts and 1x10^6 keratinocytes. Black dashed line indicates dermal-epidermal junction.*

Figure 3.4 shows the H&E staining of the full thickness model for donor 8. Results were comparable to those observed for donor 7. Figure 3.4A shows the model containing $0.5x10^6$ fibroblasts and $1x10^6$ keratinocytes. Poor formation of the dermal layer with a large amount of keratinocyte infiltration as observed for donor 7. The HSE containing $1x10^6$ fibroblasts and $1x10^6$ keratinocytes (Figure 3.4B) showed a similar result to that observed in Figure 3.4A, with slightly less keratinocyte infiltration into the dermal layer as shown in the initial experiments. The HSE which contained $1.5x\ 10^6$ fibroblasts and $1x10^6$ keratinocytes (Figure 3.4C) showed no visible keratinocyte infiltration and much-improved development of the dermal compartment. There was also improved development of the epidermal layer showing a well organised epidermis, with a nicely defined dermal-epidermal junction. The epidermis contained a well-developed spinous stratum with the early formation of a granular strata visible. In comparison to donor 7, donor 8 appeared to form an overall better HSE. The full thickness HSE which contained $2x10^6$ fibroblasts and $1x10^6$ keratinocytes produced a well-developed HSE as shown in Figure 3.4D. This HSE showed no visible keratinocyte infiltration into the dermal compartment. The fibroblasts adequately covered the surface of the scaffold and produced enough ECM to support the keratinocytes resulting in a clear dermal-epidermal junction, allowing epidermal formation. Notably, the increase in fibroblasts in the dermis from $1.5x10^6$ cells to $2x10^6$ cells appeared to result in a thicker epidermis, this was also observed in donor 7. A good columnar organisation of basal keratinocytes provided a self-renewing population of keratinocytes within the epidermis. As a result, a more densely populated epidermal layer was observed which was more clearly defined. More undifferentiated keratinocytes were visible resulting slightly better formation of the basal strata visible immediately above the black dashed line. The epidermis of this HSE also featured a thicker spinous layer with the presence of granular keratinocytes and a thin cornified envelope.

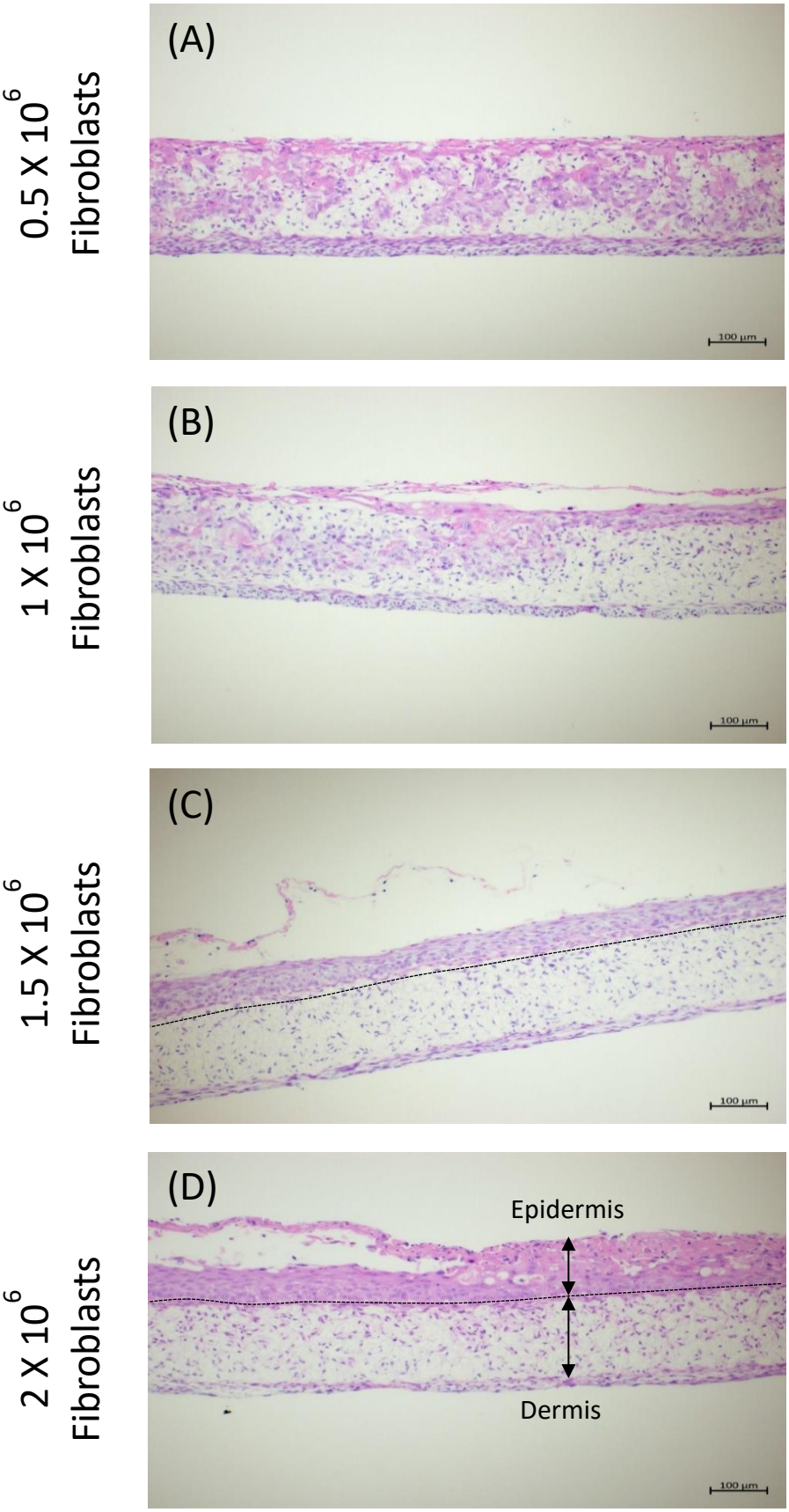

Figure 3.4 H&E staining of HSEs made with cells from donor 8. (A) *HSE made with 0.5x10^6 fibroblasts and 1x10^6 keratinocytes. (B) HSE made with 1x10^6 and 1x10^6 keratinocytes. (C) HSE made with 1.5x10^6 fibroblasts and 1x10^6 keratinocytes. (D) HSE made with 2x10^6 fibroblasts and 1x10^6 keratinocytes. Black dashed lines indicate dermal-epidermal junction.*

The full-thickness HSEs made with cells from donor 9 are shown in Figure 3.5. The HSE made with $0.5x10^6$ fibroblasts and $1x10^6$ keratinocytes showed a low number of fibroblasts within the scaffold (Figure 3.5A). As a result, no fibroblasts-ECM layer was visible at the top of the scaffold, which caused keratinocytes to infiltrate the dermis. Figure 3.5B shows the HSE developed with 1 $x10^6$ fibroblasts and $1x10^6$ keratinocytes. The dermis partially formed with an inconsistent fibroblast-ECM layer supporting some keratinocytes, large pockets of the dermis displayed keratinocyte infiltration. Interestingly those keratinocytes that did not infiltrate the dermis appeared to partially form the basal strata featuring columnar keratinocytes. The use of $1.5x10^6$ fibroblasts and $1x10^6$ keratinocytes (Figure 3.5C) showed partial dermal formation with some keratinocytes infiltrating the dermis and some epidermal formation. The full thickness HSE shown in Figure 3.5D contained $2x10^6$ fibroblasts and $1x10^6$ keratinocytes. This HSE formed a fully developed dermis featuring a fibroblast-ECM layer lining the dermal-epidermal junction with no keratinocyte infiltration of the dermis. This allowed the dermis to support the keratinocytes facilitating epidermal formation. Clear columnar organisation of basal keratinocytes suggested good formation of a basal strata. Some stratification could be observed with a spinous layer of differentiating and flattening keratinocytes directly above the undifferentiated stratum basale. Partial formation of the stratum granulosum could be observed with some granulated cells above the spinous strata. There was no cornified envelope visible.

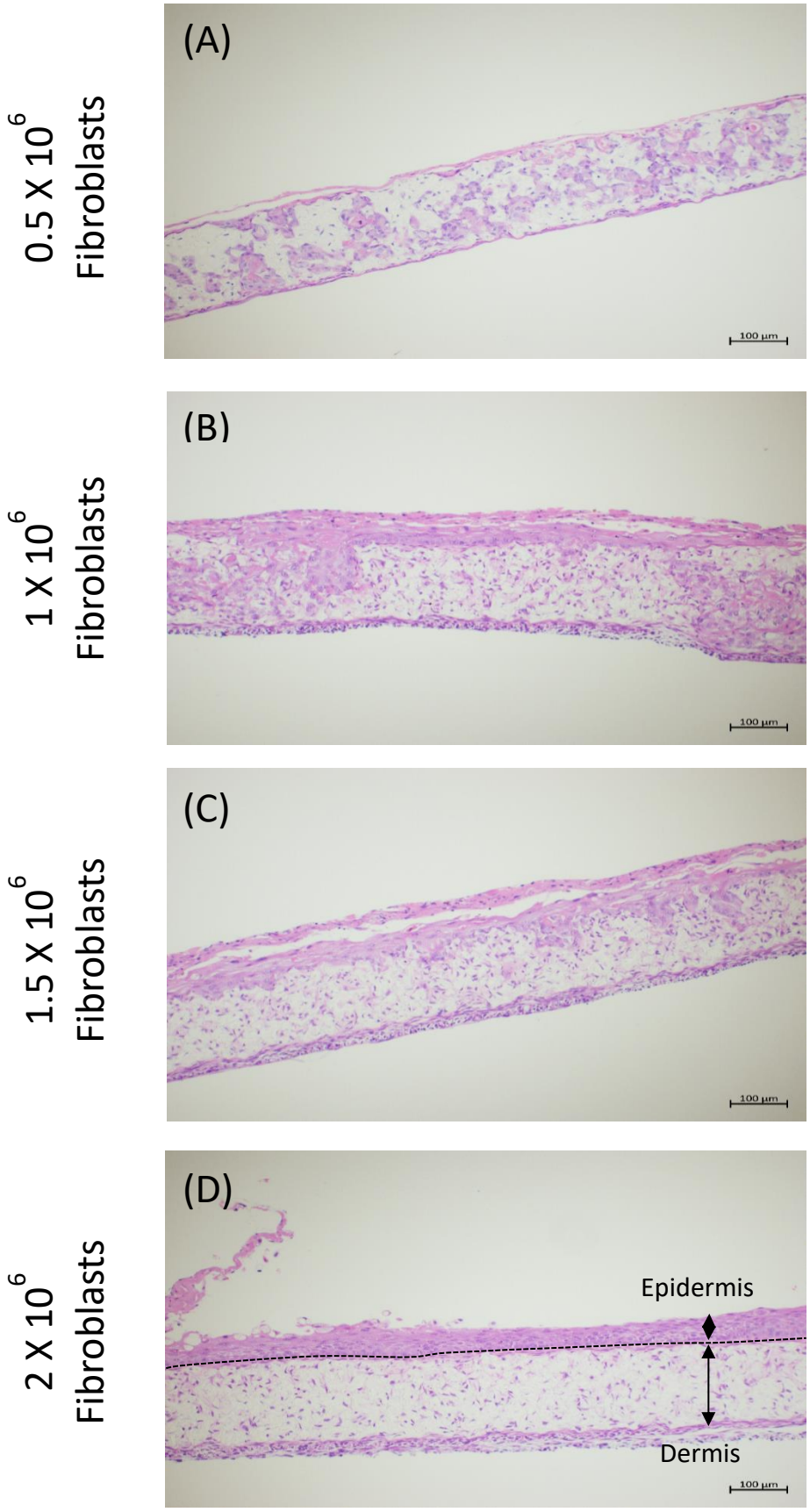

Figure 3.5 H&E staining of HSEs made with cells from donor 9. (A) *HSE made with 0.5x10^6 fibroblasts and 1x10^6 keratinocytes. (B) HSE made with 1x10^6 and 1x10^6 keratinocytes. (C) HSE made with 1.5x10^6 fibroblasts and 1x10^6 keratinocytes. (D) HSE made with 2x10^6 fibroblasts and 1x10^6 keratinocytes. Black dashed line indicates dermal-epidermal junction.*

To visualise dermal extracellular matrix, HSEs were stained with Picro-Sirius Red, which is a specific stain for collagen (Figure 3.6). Sirius red stains collagen red while staining cell nuclei and cytoplasm yellow. The stain allowed qualitative insight into the extent of ECM being produced by the dermal fibroblasts. The production of ECM is critical to the formation of a complete dermal equivalent. Inadequate production of ECM resulted in a porous dermal substrate preventing keratinocytes forming a complete monolayer on top of the dermis. Therefore, poor ECM production could directly affect epidermal formation. The staining showed poor ECM production and dermal formation in Figure 3.6A ($0.5x10^6$ fibroblasts) and 3.6B ($1x10^6$ fibroblasts). By increasing the number of fibroblasts to $1.5x10^6$ there was a visible improvement in ECM production and dermal development (Figure 3.6C). HSE's made with $1.5x10^6$ fibroblasts showed improved formation of a collagen mesh (black arrow) at the top of the Alvetex® scaffold. This allowed partial epidermal development, however, $1.5x10^6$ fibroblasts still resulted in a patchy dermal equivalent with a lack of collagen in some regions resulting in infiltration of keratinocytes into the dermal compartment. Figure 3.6D shows that a further increase of fibroblasts to $2x10^6$ resulted in a complete collagen mesh formation at the dermal epidermal junction indicated by the red staining (black arrow). This provided the keratinocytes with a solid foundation to form an epidermis without cells falling into the dermal equivalent. The yellow staining above the dermis represents staining of epidermal keratinocytes which have not fallen into the dermal equivalent resulting in the full thickness HSE. Overall, 100% of HSEs developed with $2x10^6$ fibroblasts produced full bilayer constructs.

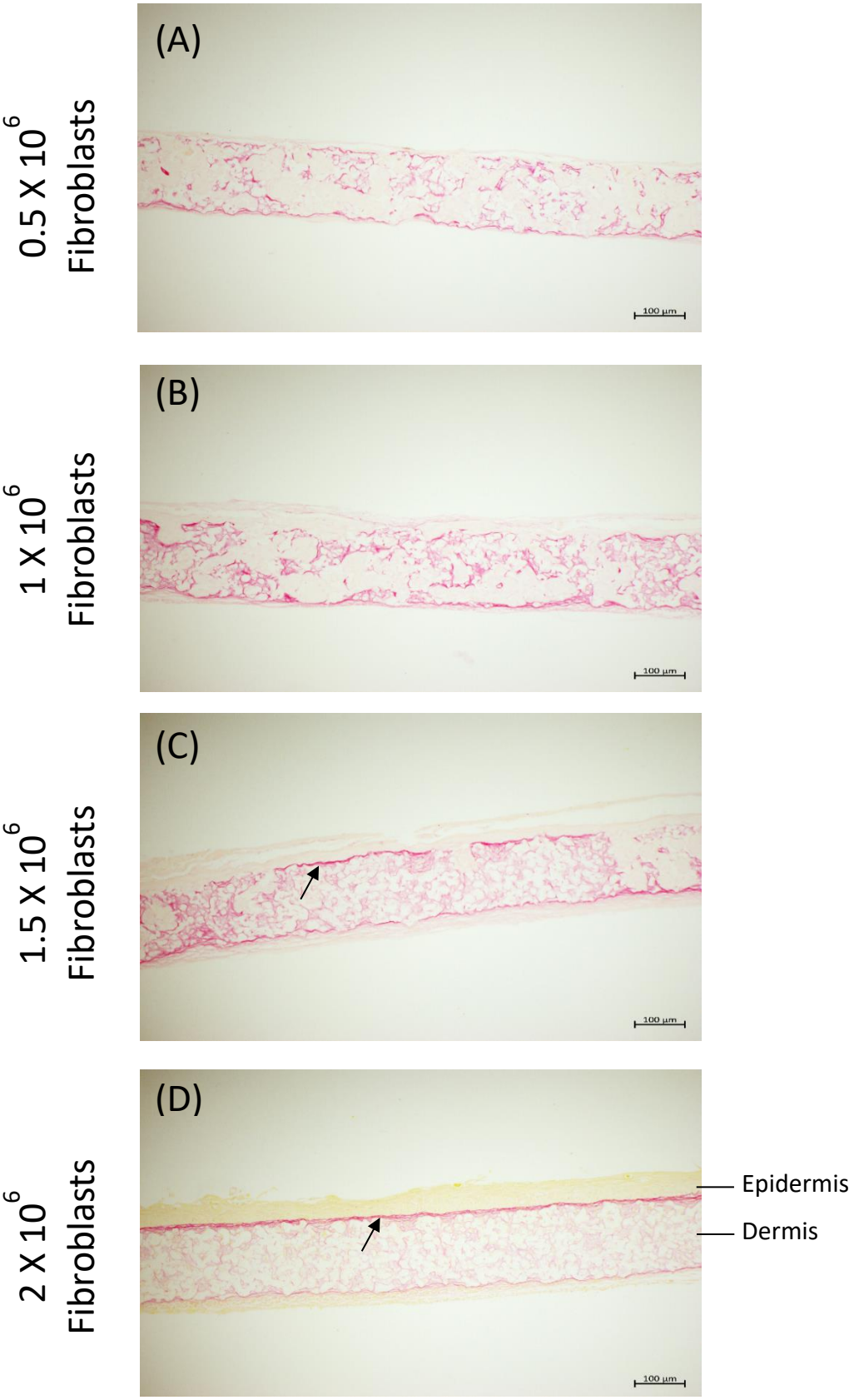

Figure 3.6 Picro-Sirius Red staining of HSEs made with a range of keratinocytes. *A) HSE made with 0.5x10^6 fibroblasts and 1x10^6 keratinocytes. (B) HSE made with 1x10^6 and 1x10^6 keratinocytes. (C) HSE made with 1.5x10^6 fibroblasts and 1x10^6 keratinocytes. (D) HSE made with 2x10^6 fibroblasts and 1x10^6 keratinocytes. Cell cytoplasm and nuclei were stained yellow while collagen was stained red. Black arrow indicates fibroblast-ECM mesh*

3.3.3 Comparison of histological techniques

The titration of antibodies specific for human cytokeratin 10 and human loricrin using sections of physiological human skin are shown in Figure 3.7 and Figure 3.8, respectively. Titration of rabbit anti-human cytokeratin 10 showed that the primary antibody was highly specific for human epidermal cytokeratin 10 as staining was highly localised at the spinous and granular strata of the epidermis. Titration of the rabbit anti-human loricrin antibody showed specificity for the stratum corneum of the epidermis in physiological human skin. Whilst use of the primary antibody at a 1:125 dilution yielded limited expression due to peeling of the stratum corneum during sectioning, loricrin could be identified in the epidermis of other concentrations.

Staining of dermal collagen type III in physiological human skin using a mouse anti-human is shown in Figure3.9. At a concentration of 1:250 some staining could be observed in the dermis of the human skin however the staining was limited. Staining was also observed in the epidermis of the skin which was not expected. When the concentration of the primary antibody was increases to 1:125 the extent of staining in both the dermis and epidermis increased.

Immunofluorescent staining for the basement membrane at the dermal-epidermal junction of human skin in by staining for collagen IV, collagen VII and laminin-5 are shown in Figure 3.10, Figure 3.11, and Figure 3.12, respectively. As concentration of the mouse anti-human collagen IV antibody increased so did the expression within the dermal region of the human skin (Figure 3.10). However, despite this increasing expression specific staining of the basement membrane at the dermal-epidermal junction was not detected in human skin. A similar trend was seen when staining for dermal collagen VII in human skin where an increase in concentration resulted in increasing staining in the dermis yet there was no specific staining of the basement membrane structure. (Figure 3.11). Laminin-5 staining was conducted with a wide range of concentrations most of which did not produce any staining (Figure 3.12). Staining at a high concentration of 1:25 produced expression in the dermis. This expression was mostly located in the upper dermis but was not specific for the basement membrane at the dermal-epidermal junction.

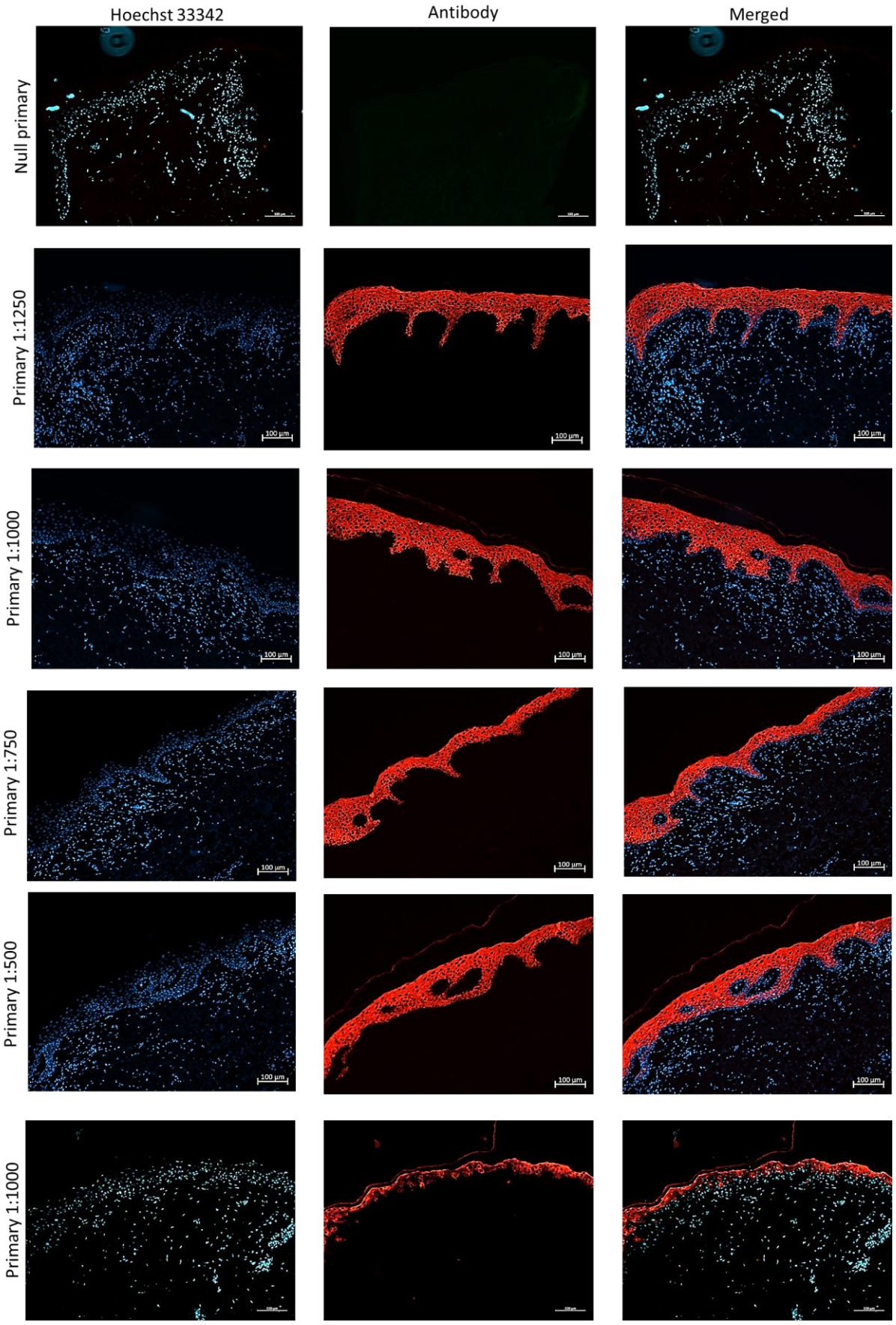

Figure 3.7 Titration of rabbit anti-human cytokeratin-10 antibody using physiological human skin. Cytokeratin-10 is shown in red. Hoechst nuclear staining is blue. Scale bar:100µm.

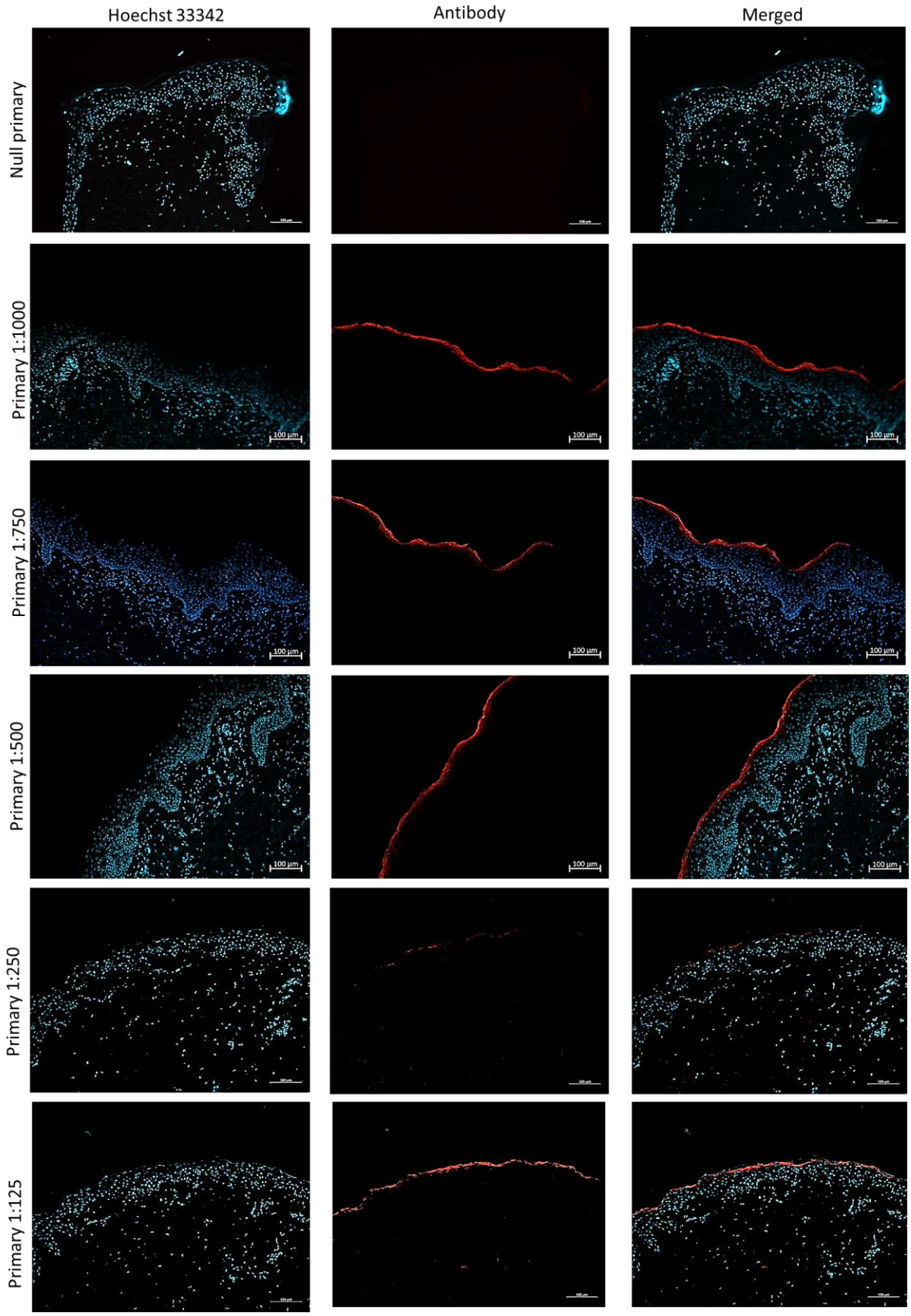

Figure 3.8. Titration of rabbit anti-human loricrin antibody in physiological human skin. Loricrin is shown in red. Hoechst nuclear staining is blue. Scale bars:100µm.

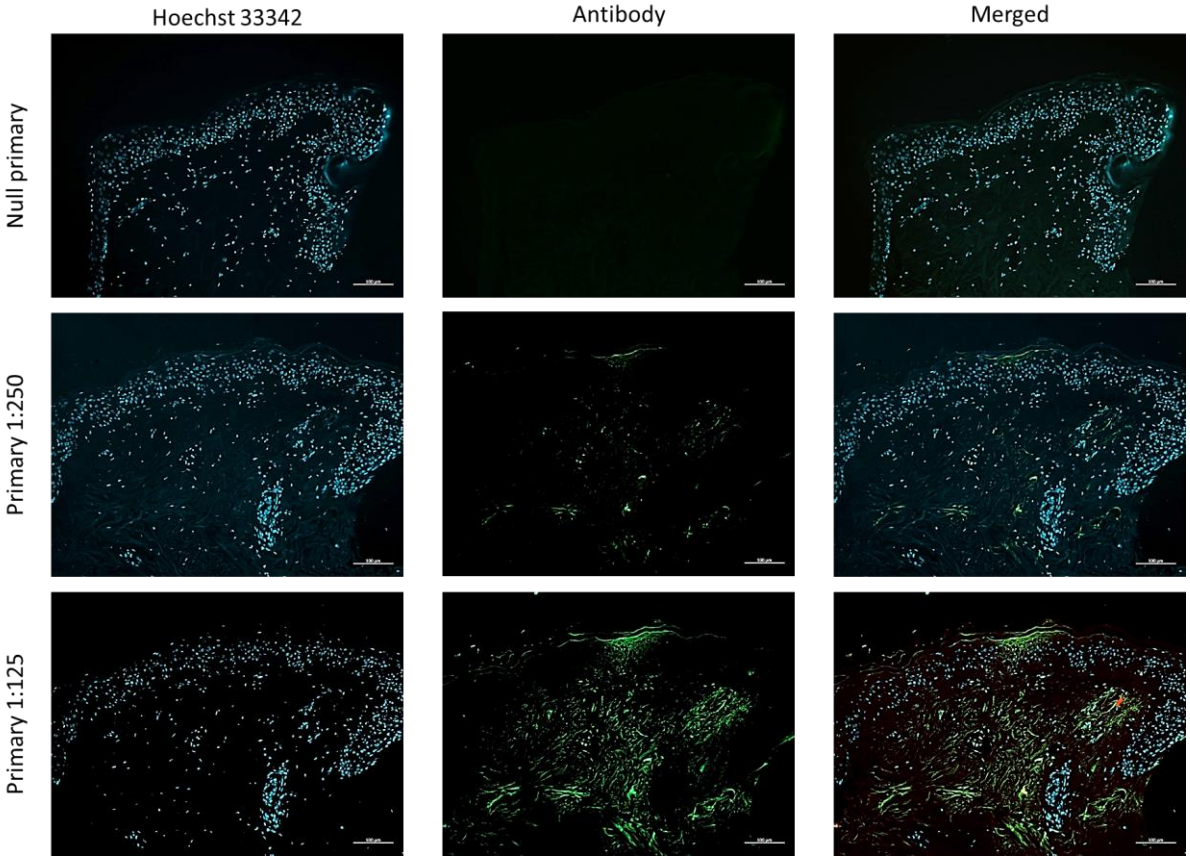

Figure 3.9. Immunofluorescent staining for collagen III using physiological human skin. Collagen III is shown in green. Hoechst nuclear staining is blue. Scale bars:100µm.

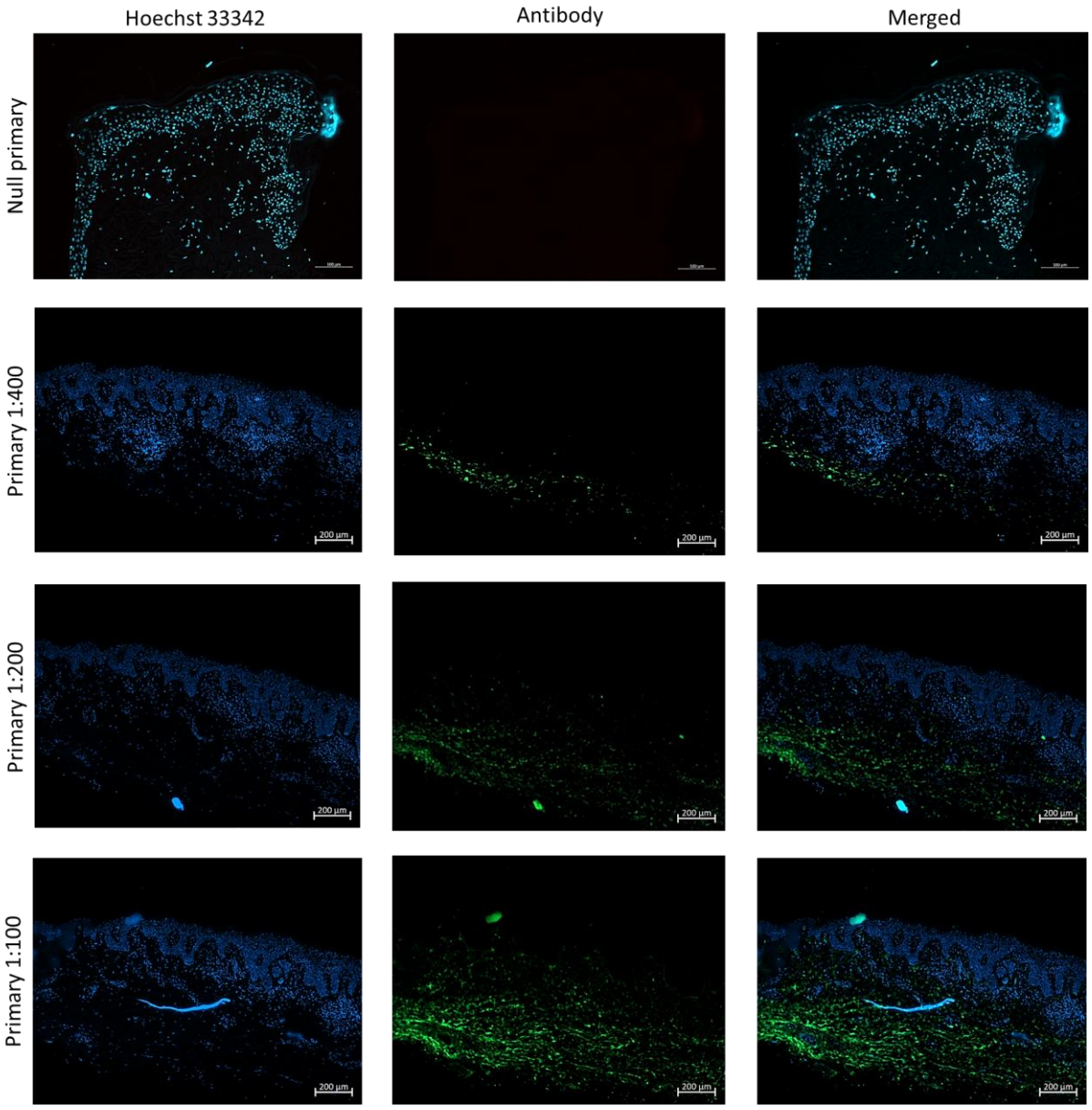

Figure 3.10 Immunofluorescent staining of basement membrane collagen IV in physiological human skin. Collagen IV is shown in green. Hoechst nuclear staining is blue. Scale bars:100µm.

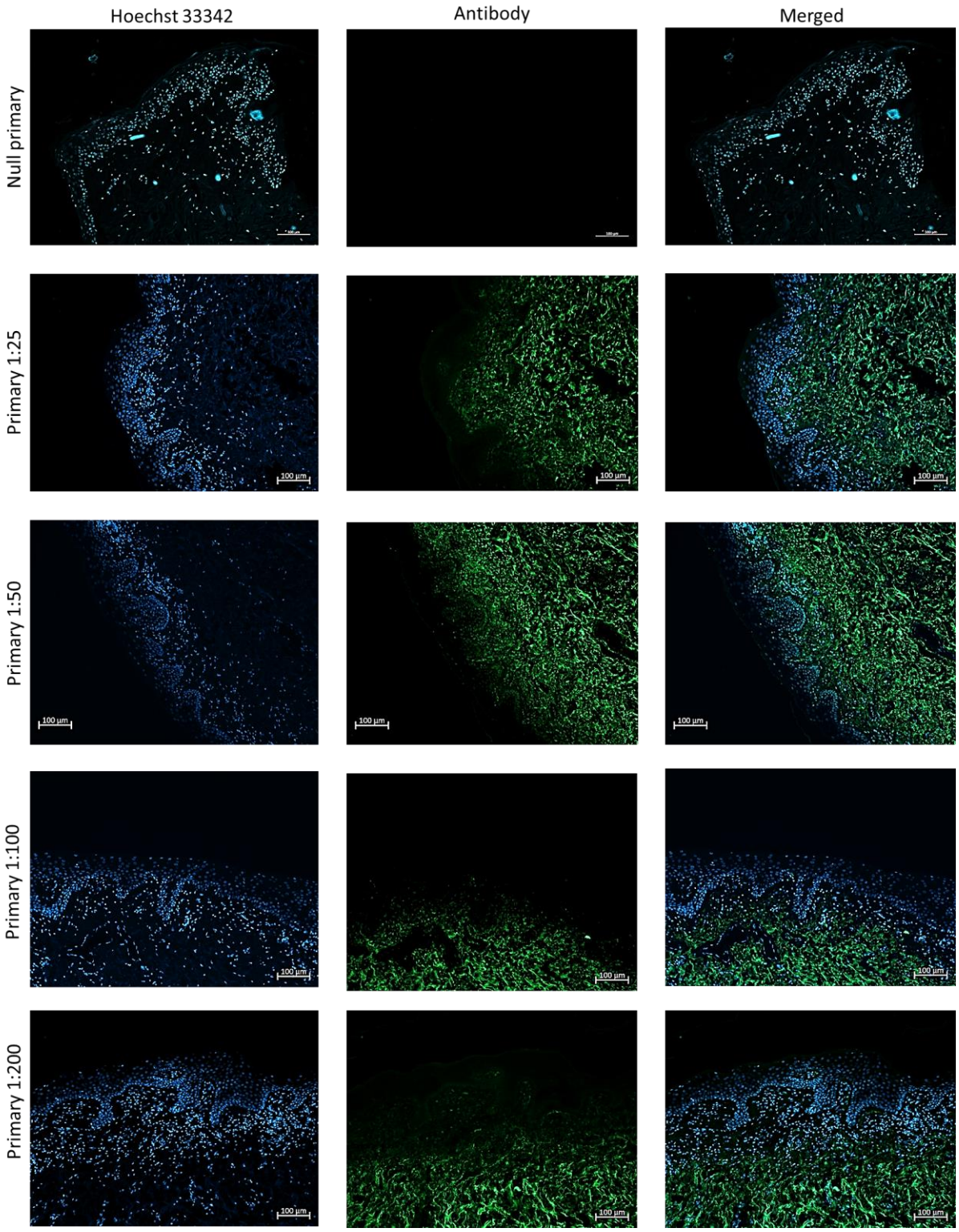

Figure 3.11. Immunofluorescent staining of basement membrane collagen VII in physiological human skin. Collagen VI is shown in green. Hoechst nuclear staining is blue. Scale bar:100µm.

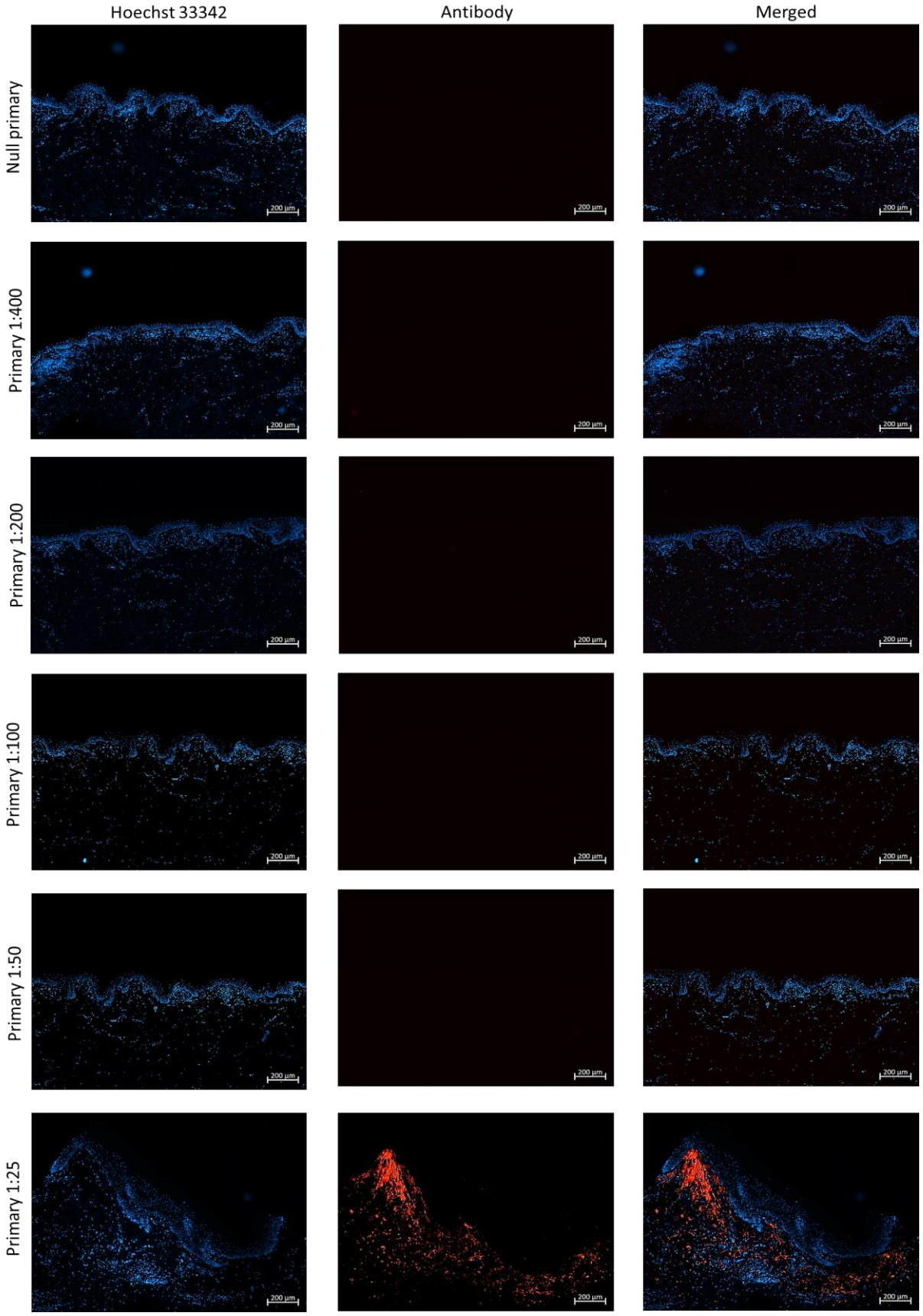

Figure 3.12. Immunofluorescent staining of basement membrane laminin-5 in physiological human skin. Laminin-5 is shown in red. Hoechst nuclear staining is blue. Scale bar:100µm.

3.3.4 Histological comparison of skin equivalents to physiological human skin

To determine if the HSEs were representative of physiological human skin, human skin biopsies were paraffin embedded, sectioned, and stained with H&E and Picro-Sirius Red for histological analysis. The skin biopsies (Figure 3.13) showed two very clearly defined layers (dermis and epidermis) which were separated by a dermal/epidermal junction (dotted line) as seen in Figure 3.13A. The epidermis of the human skin contains stratified sublayers which were also visible in the skin equivalents optimised with $2x10^6$ fibroblasts and $1x10^6$ keratinocytes as shown previously, which indicates that the development of the HSEs were representative of human skin.

The physiological human skin was also stained with Picro-Sirius Red. The Picro-Sirius Red staining revealed two sublayers of the dermis, the papillary dermis and the reticular dermis separated by the blue dashed line (Figure 3.13B). The papillary dermis in human skin contains smaller and thinner collagen fibres (Rognoni and Watt 2018) much like those seen in the optimised full thickness HSE's suggesting that the dermis formed in the HSE's is more physiologically representative of the papillary dermis. The collagen in the reticular dermis in human skin was observed to consist of much larger, more organised and cross-linked collagen resulting in reticular connective tissue (Rognoni and Watt 2018). This was shown by the larger areas of strong red staining in the reticular dermis. Such organised reticular ECM, consisting of larger collagen fibres were not seen in the full thickness HSE's, further indicating that the dermis of the HSE's were more representative of the papillary dermis. This shows that the HSE's were therefore physiologically accurate.

To compare the development of the basement membrane in HSE's to physiological human skin, periodic acidic Schiff staining was performed. Periodic acidic Schiff stains the glycoproteins found within the basement membrane a magenta colour whilst staining cells dark blue. Figure 3.14A shows the magenta staining representing the glycoproteins in the basement membrane of physiological human skin at the dermal-epidermal junction. This membrane is shown to be present directly underneath the basal strata of the epidermis. In the HSEs (Figure 3.14B) the presence of fibroblasts lining the dermal epidermal junction directly beneath the basal keratinocytes resulted in a strong dark blue stain with some traces of the magenta stain representing the basement membrane visible between the two layers of the HSE. However, the large population of both fibroblasts and keratinocytes at the dermal/epidermal junction

resulted in dark blue staining at the dermal-epidermal junction which could have masked the magenta stained basement membrane.

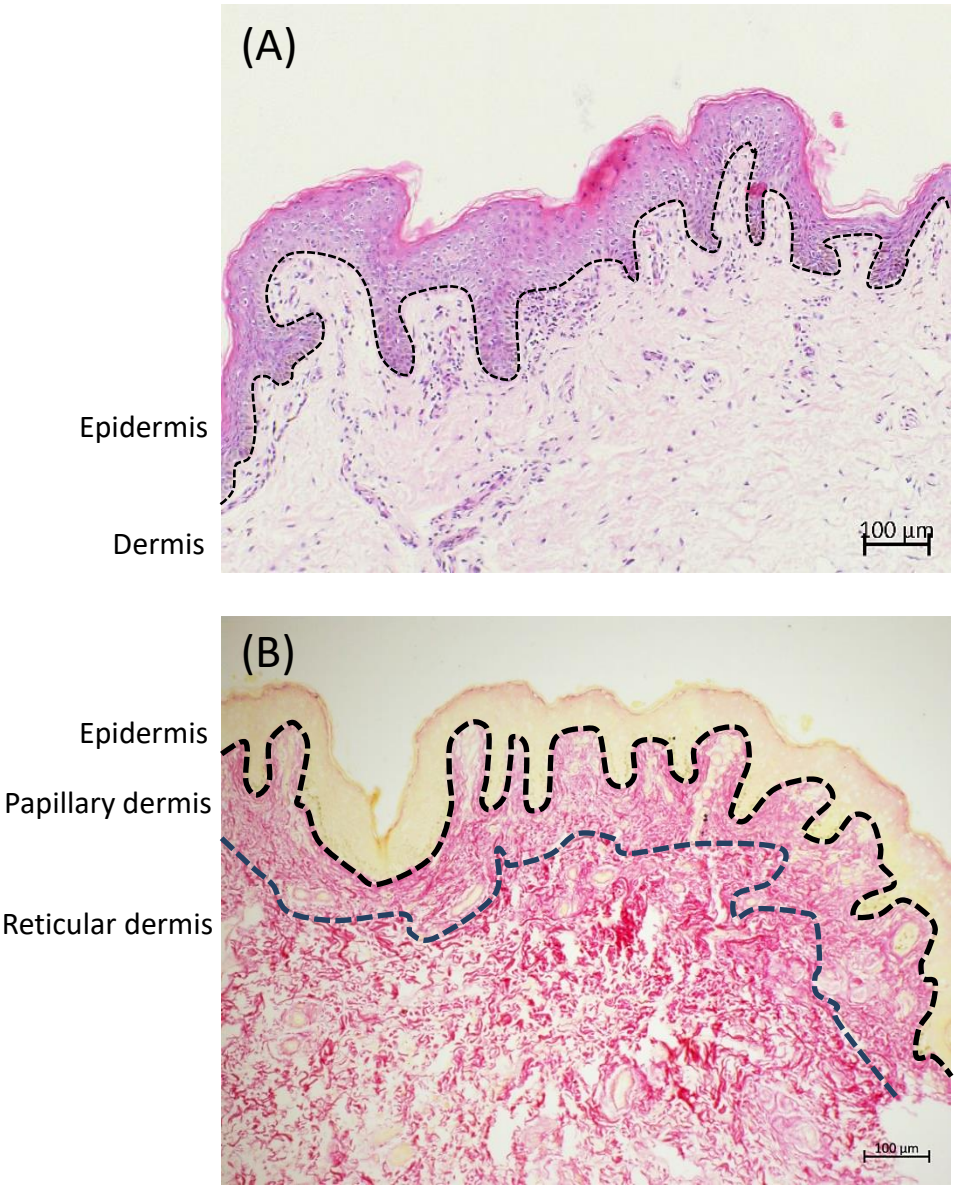

Figure 3.13 Representative histology images of staining of normal healthy human skin. (A) *H&E of a normal human skin biopsy. Black dotted line indicates the dermal-epidermal junction. (B) Picro-Sirius Red staining of a normal human skin biopsy. Black dotted line indicates the dermal-epidermal junction. Blue dotted line indicates the junction of the papillary dermis and the reticular dermis.*

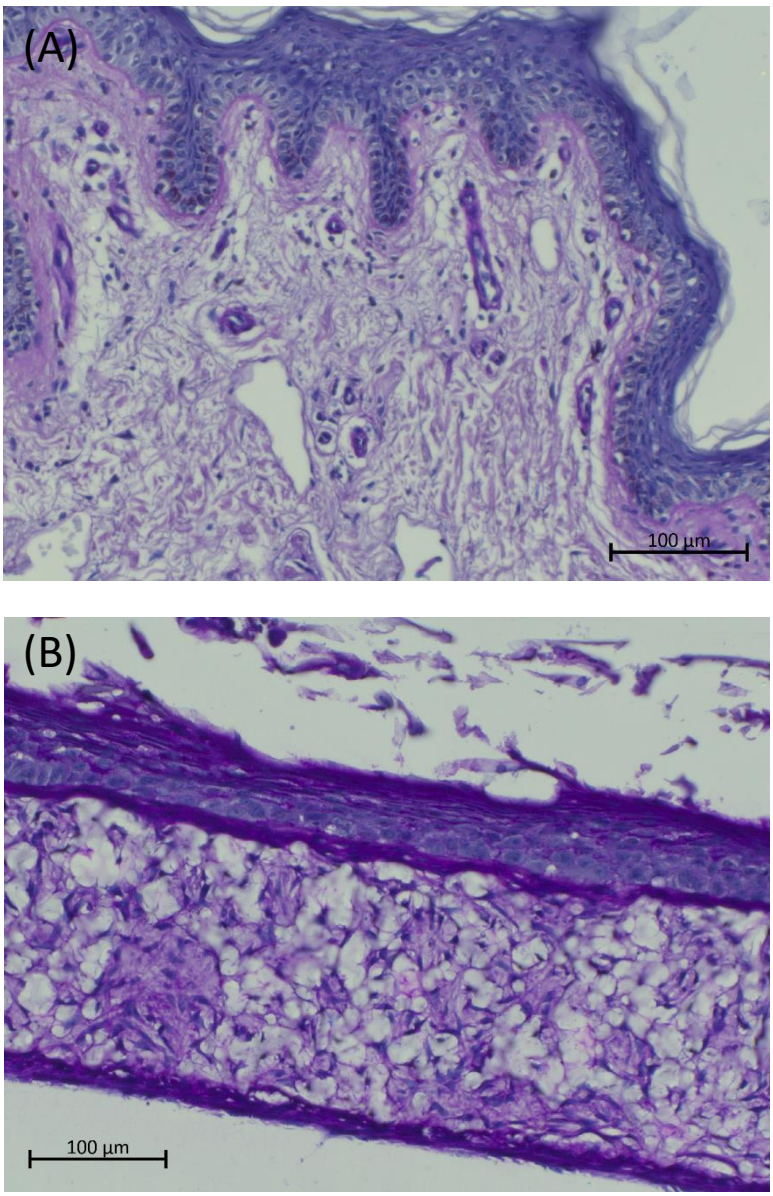

Figure 3.14. Representative images for Periodic Acidic Schiff staining of both a healthy human skin biopsy and a fully formed full-thickness HSE*. (A) Human skin biopsy. (B) Optimised full-thickness HSE.*

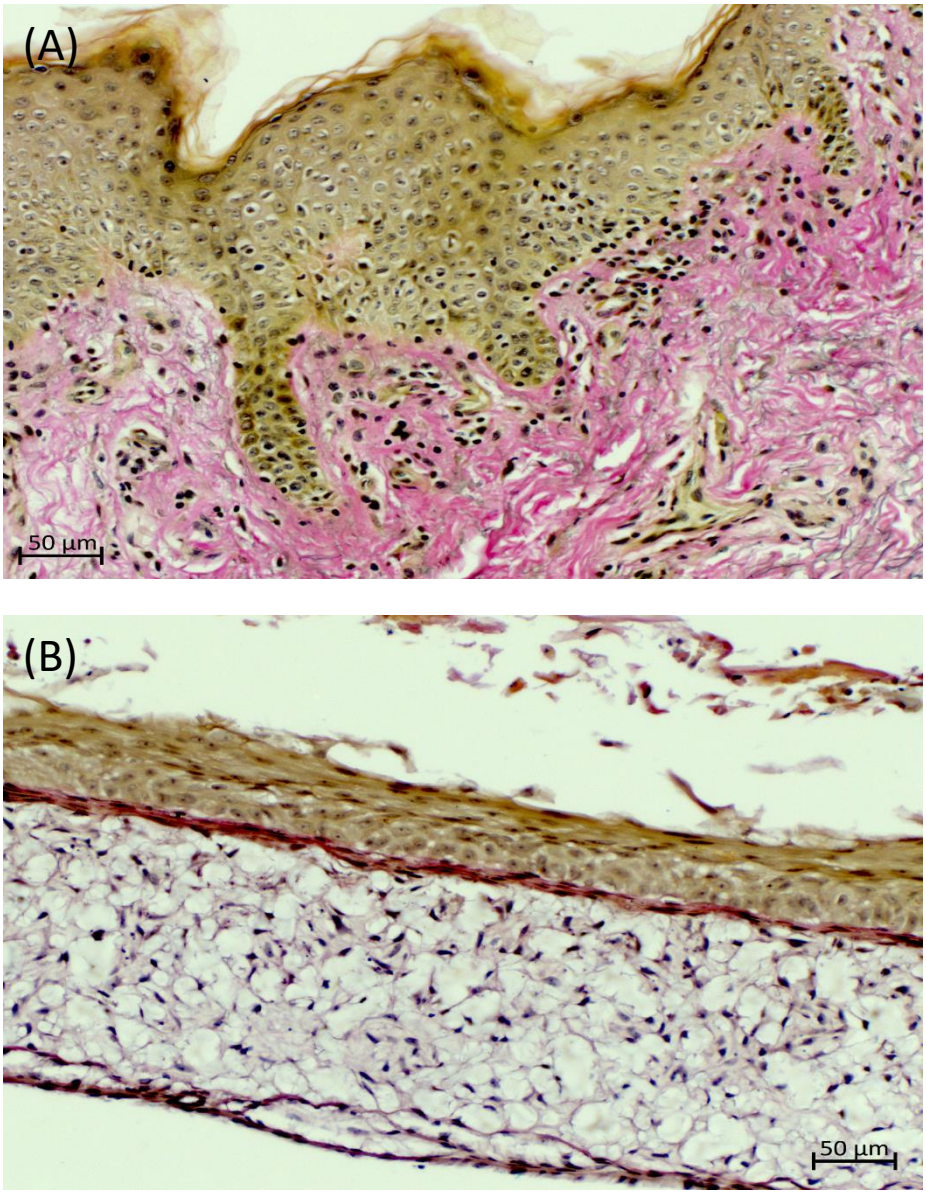

Figure 3.15 Representative histology images of Verhoeff van-Geison staining of both a physiological human skin (A) and HSE (B).

Physiological human skin and the HSEs were stained for elastin using Verhoeff van-Geison staining. The Verhoeff van-Geison stains cell nuclei black, cytoplasm brown, ECM pink and elastin fibres black. In physiological human skin, elastin fibres in the dermal region close to the epidermis (papillary dermis) were shown to be small and thin grey fibres which are difficult to detect (Figure 3.15B). These fibres become larger and thicker with darker staining further into the reticular dermis. These elastin fibres were not visible in the HSE's (Figure 3.15A).

Immunofluorescent staining was used to stain different markers present throughout various strata of the epidermis in both physiological human skin (Figure 3.16) and HSE's (Figure 3.17). In the basal strata of the epidermis in physiological human skin, basal keratinocytes which are healthy, proliferating, and undifferentiated contain cytokeratin 14 (Figure 3.16A), which is an intermediate filament within the cytoskeleton of basal keratinocytes. Positive staining for cytokeratin 14 indicates keratinocytes with a basal phenotype were present. In the HSE's, cytokeratin 14 was also detected (Figure 3.17A) directly above the dermal/epidermal junction (dashed line). As the keratinocytes begin to differentiate and stratify, they begin to express cytokeratin 10, which also is a component of the cytoskeleton. Cytokeratin 10 is expressed in the spinous and granular strata in the epidermis of physiological human skin. In physiological human skin, cytokeratin-10 (Figure 3.16B) was present above the basal strata of the epidermis. Cytokeratin 10 was also detected above the basal layer in the HSE's (Figure 3.17B). Involucrin, a precursor of the stratum corneum is found in the granular and upper spinous strata. Both physiological skin and the HSE's expressed involucrin in the spinous and granular strata (Figure 3.16C and Figure 3.17C). Loricrin is present in the corneal envelope of the epidermis and in the human skin it was found to be in the uppermost strata of the epidermis (Figure 3.16D). In the HSE's, the loricrin staining was positively detected, however, it was not as clearly defined as that observed in physiological human skin due to artefact during tissue processing (Figure 3.17D). The null primary images (negative controls) for immunofluorescent staining are shown in Figure 3.18.

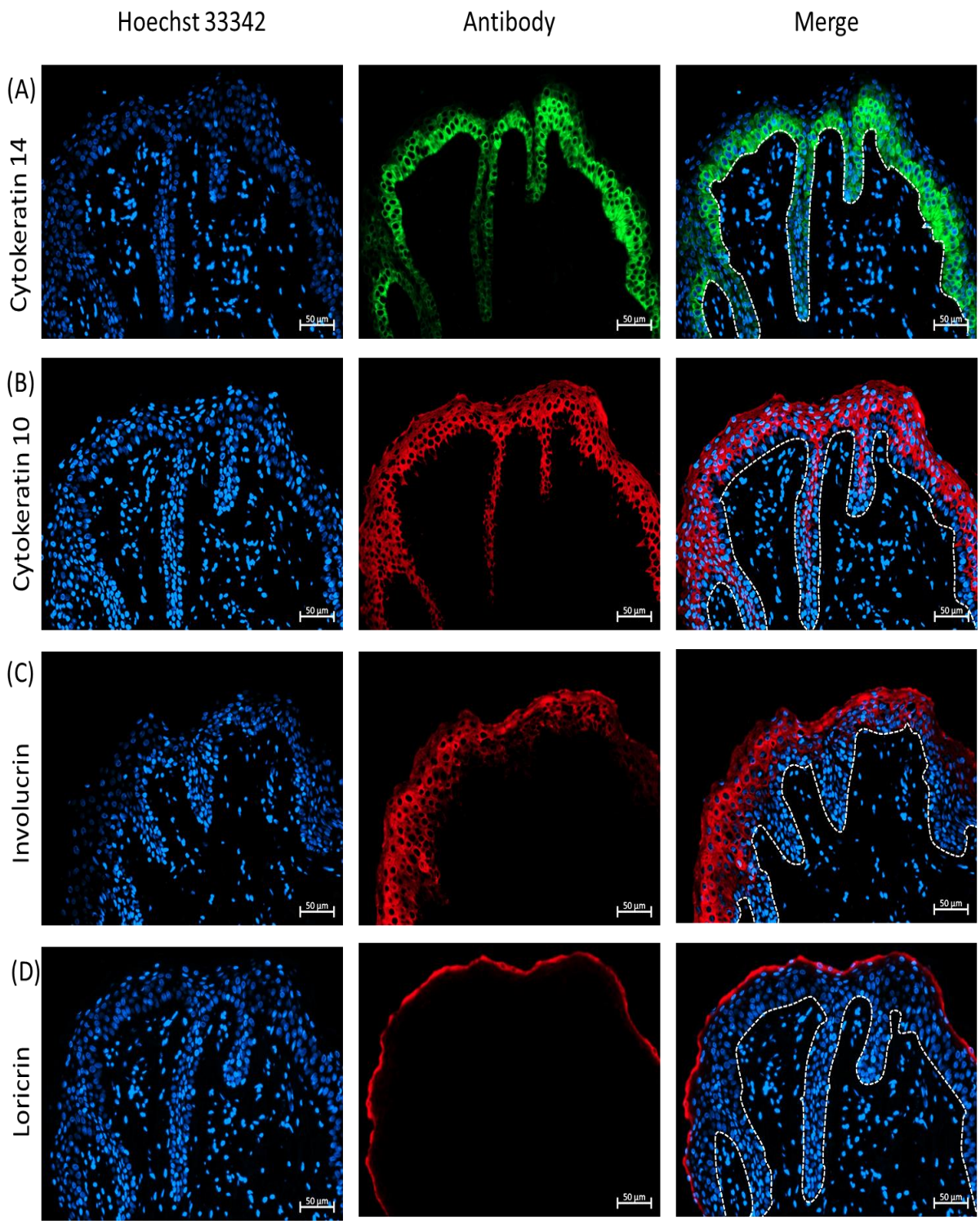

Figure 3.16. Representative images of human skin biopsies stained with immunofluorescent staining. (A) *Cytokeratin 14 (green) staining of human skin. (B) Cytokeratin 10 (red) staining of human skin. (C) Involucrin (red) staining of human skin. (D) Loricrin (red) staining of human skin. White dashed line indicates dermal-epidermal junction. Cell nuclei are were stained blue with Hoechst 33342.*

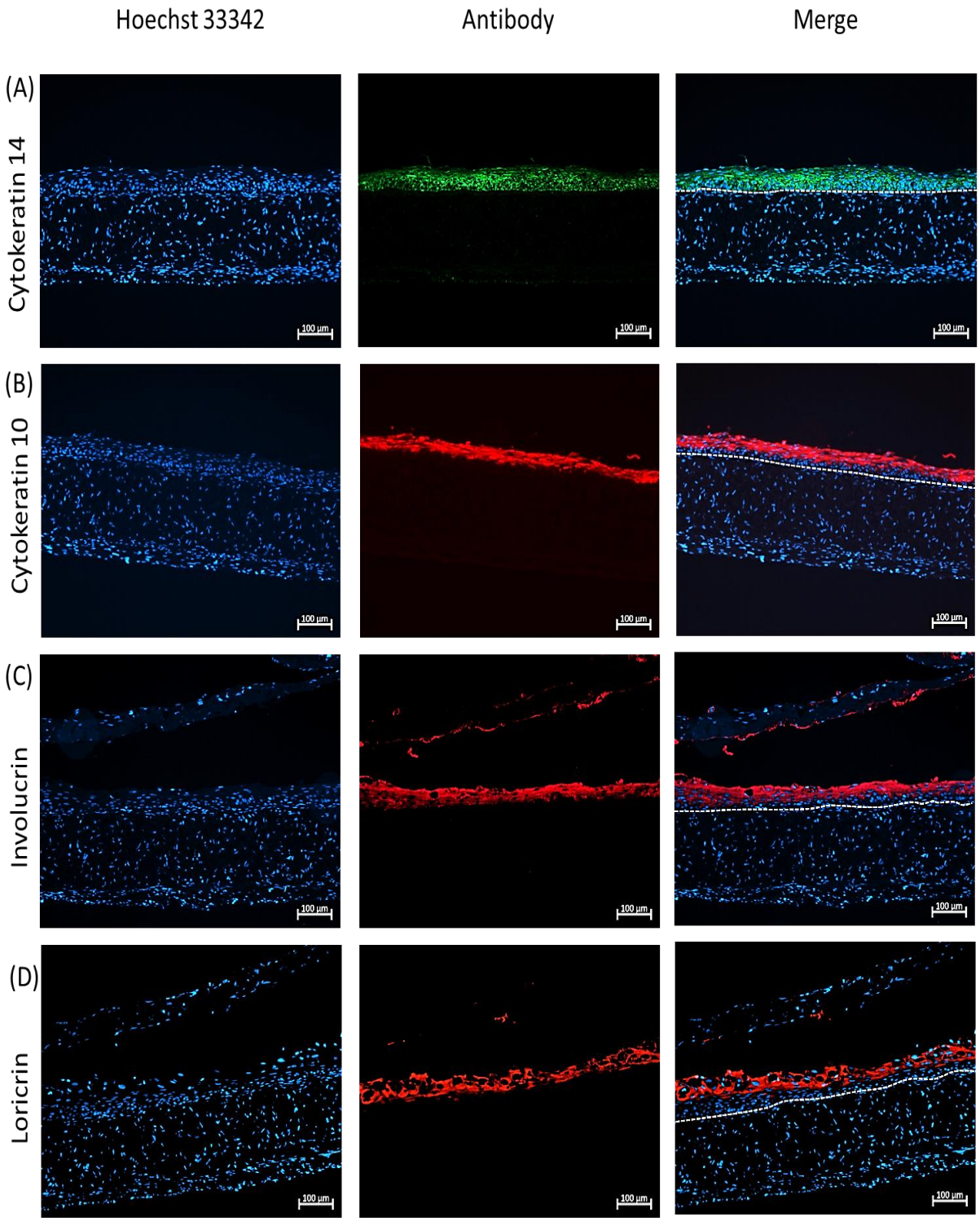

Figure 3.17. Representative images of HSEs stained with immunofluorescent staining. **(**A*) Cytokeratin-14 (green) staining of HSE. (B) Cytokeratin-10 (red) staining of HSE. (C) Involucrin (red) staining of HSE. (D) Loricrin (red) staining HSE. White dashed line indicates dermal-epidermal junction. Cell nuclei are were stained blue with Hoechst 33342.*

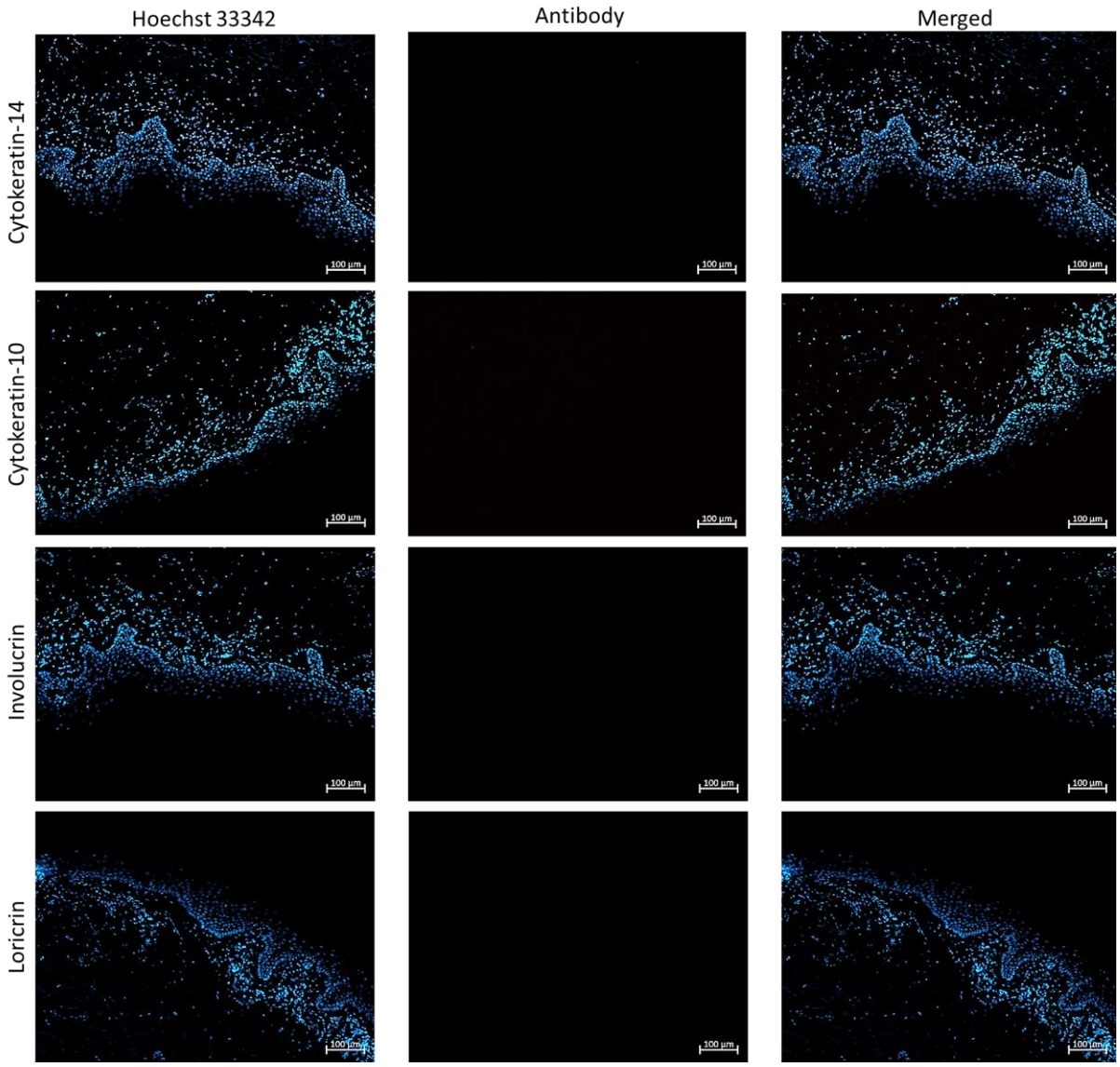

Figure 3.18. Null primary images (negative controls) from immunofluorescent staining of human skin equivalents.

To minimise the incubation time and cost of additional antibody diluent and washing buffer (~£1.50 per slide) associated with evaluating the HSE's for differentiation markers immunofluorescence double staining was established using two different combinations of antibodies. Figure 3.19 shows staining for Involucrin and cytokeratin 14 in both human skin (Figure 3.19A) and HSE (Figure 3.19B). Performing the double stain on a single section more clearly defines the separate layers of the epidermis and gives a better outline and a more direct comparison of the formation of the different sublayers of the epidermis.

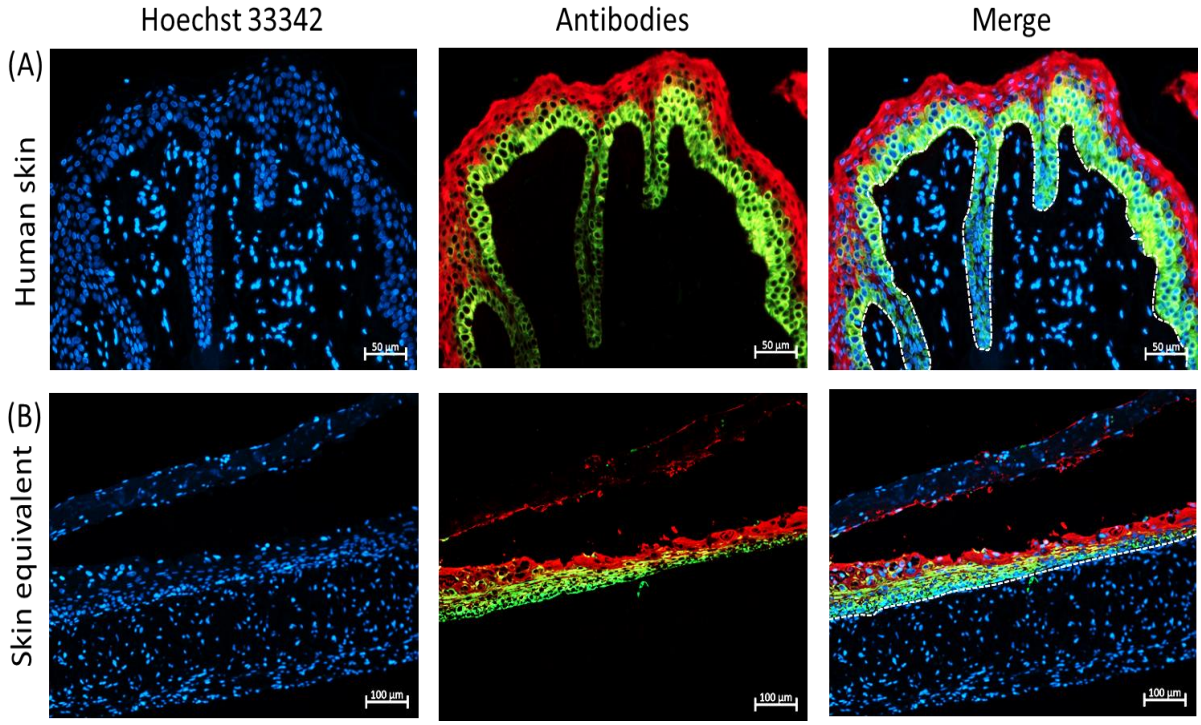

Figure 3.19. Representative images of double immunofluorescent staining for cytokeratin-14 and Involucrin in human skin biopsies and HSEs. (A*) Staining of human skin biopsy. (B) Staining of HSE. White dotted line indicates dermal-epidermal junction. Cell nuclei were stained blue with Hoechst 33342*

3.4 Discussion

The initial 24-well format Skimune 3D® protocol provided by Alcyomics yielded models which did not fully develop, the histological analysis of each model suggested the same cause of failure. While the extent of development varied from donor to donor, each donor demonstrated insufficient cell numbers and ECM production to prevent the fall through of keratinocytes into the dermal equivalent. Therefore, the tissues formed were not physiologically accurate as there was no reproducible formation of a dermis and a separate epidermal layer with relevant strata. To form a well-developed dermis, sufficient cell numbers and ECM would be required to plug the pores of the inert Alvetex® scaffold thereby blocking any keratinocytes from entering the scaffold. This could be achieved in two ways; firstly, by increasing the number of dermal fibroblasts seeded; and secondly, by encouraging an increase in proliferation or ECM production by adjusting the contents of the dermal culture media. The Skimune 3D® model relies on ascorbic acid to encourage dermal fibroblasts to produce ECM (Hill *et al*. 2015). Collagen is one of the main components in the ECM of human skin with collagen type I making up to 85-90% of total collagen, while collagen type III comprises of 8-11% of total collagen (Smith, Holbrook, and Madri 1986). While ascorbic acid has been shown to increase proliferation of dermal fibroblasts, ascorbic acid also specifically upregulates collagen type I and type III synthesis by increasing the synthesis of precursor collagen chains proα1(I) and proα1(III) (Hata *et al*. 1988; Phillips, Combs, and Pinnell 1994). To further encourage ECM production, the use of additional growth factors such as transforming growth factor beta 1 (TGF-β1) was considered. The effects of TGF-β1 on the proliferation and ECM synthesis of dermal fibroblasts has been well documented (Chen and Thibeault 2012; Grouf *et al*. 2007; Phillips, Combs, and Pinnell 1994). TGF-β1 increases the proliferation of dermal fibroblasts and the synthesis of dermal ECM by increasing overall protein synthesis (Phillips, Combs, and Pinnell 1994). However more recently the use of TGF-β1 has been shown to alter the phenotype of dermal fibroblasts. TGF-β1 has been implicated in the lineage reprogramming (trans-differentiation) of dermal fibroblasts to myofibroblasts by upregulation of microRNA-21 (miR-21) (Liu *et al*. 2016; Midgley *et al*. 2013). TGF-β1 induced trans-differentiation of fibroblasts to myofibroblasts is a factor in the formation of scar tissue (Midgley *et al*. 2013). Therefore, the use of TGF-β1 in developing the dermal equivalent may result in a dermal equivalent containing ECM like that of keloid scar tissue with the presence of myofibroblasts and therefore be less physiologically representative of normal healthy human skin.

The introduction of additional growth factors into the media would also influence the development cost of Skimune3D®. It was therefore determined that rather than adding additional growth factors to improve dermal development, investigating how increasing the number of fibroblasts initially seeded into the scaffold would impact the formation of the dermal equivalent could be more economically beneficial for development costs. By doubling the number of dermal fibroblasts seeded initially from $1x10^6$ to $2x10^6$ the production of a dermal equivalent was shown to be robust and reproducible across donors. The variability of the proliferative capacity and ECM synthesis of dermal fibroblasts was highlighted by equivalents using $1.5x10^6$ fibroblasts which produced variable results. Of the three donors used, only two donors developed a dermis with $1.5x10^6$ fibroblasts capable of supporting keratinocytes with little or no epidermal infiltration into the dermis. The same donors also demonstrated the impact that number of fibroblasts can have on keratinocyte proliferation. An increase in epidermal thickness and improved epidermal development was seen when the number of fibroblasts was increased from $1.5x10^6$ to $2x10^6$. The improved stratification and thicker epidermis of equivalents made with $2x10^6$ fibroblasts compliments the findings of previous studies (el-Ghalbzouri *et al*. 2002; Sun *et al*. 2008; Wang *et al*. 2012). The increase in fibroblasts may well have resulted in increased cell-cell contact and cross-talk between the fibroblasts and keratinocytes, thereby resulting in overall improvement in HSE formation. As reported by Wang *et al* an increase in direct fibroblast-keratinocyte contact can increase the proliferation of keratinocytes (Wang *et al*. 2012). The increasing intensity of red PSR staining of skin equivalents suggested that increasing the number of fibroblasts initially seeded appeared to affect the extent to which collagen type I and type III was produced within the scaffold. Thinner collagen fibres were visible within and underneath the dermal component. Interestingly the collagen located at the surface of the scaffold (dermal-epidermal junction) suggested the presence of more compact collagen. This could be explained by the high number of fibroblasts present at the dermal-epidermal junction. Evidently without an adequate cell-ECM layer at the dermal-epidermal junction skin equivalents failed to form. Overall optimal dermal and epidermal development occurred when seeding $2x10^6$ fibroblasts consequently forming full-thickness skin equivalents which were highly comparable to physiological human skin.

In healthy normal human skin, the epidermis and the dermis are separated by a basement membrane at the dermal-epidermal junction. This feature was not detected

when using immunofluorescence to stain for basement specific proteins such as collagen IV, collagen VII, and laminin-5 due to the lack of specificity of the primary antibodies. In contrast the basement membrane was positively detected in skin biopsies by staining for glycoproteins using periodic acid-Schiff PAS. In skin equivalents PAS staining was inconclusive. The columnar organisation of basal keratinocytes in H&E stained sections appeared to suggest the formation of a basement membrane however only very subtle traces of glycoproteins were visible when stained with PAS. The high density of dark blue stained dermal fibroblasts at the dermal-epidermal junction may have masked the PAS staining of the basement membrane glycoproteins. Analysis of elastin in skin equivalents using Verhoeff–Van Gieson staining, revealed no visible production of elastin fibres as the fibroblasts were supplemented with ascorbic acid to promote collagen synthesis, rather than increase general protein synthesis. In human skin biopsies a gradient of elastin fibres was observed with very little to no elastin fibres in the papillary dermis and fibres increasing in number and size further into the reticular dermis. When comparing the elastin content of the skin equivalents to healthy human skin the HSEs appeared to more closely represent the papillary dermis than the reticular dermis suggesting that the dermal compartment of skin equivalents was physiologically accurate.

Epidermal differentiation and stratification were characterised by the detection of cytoskeletal keratins, a cornified envelop precursor and a marker of a cornified envelope by immunofluorescent staining. The detection of cytokeratin-14 directly above the dermal-epidermal junction confirmed the formation of a basal strata containing healthy undifferentiated “stem cell” like keratinocytes. Suprabasal expression of cytokeratin-10 and involucrin indicate a layer of keratinocytes in the process of undergoing terminal differentiation above the basal strata much like epidermal formation in physiological human skin. The combined staining of cytokeratin-14 and involucrin demonstrated epidermal stratification in skin equivalent. Suprabasal detection of loricrin in skin equivalents suggested the presence of a cornified envelope in the epidermis.

Overall, this chapter demonstrates importance of optimising cell numbers and seeding ratios by increasing the number of fibroblasts used to form the dermal compartment of the HSE. The amount of ECM produced could be increased by increasing cell numbers allowing an improvement in dermal formation which in return resulted in prevention of keratinocyte infiltration into the dermal layer. This further resulted in a better and more

complete formation of an epidermal layer allowing an overall more physiologically relevant HSE to be produced. When compared to the work of Hill *et al* (Figure 3.20) the optimised 24-well HSE presented in this chapter was physiologically similar to the original Skimune3D® HSE first developed by Hill *et al* (Hill et al. 2015). Both the 24-well HSE and the original HSE feature a bilayer construct with a densely populated dermis and a stratified epidermis.

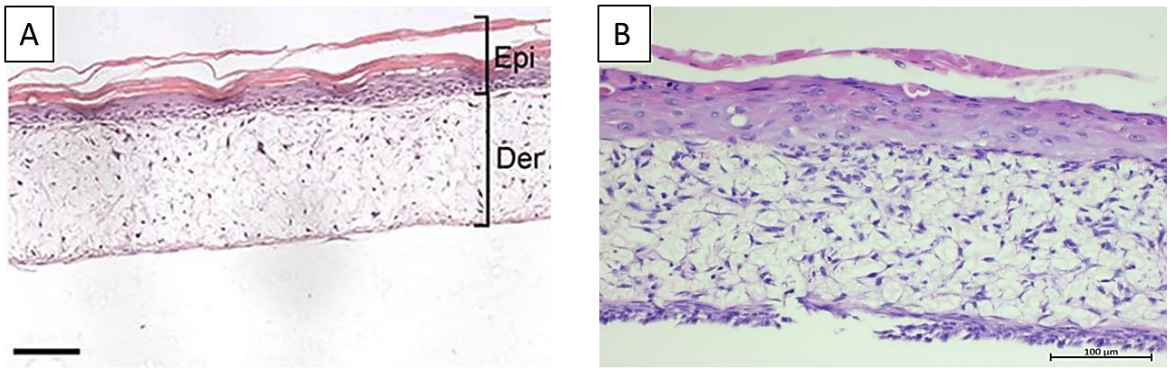

Figure 3.20. Comparison of original Skimune to optimised 24-well skin equivalents. *A) Original 6-well HSE developed by Hill et al (adapted from Hill et al 2015), Scale bar: 100µm. B) Handmade 24-well HSE, scale bar: 100µm.*

To improve the scalability of the Skimune3D® HSE the next iterations of the HSE would require a reduction in size to facilitate the reduction in the number of cells necessary to construct HSEs using primary human skin cells. This would require a reduction in format from the 24-well transwell system presented in this chapter.

Chapter 4 Development of a Handmade 96-well Skin Equivalent

4.1 Introduction

In this chapter human skin equivalents (HSEs) were scaled to the 96-well format using prototype transwell inserts. The rationale for scaling HSEs to the 96-well format was to minimise the number of cells that would be required to manufacture HSEs and to maximise the number of HSEs that per could be produced per healthy donor. This chapter describes the work to establish a handmade 96-well HSE by first establishing a protocol for manufacturing a dermal equivalent then proceeding to use dermal equivalents to create full-thickness HSEs. The structure of the optimised HSEs were stained using basic histological and immunohistological techniques to visualise dermal extra-cellular matrix (ECM) and epidermal markers.

4.2 Aims

The aims of the work described in this chapter were:

1. Establish a protocol for creating a 96-well format dermal equivalent.
2. Develop a 96-well full-thickness skin equivalent using the dermal equivalent protocol.
3. Use immunohistochemistry to validate the structure of the epidermis.

4.3 Results

4.3.1 Developing a 96-well dermal equivalent

The representative dermal equivalents harvested at day 10 are shown in Figure 4.1. The H&E staining of dermal equivalents made with $1x10^5$ dermal fibroblasts showed a good distribution of fibroblasts within the Alvetex® scaffold with slightly fewer cells being present at the bottom of the scaffold. While cells were distributed through the scaffold the cellularity of the scaffold was poor. Thin fibroblast layers were observed at both the top and bottom surfaces of the scaffolds. Picro-Sirius Red staining of the dermal equivalents made with $1x10^5$ fibroblasts revealed that the fibroblasts had begun to produce small uncross-linked collagen fib res as indicated by the faint red staining within scaffold. The use of $3x10^5$ fibroblasts resulted in a good distribution of cells within the scaffold with a fibroblasts layer at the top and bottom of the scaffold. Small traces of collagen were also present when stained with Picro-Sirius Red. Seeding $5x10^5$ fibroblasts resulted in a large majority of the cells being located near the bottom of the scaffold at day 10. The layer of fibroblasts at the bottom of the scaffold was thicker with several layers of cells visible, however, the fibroblast layer at the top of the

scaffold was incomplete with visible gaps between cells. No collagen was visible when stained with Picro-Sirius Red. Dermal equivalents made with $7x10^5$ fibroblasts were densely populated. Most of the dermal fibroblasts were located at the bottom of the scaffold where a thick fibroblast layer was noticeable. No collagen was visible in dermal equivalents with $7x10^5$ fibroblasts after 10 days.

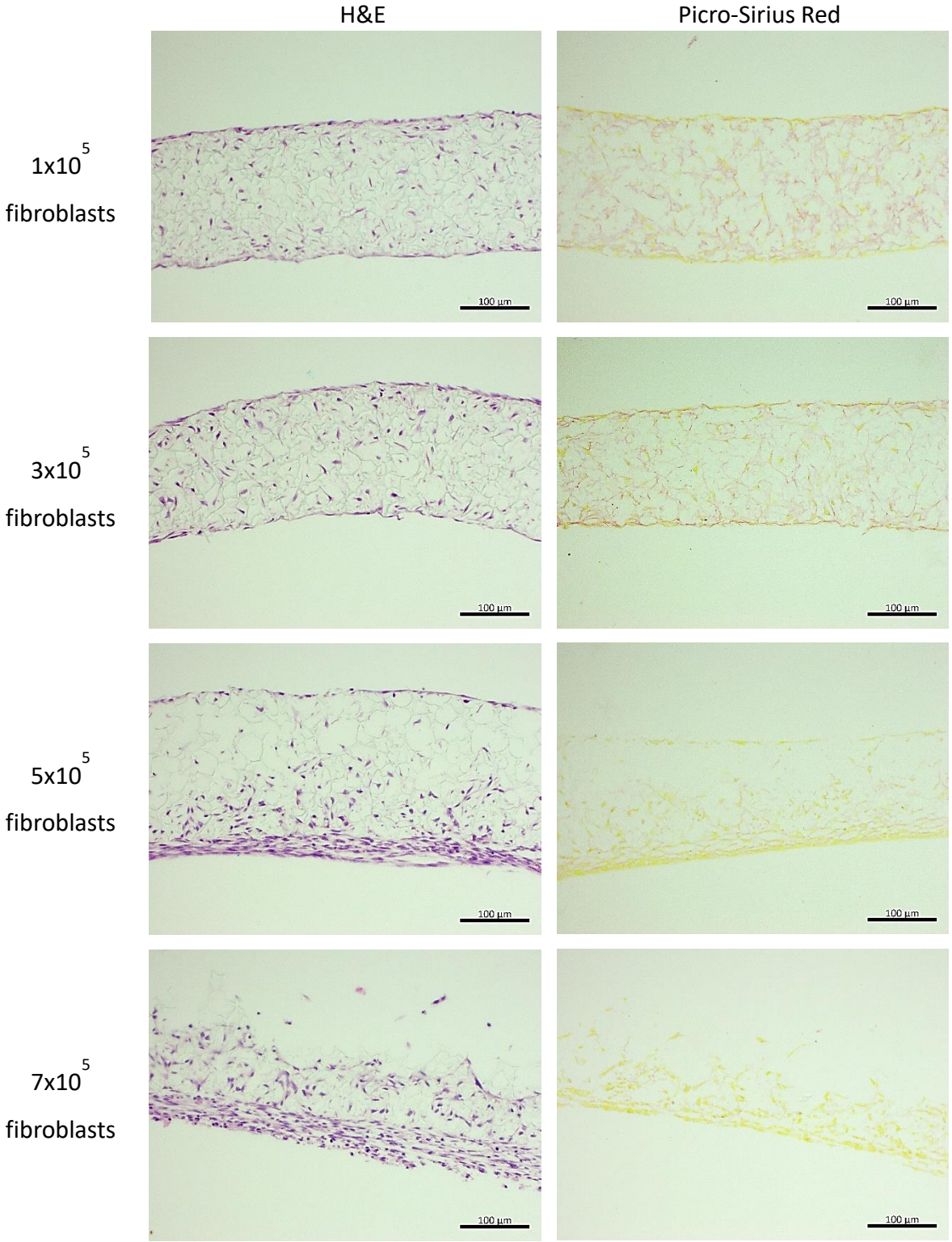

Figure 4.1. Representative dermal equivalents grown for 10 days stained with H&E and Picro-Sirius Red. *Dermal equivalents incubated for 10 days and stained with both H&E to show the location of cells and Picro-Sirius Red to visualise dermal collagen. Dermal equivalents were also cultured with a range of dermal fibroblasts which include $1x10^5$, $3x10^5$, $5x10^5$ and $7x10^5$ cells. Scale bars: 100µm.*

Representative H&E and Picro-Sirius Red staining of dermal equivalents incubated for 14 days can be seen in Figure 4.2. The dermal equivalents made with $1x10^5$ fibroblasts maintained a good distribution of cells within the scaffold however the scaffold was still thinly populated. A fibroblast layer at the top and the bottom of the scaffold were still visible. Picro-Sirius Red staining revealed a noticeable increase in dermal collagen. The collagen staining at day 14 was slightly stronger than those observed at day 10, with the collagen appearing more complete fewer gaps in the extracellular space, particularly in the fibroblast layer at the top and the bottom of the scaffold. While there was a complete cell layer at the top of the scaffold the formation of a collagen mesh was not complete as there were many regions where fibroblasts had not yet produced collagen. H&E staining of dermal equivalents made with $3x10^5$ fibroblasts revealed that most fibroblasts were present at the bottom of the scaffold which contained a thick fibroblast layer. The layer of fibroblasts at the top of the scaffold remained thin with some gaps between cells observed. The collagen stained with Picro-Sirius Red was observed more strongly stained indicating the presence of more collagen which appeared to be largely unorganised. Darker red staining at the bottom of the scaffold suggested the presence of cross-linked collagen. Conversely the collagen at the top of the scaffold was observed to consist of rather thinly distributed indicating that a collagen mesh had not formed at the top of the scaffold. As expected, the representative H&E of dermal equivalents containing $5x10^5$ fibroblasts was more densely populated. A good layer of dermal fibroblasts was observed at the top of the scaffold with a thicker fibroblast layer present at the bottom of the scaffold. The collagen staining displayed thick reticular like collagen at the bottom of the scaffold with less intensely stained collagen within the scaffold. Thicker layers of collagen were also observed at the top of the scaffold partially forming a collagen-cell mesh although some gaps were observed. The cells in dermal equivalents made with $7x10^5$ were shown to be mostly located at the bottom of the scaffold with some cells located towards the middle of the scaffold. Some fibroblasts were visible at the top of the scaffold though there were not enough cells to create a layer at the top of the scaffold. Picro-Sirius Red staining of the scaffold showed very little red staining, indicating that there was there was very little collagen present within the scaffold. The faint red of collagen was located towards the bottom of the scaffold where most of the cells were present.

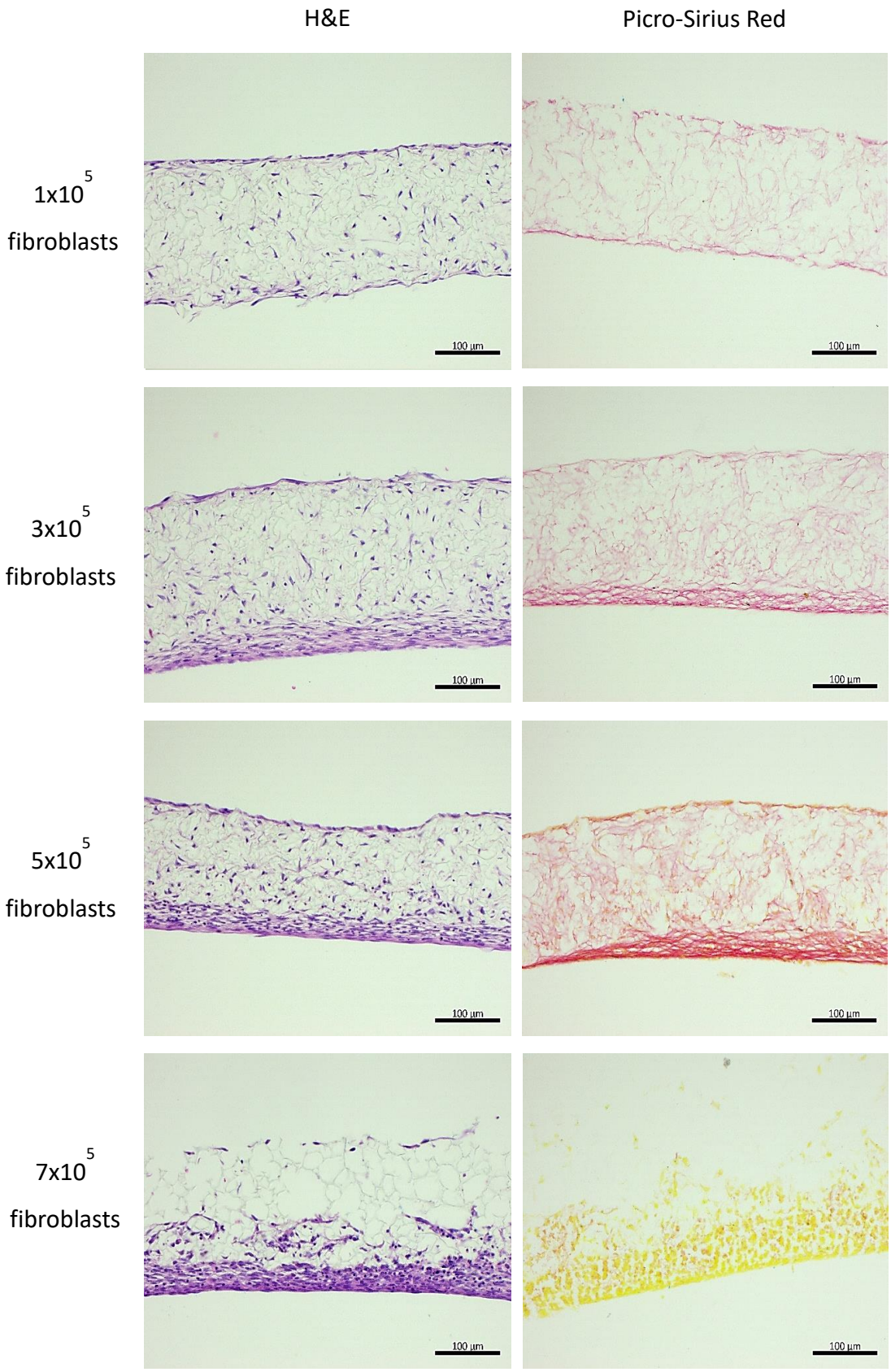

Figure 4.2 Representative dermal equivalents grown for 14 days stained with H&E and Picro-Sirius Red. *Dermal equivalents incubated for 14 days and stained with both H&E to show the location of cells and Picro-Sirius Red to visualise dermal collagen. Dermal equivalents were also cultured with a range of dermal fibroblasts which include $1x10^5$, $3x10^5$, $5x10^5$ and $7x10^5$ cells. Scale bars: 100µm.*

Representative H&E and Picro-Sirius Red staining of dermal equivalents incubated for 18 days are shown in Figure 4.3. By day 18 dermal equivalents had developed with various states of collagen production. $1x10^5$ fibroblasts produced a dermal equivalent with a good distribution of cells throughout the scaffold and a thin layer of fibroblasts was observed at the top of the scaffold. When stained with Picro-Sirius Red there was a noticeable increase in dermal collagen. Stained collagen was present throughout the scaffold with the light red staining suggesting that most of the dermal ECM was not cross-linked. Small areas of darker staining were noticeable at the top and the bottom of the scaffold indicating that crosslinking of collagen had occurred in these regions, however cross-linked collagen was not consistent across the top of the scaffold. Dermal equivalents made with $3x10^5$ fibroblasts resulted in most of the cells being present at the bottom of the scaffold at day 18. Some cells were visible in the middle of the scaffold with a layer of fibroblasts visible at the top of the scaffold. When stained with Picro-Sirius red slight thickening of the collagen at the top of the scaffold was visible. The inner scaffold appeared more densely packed with collagen compared to earlier time points. Some thickening of collagen at the bottom of the scaffold was observed. Dermal equivalents containing $5x10^5$ fibroblasts were well populated. A thick layer of fibroblasts was visible at the bottom of the scaffold with cells appearing to migrate superficially through the scaffold. The fibroblasts had formed a monolayer at top of the scaffold. A good layer of collagen was present at the top of the scaffold with well stained ECM lining the top of the Alvetex®. Large layers of collagen were stained at the bottom of the scaffold where most of the cells were located. After 18 days of incubation, dermal equivalents made with $7x10^5$ fibroblasts showed a large outgrowth of cells from underneath the scaffold could be seen. Within the outgrowth a large layer of cells could be seen with irregular morphology. The fibroblasts appeared swollen with larger nuclei much like cells to undergoing necrosis. Inside the scaffold the fibroblasts were mostly located in the lower regions. A layer of fibroblasts was found to be present at the top of the scaffold although some gaps were visible. Very little collagen production in the scaffold was observed when stained with Picro-Sirius Red. A thin and patchy layer of collagen lined the top of the scaffold while very little collagen was visible within the scaffold. Collagen was visible in the layer of swollen cells of the fibroblast outgrowth.

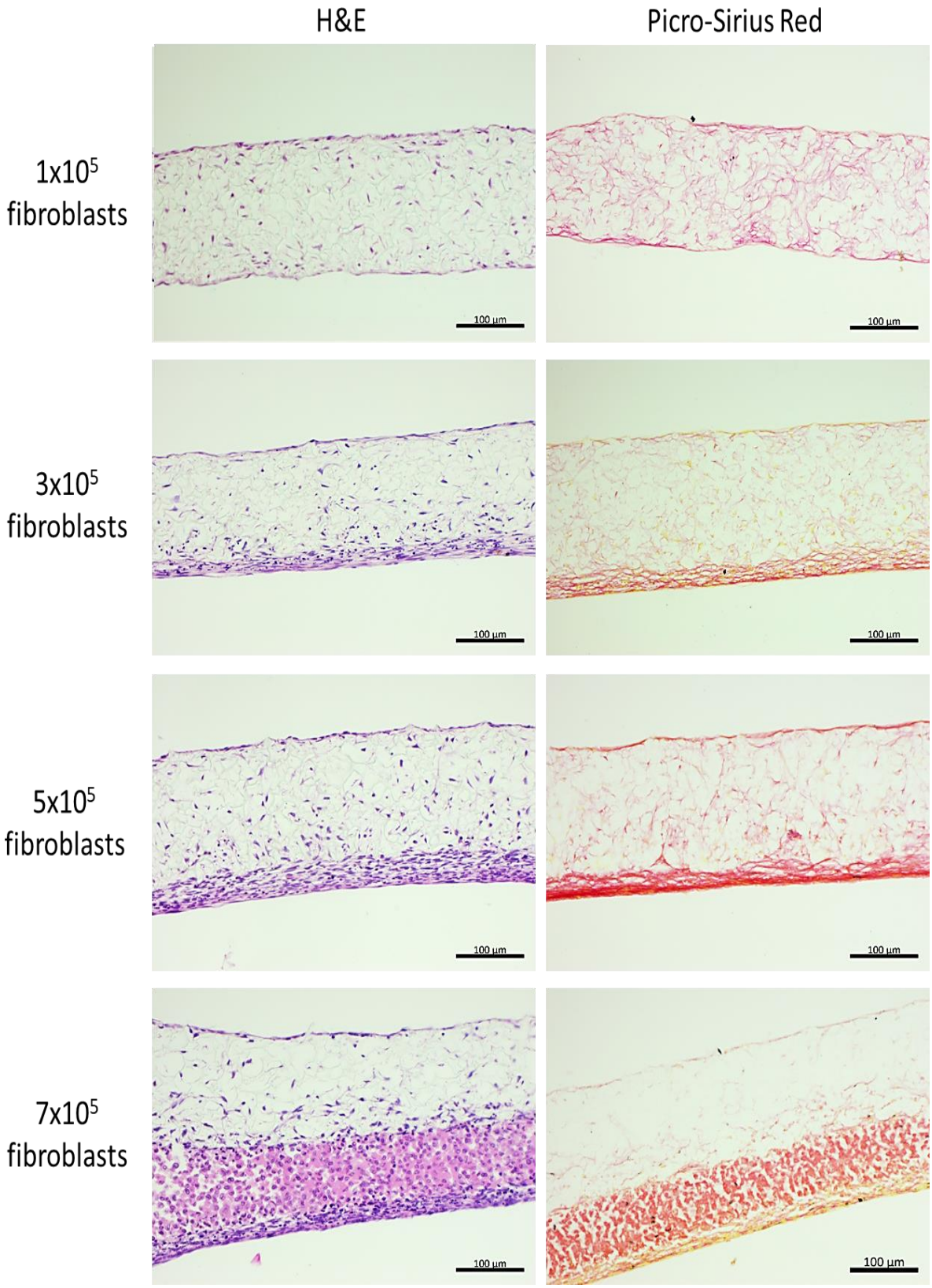

Figure 4.3. Representative dermal equivalents grown for 18 days stained with H&E and Picro-Sirius Red. *Dermal equivalents incubated for 18 days and stained with both H&E to show the location of cells and Picro-Sirius Red to visualise dermal collagen. Dermal equivalents were also cultured with a range of dermal fibroblasts which include 1x10^5, 3x10^5, 5x10^5 and 7x10^5 cells. Scale bars: 100µm.*

4.3.2 Developing a 96-well full-thickness skin equivalent

H&E staining of dermal equivalents constructed with $3x10^5$ and $5x10^5$ fibroblasts and seeded with keratinocytes are shown in Figure 4.4. The use of $3x10^5$ fibroblasts in dermal equivalents resulted in complete infiltration of epidermal keratinocytes into the dermal compartment. As shown in Figure 4.4 all the $3x10^5$ dermal equivalents seeded with $1x10^5$, $3x10^5$, $5x10^5$ or $7x10^5$ keratinocytes were unable to support the formation of an epidermis without infiltrating keratinocytes.

H&E stained skin equivalents constructed using $5x10^5$ fibroblasts and keratinocytes are shown in Figure 4.5. Skin equivalents seeded with $1x10^5$ keratinocytes developed a very thin epidermis with only the granular stratum and the stratum corneum visible. There were visible gaps in the epidermis with delamination occurring between the layers of differentiated keratinocytes. The dermis was well formed with no visible keratinocyte infiltration. Seeding $3x10^5$ keratinocytes produced well-formed skin equivalent. The epidermis included a basal layer above the dermal-epidermal junction (dotted line) which mostly covered the dermal equivalent with undifferentiated keratinocytes, a spinous layer, and a granular layer. The flattened nuclei of differentiating keratinocytes could be seen in the spinous strata (black arrow) directly above the basal strata, some vacuoles (red arrow) were also visible in the spinous strata. The granular layer which separated from the skin equivalent during sectioning was visible. The dermal equivalent was well formed with a fibroblast/ECM layer supporting the epidermis, there was no visible keratinocyte infiltration into the dermis. Skin equivalents containing $5x10^5$ keratinocytes featured a partial basal layer in the epidermis above the dermal-epidermal junction (black dotted line). The basal strata containing undifferentiated keratinocytes was inconsistent across the dermal equivalent. Alongside the columnar undifferentiated basal keratinocytes, were cells that were undergoing differentiation with some degree of vacuolisation occurring (blue arrow). Directly above the partial basal strata was a consistent but thin spinous stratum with some separation visible between the layers of differentiating cells. Above the spinous strata was a layer of keratinocytes which appeared to be dyskeratotic (blue arrows). This layer of keratinocytes, which adhered poorly to the spinous strata, were heavily stained with eosin and contained shrunken pyknotic and hyperchromatic nuclei (green arrow). Seeding $7x10^5$ keratinocytes onto dermal equivalents resulted in complete infiltration of the dermal equivalent by keratinocytes resulting in failure to form a dermal equivalent.

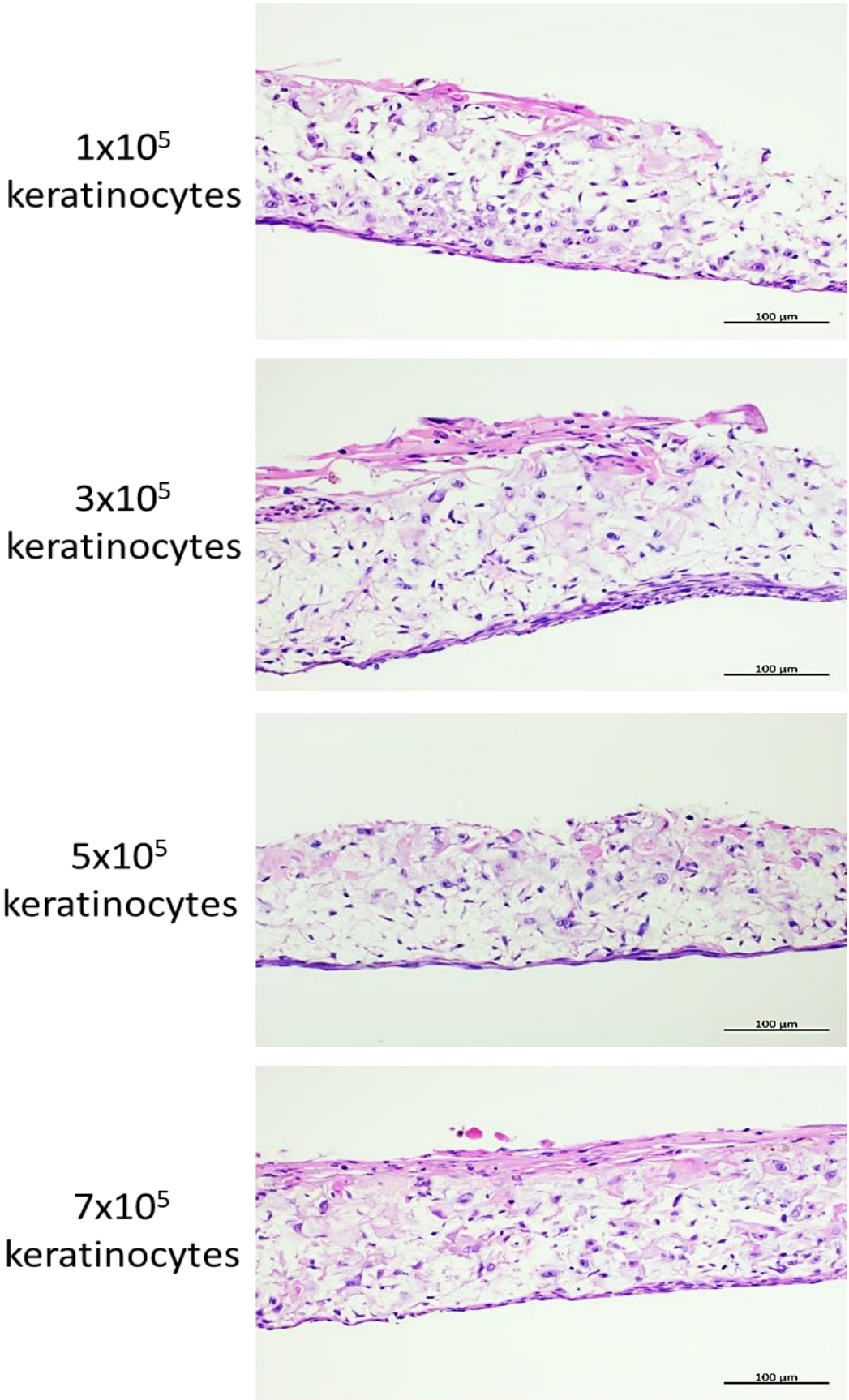

Figure 4.4. HSEs developed with 3x10^5 fibroblasts stained with H&E. *Dermal equivalents constructed with 3x10^{5}fibroblasts were grown for 18 days and seeded with 1x10^5, 3x10^5, 5x10^5, or 7x10^5 keratinocytes. Scale bars: 100µm*

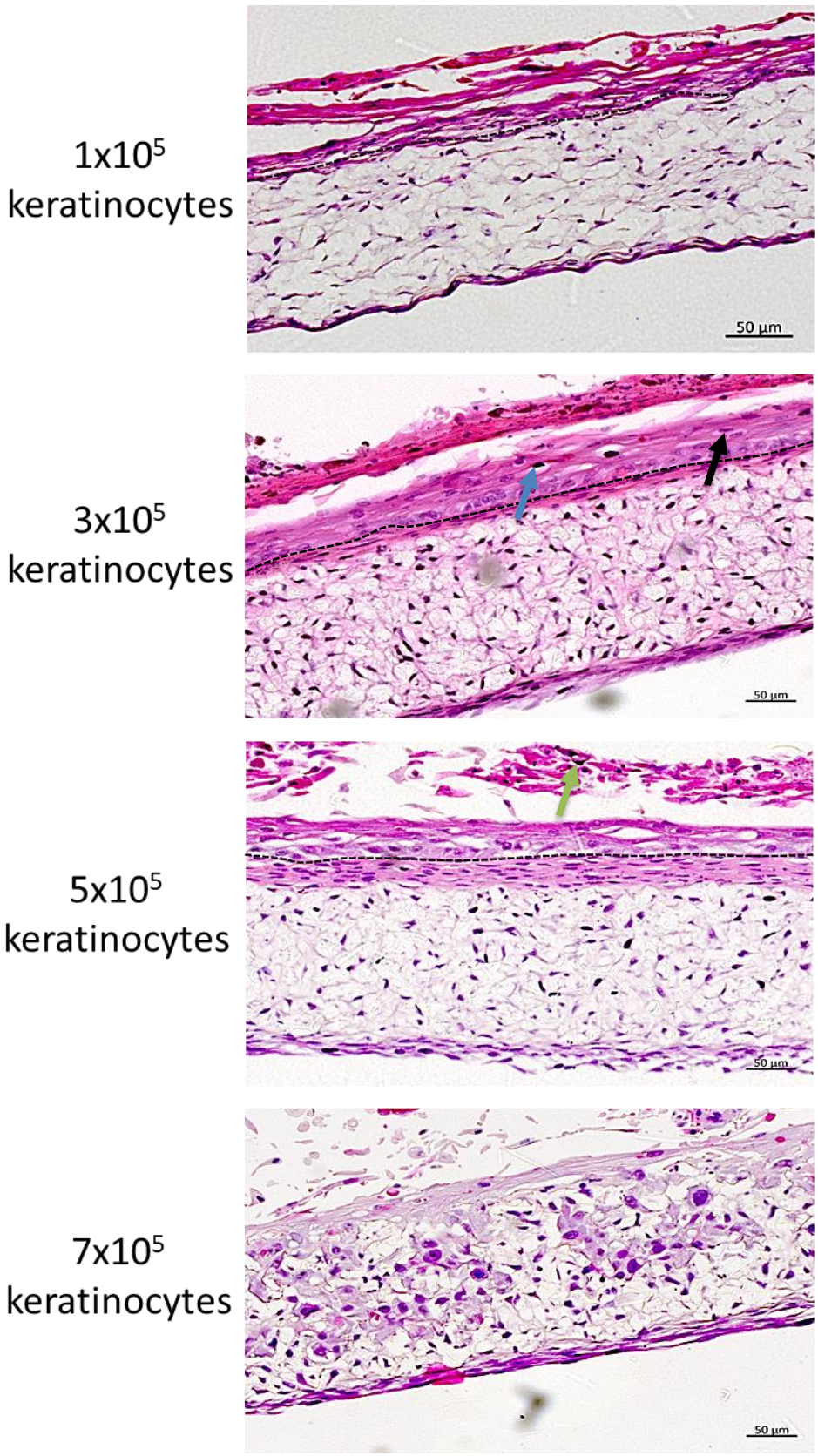

Figure 4.5. HSEs developed with 5x10^5 fibroblasts stained with H&E. *Dermal equivalents constructed with 5x10^5 fibroblasts were grown for 18 days and seeded with 1x10^5, 3x10^5, 5x10^5, and 7x10^5 keratinocytes. Differentiating keratinocytes are shown by the black arrow, Blue arrow points to a dyskeratotic keratinocyte. Green arrows indicate pyknotic and hyperchromatic nuclei. Scale bars:100µm.*

To further improve the overall thickness and cellularity of the epidermis in HSEs the number of keratinocytes seeded into the scaffold were increased to $4x10^5$ keratinocytes while the number of fibroblasts per skin equivalent remained at $5x10^5$. HSEs constructed with $4x10^5$ keratinocytes and $5x10^5$ fibroblasts were stained with H&E to visualise the overall structure of the HSEs, Picro-Sirius Red to detect dermal collagen, periodic acidic-Schiff (PAS) to stain mucosubstances found in basement membranes and Verhoeff-van Gieson staining to distinguish any elastin fibres from collagen. The representative images of 96-well HSEs made with the final protocol are presented in Figure 4.6. The representative H&E staining of HSEs showed two separate distinct layers Figure 4.6A. The epidermis was thick with undifferentiated keratinocytes forming a sparsely populated basal layer above the dermal-epidermal junction (black dotted line). The keratinocytes had migrated superficially while differentiating to produce a good stratum spinosum although some vacuoles could be seen (back arrow). Above the spinous strata a single layer of granular keratinocytes forming the stratum granulosum was visible and consistent across the HSE (red arrow). Thin layers of the final layer of the epidermis, the stratum corneum were located directly above the stratum granulosum (blue arrow). The stratum corneum appeared to delaminate and peel from the epidermis possibly as an artefact of sample processing or sectioning. As expected, the Picro-Sirius Red staining of the full-thickness HSE (Figure 4.6B) revealed a network of dermal collagen throughout the Alvetex® scaffold with thicker layers located at the dermal-epidermal junction and the bottom of the scaffold. The cell nuclei and cytoplasm were stained dark orange rather than yellow due to over exposure to ethanol during stain differentiation and section dehydration. The PAS staining failed to clearly detect any glycoproteins that would constitute a basal membrane at the dermal-epidermal junction (Figure 4.6C). When stained for elastin using Verhoeff-van Gieson staining (Figure 4.6D), elastin fibres which would stain grey/black could not be seen.

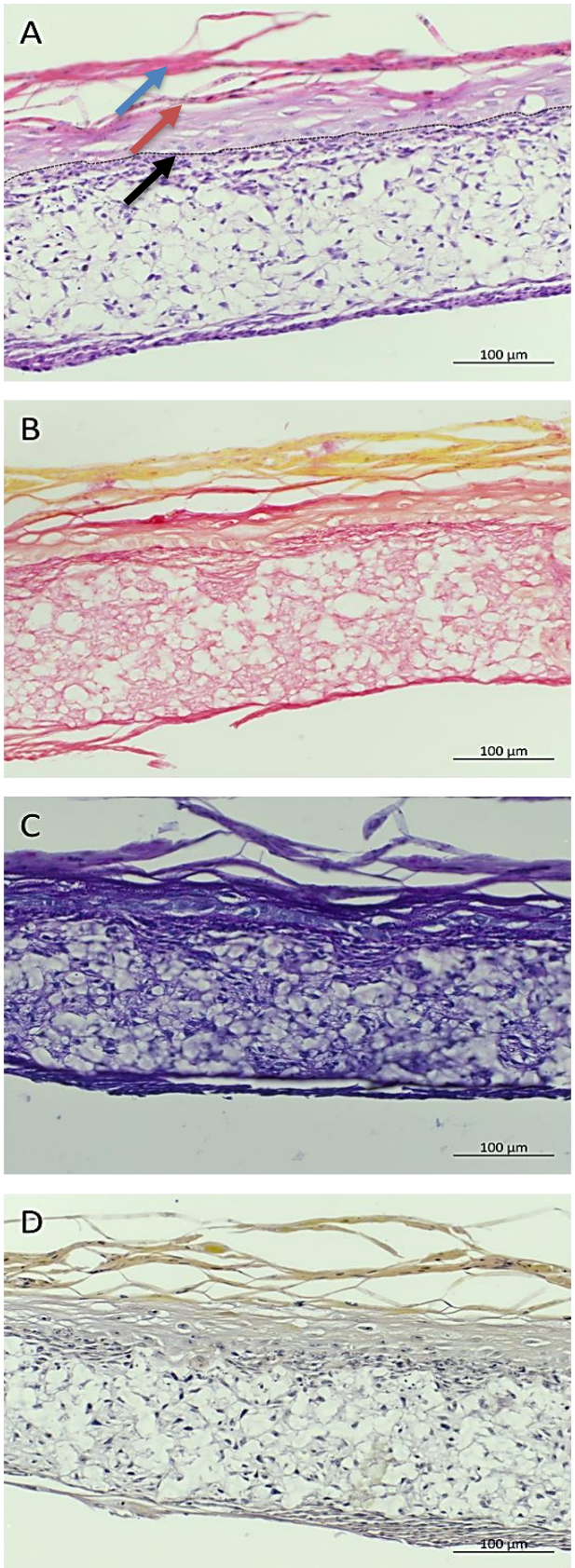

Figure 4.6. Representative staining of Full-thickness HSEs constructed with 5x10^5 fibroblasts and 4x10^5 keratinocytes stained. *A) H&E staining of HSE. Black dotted line indicates the dermal epidermal junction. Black arrow indicates vacuoles. Red arrow indicates granular strata. blue arrow indicates stratum corneum B) Picro-Sirius red of HSE. C) Periodic acidic-Schiff staining of HSE. C) Period acidic-Schiff staining of HSE. D) Verhoeff-van Geison staining of HSE. Scale bars: 100µm.*

Immunofluorescence staining was used to stain various markers present throughout the different strata of the epidermis in handmade 96-well HSEs. Representative images of HSEs stained using immunofluorescence as shown in Figure 4.7. The null primary images are shown in Figure 4.8. Cell nuclei were stained blue with Hoechst 33342. Cytokeratin-14 is a cytoskeletal intermediary keratin filament of healthy undifferentiating basal keratinocytes. As shown in Figure 4.7 the lowest strata of the epidermis stained positively for cytokeratin-14 directly above the dermal-epidermal junction (green stain). HSEs were also stained for Cytokeratin-10. Cytokeratin-10 is a cytoskeletal intermediary filament present in keratinocytes undergoing differentiation in the spinous and granular strata of the epidermis. In handmade 96-well HSEs cytokeratin-10 was detected in the epidermis above of the basal layer (red stain). The expression of cytokeratin-10 above the basal keratinocytes confirmed the formation of a thin stratum spinosum. Involucrin is precursor of the epidermal corneal envelope and is found in the same regions of epidermis as cytokeratin-10. In Figure 4.7 staining involucrin (red stain) was detected in the upper strata of the epidermis as expected. In healthy human skin loricrin is found in the stratum corneum of human skin. Loricrin was positively detected in the epidermis of 96-well (red stain).

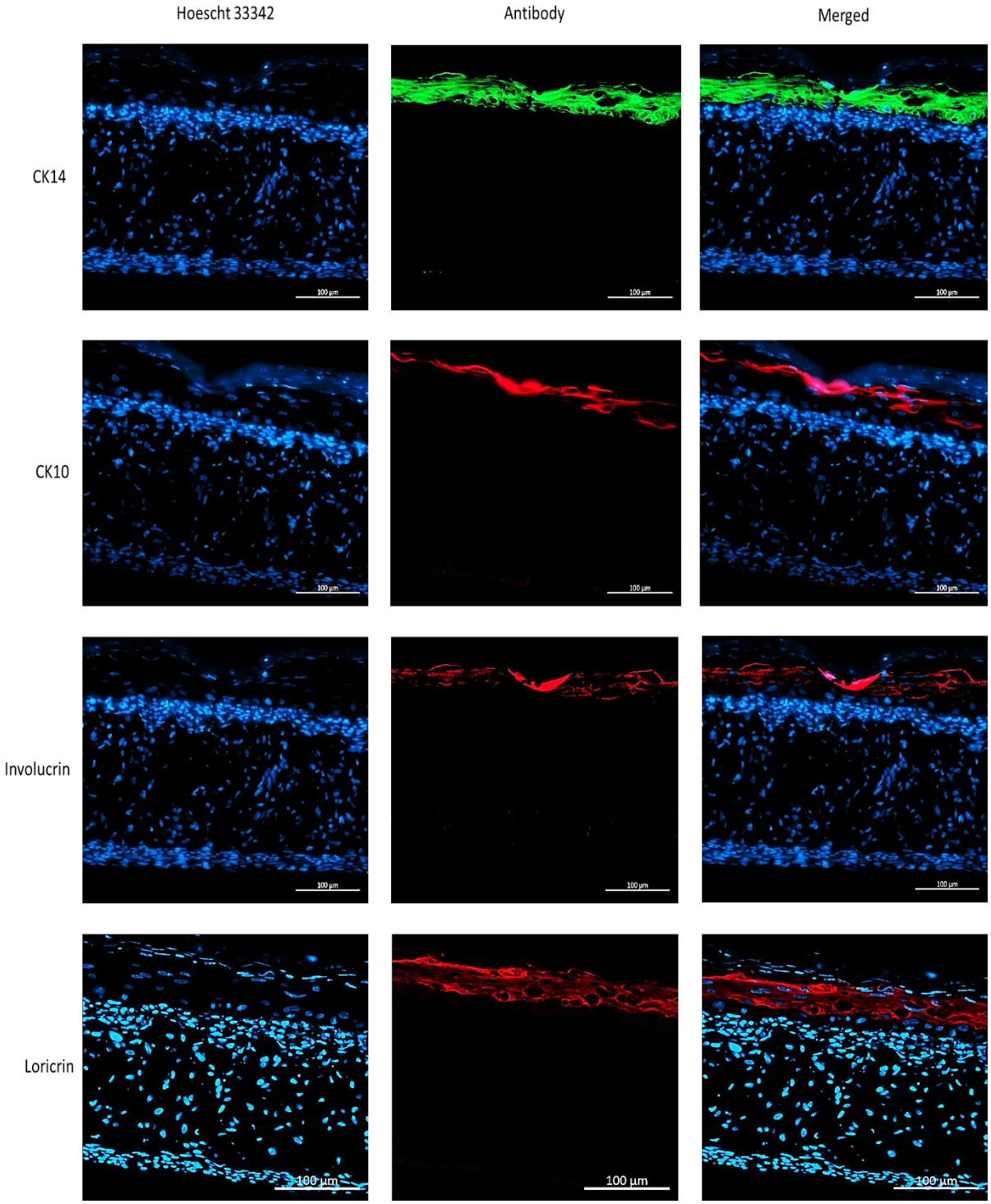

Figure 4.7. Immunofluorescent staining of handmade 96-well HSEs. *Full-thickness HSEs made with 5x10^5 fibroblasts and 3x10^5 keratinocytes, stained for cytokeratin-14 (green), cytokeratin-10 (red), Involucrin (red) and loricrin (red). Cell nuclei stained blue with Hoechst 33342. Scale bars: 100µm.*

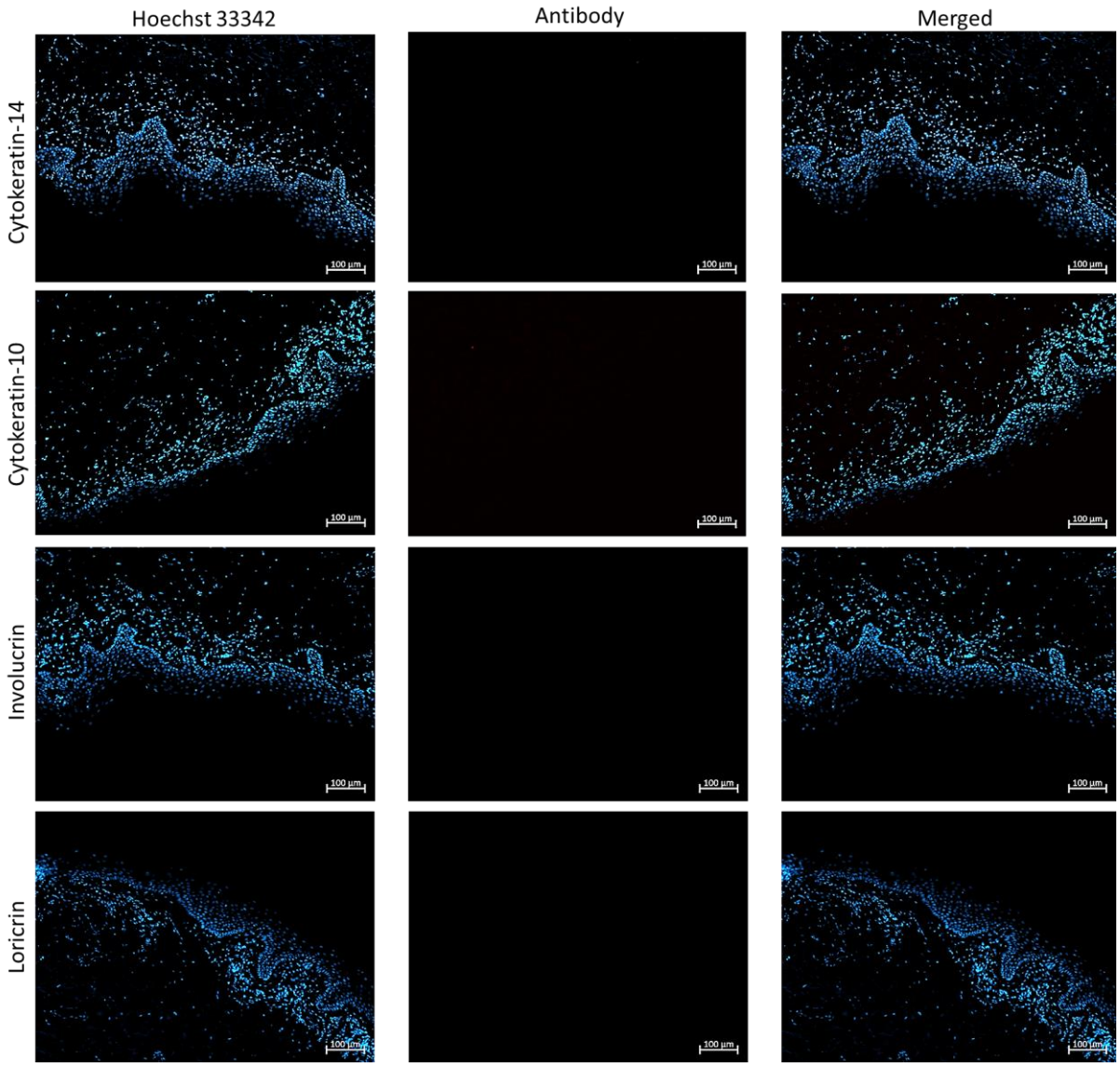

Figure 4.8. Null primary (negative controls) for immunofluorescent staining of handmade 96-well HSEs. *Hoechst nuclear stain shown in blue. Scale bars: 100µm.*

4.4 Discussion

Overall, the transition from a 24-well format HSE to a 96-well format HSE required the optimisation of the cellularity of the HSEs. As summarised in chapter 3, for a dermal equivalent to support an epidermis the production of dermal collagen is vital. Dermal development was investigated with the aim of minimising overall lead time and cell requirement to maximise output. The production of cross-linked dermal ECM appeared to largely occur between days 10 and day 14. The difference in dermal ECM between day 14 and day 18 was less noticeable. The key difference between dermal equivalents incubated for 14 days and 18 days was the thickening of the cell/ECM mesh at the top of the dermal equivalent. While reducing the lead time of the dermal equivalent by 4 days from 18 to 14 days may slightly reduce product development costs (£0.80 of media and supplements per well not including cost of labour), the data suggested that seeding keratinocytes at day 14 would not result in a full-thickness skin equivalent and therefore was not functional. Evidently the use of lower cell numbers ($3x10^5$) to produce dermal equivalents also was not feasible. This was due to the lack of ECM production at the surface of the scaffold. In contrast HSEs developed with $5x10^5$ fibroblasts consistently supported keratinocytes without infiltration of epidermal cells into the dermis due to thicker collagen layers lining the top of the dermal equivalents. However, the data does suggest that there is some limitation to what dermal equivalents can support. HSEs seeded with $7x10^5$ keratinocytes onto the dermis resulted in keratinocyte infiltration, while HSEs seeded with fewer keratinocytes did not show this to occur. Overall, the general structures of the HSEs were accurate in comparison to the 24-well HSE presented in chapter 3. The handmade 96-well HSEs contained the relevant epidermal markers supported by a well populated and ECM laden dermal equivalent.

Epidermal formation relies on both a well-formed dermal substrate and the establishment of a layer of basal keratinocytes. The basal cells act as stem cells and provide a continuous supply of undifferentiated keratinocytes over the two weeks required for cornification (Lippens *et al*. 2005). Interestingly HSEs prepared with $1x10^5$ keratinocyte were lined with layers of terminally differentiated cells with no available basal like cells. Without a self-renewing population of undifferentiated cells, the seeded keratinocytes terminally differentiated into corneocytes which adhered poorly to the dermis. HSEs made with $3x10^5$ and $5x10^5$ keratinocytes showed marginally improved adhesion of corneocytes. Peeling of the epidermis appears more common when there

is a lack of a basal layer. As the number of keratinocytes were increased there also appeared to be an increase in the number of cells which appeared apoptotic with blebbing cytoplasm and hyperchromatic nuclei possibly due to there being too many cells seeded onto the dermal equivalents. Additionally, some HSEs also contained dyskeratotic bodies. Dyskeratotic keratinocytes are defined as the abnormal or premature differentiation of keratinocytes (Kumar *et al* 2004). Such regions also contained eosinophilic cell bodies which were similar in appearance to civatte bodies. Civatte bodies are described as being caused by damaged apoptotic basal keratinocytes (Pranay, Kumar, and Chhabra 2013). Such features may be the result of cells undergoing senescence and apoptosis during three-dimensional (3D culture).

Overall, the variation in formation of the stratum basale in the epidermis of the HSEs reflects the challenges associated with the isolation and culture of primary epidermal keratinocytes. While primary fibroblast can be cultured for at least 7 passages and maintain their healthy phenotype before the onset of senescence, this is not the case for primary keratinocytes. The initial yield of keratinocytes from 4mm punch biopsies is low and relies on the early formation of colonies which appears to vary from donor to donor. This ultimately comes at the cost of the replicative capacity of the keratinocytes, as the longer the cells are in culture the more likely they are to senesce and therefore affect the quality of the HSE. To ensure keratinocytes maintain a basal like phenotype several studies have explored temporary immortalisation of the keratinocytes through incubation with Rho kinase (ROCK) inhibitor Y-27632 (Anderson *et al*. 2018; Chapman *et al*. 2010; Chapman *et al*. 2014; Strudwick *et al*. 2015). This literature indicates that the Skimune3D® HSE development process could be improved through the application of Y-27632. As a tissue equivalent which is to be routinely developed for commercial applications the protocol for Skimune3D® HSEs must also be robust and highly reproducible from user to user.

To date this is not the first skin equivalent to be constructed in a 96-well format. There are several reconstituted human epidermis (RHE) equivalents constructed in the 96-well format which both commercially available (SkinEthic™ RHE from Episkin) a non-commercial RHEs (Pedrosa et al. 2017). Naturally as RHEs only feature one layer of skin it could be argued that such equivalents are less physiologically representative of human skin than the HSE presented in the 96-well chapter. In terms of full-thickness HSEs in a 96-well format very few have been presented in literature or otherwise. So far the only notable full-thickness 96-well HSE Schimek *et al* (Schimek et al. 2018).

Schimek *et al* used a fibrin gel the create a dermis however the source of the fibrin gel was not specified therefore it is unclear if the HSEs produced by Schimek *et al* were autologous (Schimek et al. 2018). In contrast the HSE presented in this chapter were fully autologous with the ECM entirely produced by the cells within the HSE.

When compared to handmade 24-well HSEs presented in chapter 3, the data presented in this chapter shows that the number of fibroblasts needed to produce a dermis could be reduced by a factor of 4 from $2x10^6$ in the 24-well format to $0.5x10^6$ in the 96-well format. The number of epidermal keratinocytes required per scaffold was also reduced from $1x10^6$ in the 24-well format to $0.4x10^6$

Overall, the handmade 96-well HSEs were reproducible across multiple donors and representative of human skin, therefore this platform could potentially be used for *in-vitro* testing of immunotoxicity. However, there are some practical issues with the transwell inserts. Efficiently raising the HSEs to the air-liquid interface without damaging the epidermis or leaving residual basal media atop the HSE is more technically demanding than for the 24-well system. Additionally, due to the nature of the transwell inserts acquiring sections for histology is also difficult as illustrated in Figure 2.9 of Chapter 2, section 2.10.2. As the Alvetex scaffold cannot be separated from the transwell insert without peeling of the epidermis from the HSE, it was necessary to paraffin embed the transwell cradle along with the Alvetex scaffold. The processing of multiple models is tedious while sectioning blocks containing plastic results in paraffin blocks heating up and microtome blades dulling at a faster rate than when sectioning standard tissue. As the paraffin block heats up, the resulting sections lose stability causing distortion such as ripples, fold and tears which ultimately damages the scaffold and the tissue of interest. To develop a high throughput assay alternative forms of analysis than histology would be necessary as the process of individually fixing, dehydrating, paraffin embedding, sectioning, and staining each model is both technically demanding and time-consuming.

To summarise, this chapter presents an iteration of the Skimune3D® HSE which has been further scaled down in size to the 96-well format. This scaled down HSE requires fewer dermal fibroblasts and epidermal keratinocytes to produce a structure repetitive of previous iterations of the technology and of human skin. The combination of fewer cells and smaller seeding volumes present a platform which is ideal for solenoid valve based bioprinting of HSEs.

Chapter 5 Bioprinting of a 96-well Skin Equivalent

5.1 Introduction

This chapter establishes the parameters for the bioprinting of human dermal equivalents and subsequent bioprinting of human full-thickness skin equivalents. The structure of the bioprinted human skin equivalents (HSEs) were stained using basic histological and immunohistological techniques to visualise dermal extra-cellular matrix (ECM) and epidermal markers. Finally, the functional use of Skimune3D® as a predictive *in-vitro* tool for the identification of immunotoxic therapeutic antibodies was assessed by examining cytokine expression. The aims of the work presented in this chapter were:

1. Optimise the bioprinting of skin cells to reproduce the 96-well Skimune3D® HSE.
2. Analyse the structure of the bioprinted HSEs to detect dermal extra-cellular matrix (ECM) and epidermal markers.
3. Investigate the use of Skimune3D® HSEs to detect immunotoxicity of monoclonal antibodies *in-vitro*.

5.2 Results

5.2.1 Optimisation of printing parameters

The volume dispensed per droplet at varying dwell times and positive pressures is shown in Figure 5.1. Three main observations can be made: (i) a dwell time of less than 100 µs produces no output, (ii) the volume per droplet generally increases with pressure, and (iii) the volume per droplet generally increases with dwell time.

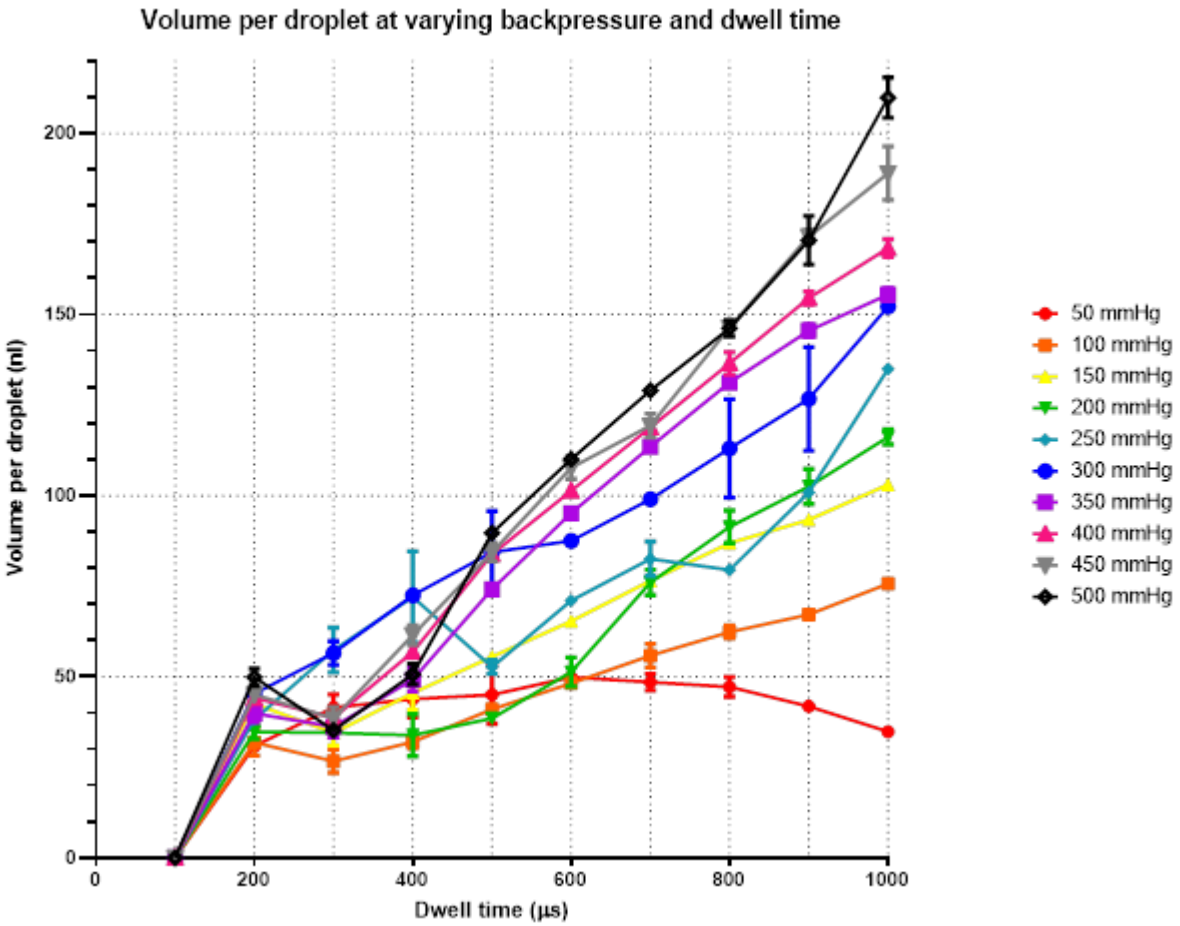

Figure 5.1. Mean volume of media dispensed per droplet at varying dwell time and positive pneumatic pressure. *Dispensing of media at different dwell times and back pressures. Error bars represent standard deviation. Some error bars could not be shown as they were smaller than the data symbols.*

When printing with a positive pressure of 50mmHg no media was dispensed at a dwell time of 100µs. As the dwell time increased the volume per droplet also increased peaking at 49.8nl at 600µs. When the dwell time was further increased from 600µs to 1000µs the mean volume per droplet steadily decreased. At 100mmHg of pressure media was not dispensed when printing with a dwell time of 100µs. The droplet volume decreased from 200µs to 300µs though steadily increased with the increasing dwell time peaking at a volume of 75.7nl per droplet when printing with a dwell time of 1000µs. Printing with a positive pressure of 150mmHg no droplets were deposited with a dwell time 100µs. As the dwell time was increased the mean droplet volume steadily increased with little variation except for printing at 300µs. The volume per droplet at 200mmHg steadily increased from 400µs to 1000µs dwell time with some variability. At 250mmHg the mean volume per droplet fluctuated from 400µs to 800µs dwell then sharply increased, topping with a mean volume per droplet of 135nl at a dwell time of 1000µs. The mean volume per droplet at 300mmHg of pressure progressively

increased as the dwell time was increased with some variability at 800µs and 900µs dwell time. The largest volume dispensed per droplet at 300mmHg was 152nl when the dwell time was 1000µs. Increasing the backpressure to 350mmHg was also resulted in an increase in the mean volume dispensed per droplet as the dwell time was increased however a dip in the volume per droplet was observed at a dwell time of 300µs. This trend was also observed when the pressure was increased to 400mmHg, 450mmHg and 500mmHg with the respective maximum volume per drop observed to be 168nl, 189nl and 209.8nl. Overall, the data suggested that a wide range of pneumatic pressures and dwell time combinations droplets could be dispensed with good consistency. As pressure and dwell time increased increases in standard deviation were recorded, suggesting that lower parameters would for a robust and reproducible printing process. Statistically parameters printed with 150mmhg were some of the most consistent with little standard deviation. Lower pressures were also preferred to reduce potential shear stress of cell during printing. Therefore, a pressure of 150mmHg and a dwell time of 900µs resulting in a mean volume per droplet of 89.9nl was used for the experiments described in the rest of this chapter.

5.2.2 Bioprinting of dermal fibroblasts

A study was designed to explore the capacity of the modified bioprinter to print a cell laden bio-ink. This study investigated the bioprinting of bio-inks with increasing concentrations of primary fibroblasts (1 x 10^6/mL, 10 x 10^6/mL, 20 x 10^6/mL and 40 x 10^6/mL) without any bio-ink purges to investigate the number of cells dispensed into multiple wells of a 24-well plate over 60 minutes. The aim of this study was to establish a range of printable cell laden bio-inks. The total cell count and cell viability was observed with a haemocytometer as described in section 2.8 of chapter 2. Viability was assessed using a trypan blue exclusion assay. Cells from three separate donors were printed and counted.

The cell count (number of cells counted) of fibroblasts printed over time is shown in Figure 5.2. The inks containing 1x10^6 cells/mL and 10x10^6 cells/mL reliably dispensed cells over 60 minutes although there was some variation in the number of cells counted at 15 minutes with both inks (Figure 5.2). As the cell concentration within the ink increased to 20x10^6 cells/mL the initial cell count w\as greater than anticipated. The cell count at 0 minutes was 2.89x10^6 which dropped to 2.25x10^6 at 15 minutes. The cell counts further decreased ending with a mean of 1.88x10^6 by 60 minutes. When printing a cell concentration of 40x10^6 cells/mL the cell count consistently decreased

at each time point. At first $4.95x10^6$ cells were printed at 0 minutes, this number decreased with each time point to $4.56x10^6$, $3.96x10^6$, $3.34 x10^6$ $2.57x10^6$ cells printed at 15, 30, 45 and 60 minutes, respectively. The increase in standard deviation at a higher cell concentration ($40x10^6$ cells/mL) and the decrease in the number of ells printed over time suggested that some degree of cell sedimentation was occurring during printing.

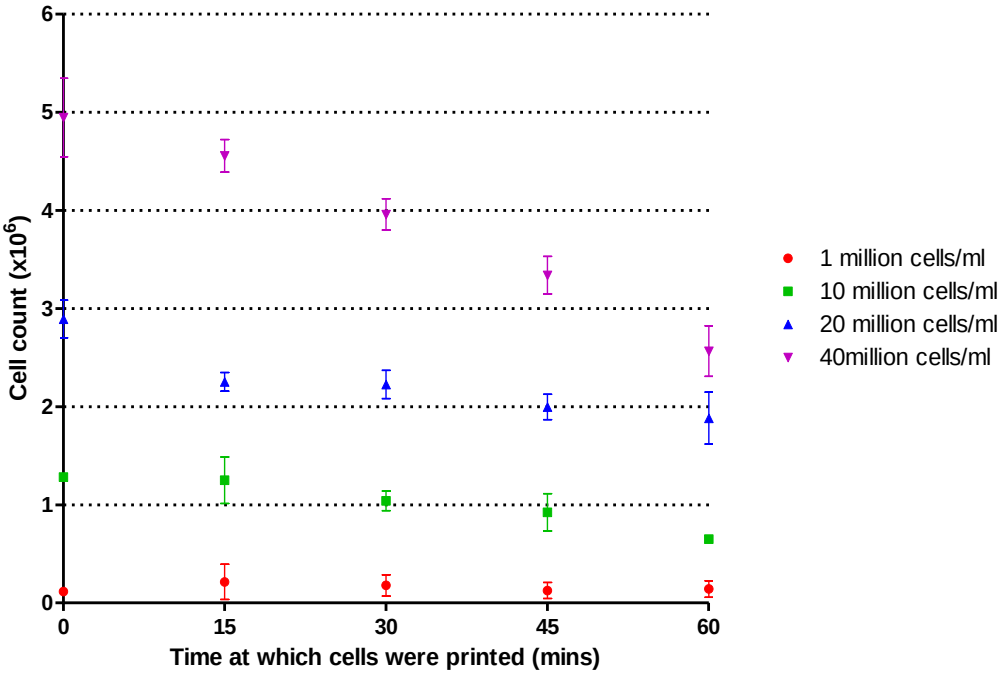

Figure 5.2. Cell count of fibroblasts bioprinted at 15 minute intervals. *The total number of cells printed and counted at time point 0, 15, 30, 45 and 60 minutes after loading into the printer reservoir. Error bars indicate standard deviation. N=3.*

The cell counts for each cell concentration were compared to anticipated cell count this is shown in table 5.1. For bio-inks containing fibroblasts at concentrations of $1x10^6$/mL, $10x10^6$/mL, and $20x10^6$/mL mean cell counts close to expected cell numbers with reasonable variation. This data suggests that the cell laden bio-inks remained stable meaning that the cells remained in suspension and were dispersed adequately in the respective inks over 60 minutes. While the cell count of inks containing $40x10^6$ fibroblasts per mL was close to the expected number of cells the variation was poor. The increase in standard deviation (Table 5.1) suggested that the bio-ink was relatively unstable during printing.

Table 5.1. Mean cell count and standard deviation of fibroblasts. *Mean and standard deviation of bioprinted fibroblasts at various bio-ink concentration. N=3.*

Bio-ink cell concentration ($x10^6$)	Expected cell count ($x10^6$)	Mean cell count over all time points ($x10^6$)	Standard deviation
1	0.1	0.155	0.0984
10	1	1.03	0.269
20	2	2.25	0.391
40	4	3.87	0.905

The mean viability of cells in the bio-inks over time can be seen in Figure 5.3. Generally, the viability of the cells in the bio-inks decreased over time. At 0 minutes the lowest viability recorded was 92%. After 15 minutes the lowest cell viability was recorded to be 86%. As time progressed further loss of cell viability was observed across all bio-inks. By 60 minutes cell viability for all bio-inks ranged from 73-79%.

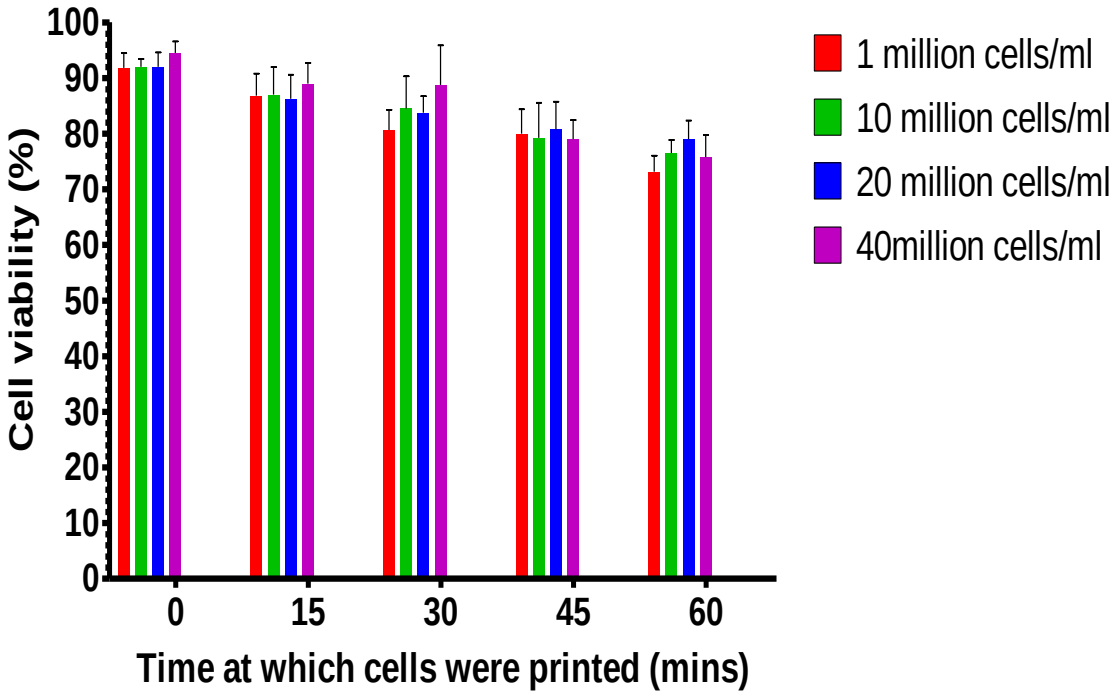

Figure 5.3 Mean viability fibroblasts bioprinted at several time points. *The viability of fibroblasts printed at time point 0, 15, 30, 45 and 60 minutes. Error bars indicate standard deviation. N=3.*

Overall, the data from this study suggested that there was some degree of sedimentation of cells when printing bio-inks containing cells at 20 million cells/mL and 40 million cells/mL. The bio-inks that containing fewer cells produced a stable output over 60 minutes, with the mean number of cells printed over 60 minutes close to the number of expected cells. However, the standard deviation increased as the cell concentration of the bio-inks increased (Table 5.1). The viability of the printed cells remained ideal within the first 30 minutes of printing. However, cells printed after 30 minutes displayed a greater loss in viability as time progressed.

5.2.3 Bioprinting of epidermal and dermal skin cells

The next steps required to bioprint HSEs, was to print the correct number of primary dermal fibroblasts and primary keratinocytes to replicate the number of cells manually seeded when producing a 96-well format Skimune3D® HSE. Like the previous study the aim was to prepare, and print bio-inks containing fibroblasts or keratinocytes and compare the output to the number of cells required per 96-well scaffold. The methodology used to calculate the number of droplets required to print 20 µL per well (capacity of transwell inserts) is defined in section 2.7.4. Using equation 3 in section 2.7.4 the size of the array needed to print 20 µL was found to be 15 droplets by 15 droplets. This methodology was also applied to the work which followed this study. The cell counts for both the fibroblasts and keratinocytes printed into the wells of a 96-well plate can be seen in Figure 5.4. The mean cell count across wells and the standard deviation are shown in Table 5.2. The dermal bio-ink containing fibroblasts at a concentration of $25x10^6$/mL reliably dispensed across wells (Figure 5.4). The mean fibroblasts cell count across all wells was $4.7x10^5$±0.4 (Table 5.2). The bio-ink containing keratinocytes was also consistent across wells with a mean cell count of $3.53x10^5$±0.17. The mean viability of both cell types across three biological replicates is shown in Figure 5.5. The mean viability of the printed fibroblasts was 92±3%. The mean viability of the printed keratinocytes was 82±9%.

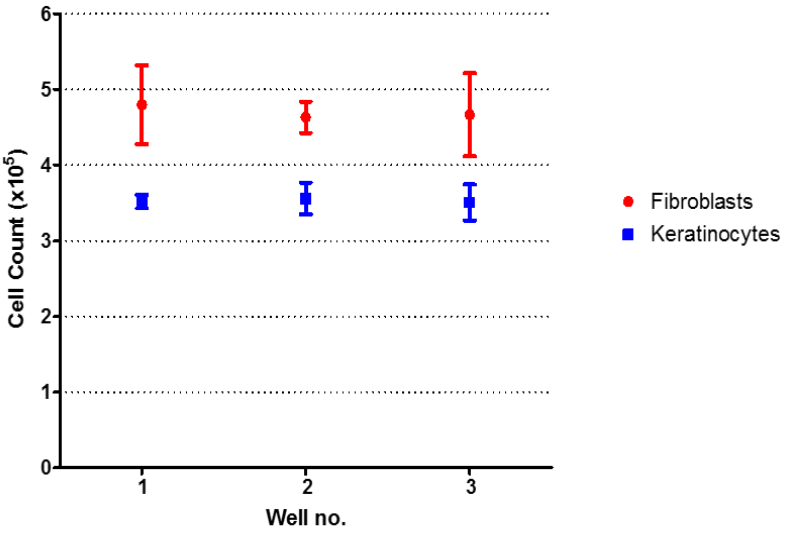

Figure 5.4. Cell counts of bioprinted skin cells. The mean cell counts of printed fibroblasts and keratinocytes across 3 wells. N=3.

Cell type	Bio-ink cell concentration ($x10^6$/mL)	Required cell count ($x10^5$)	Mean cell count ($x10^5$)	Standard deviation
Fibroblasts	25	5	4.7	0.4
Keratinocytes	20	3.5	3.53	0.17

Table 5.2. Mean cell count and standard deviation of cells printed over a period of 60 minutes. *Mean and standard deviation of bioprinted fibroblasts at various bio-ink concentration. N=3.*

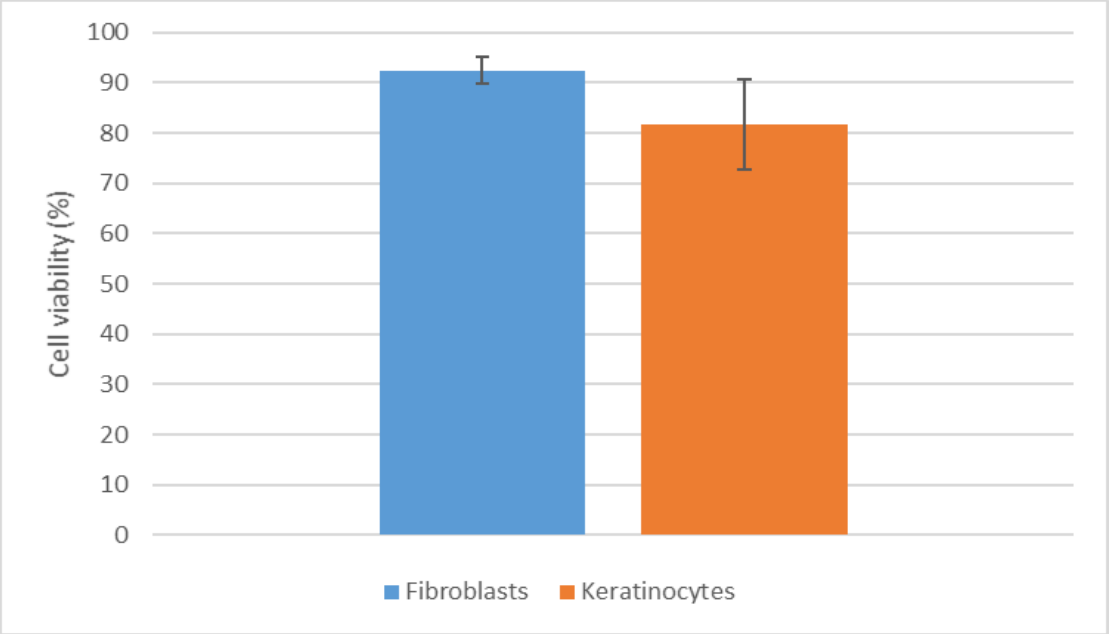

Figure 5.5 Mean viability of bioprinted fibroblasts and keratinocytes. *The viability of both fibroblasts and keratinocytes. Error bars indicate standard deviation. N=3.*

5.2.4 Bioprinting of human full-thickness skin equivalents

To bioprint a 96-well based full-thickness skin equivalent the parameters, ink formulations and array size stablished in sections 5.2.1, 5.2.2 and 5.2.3 were used to sequentially print dermal and full-thickness skin equivalents. The culture media and incubation conditions use were defined in section 2.6.2. The resulting dermal and full-thickness HSEs were formalin fixed, paraffin embedded, sectioned, and stained. Haematoxylin and eosin (H&E) staining was used to visualise the overall structure of the HSEs.

Representative images of H&E stained bioprinted dermal and full-thickness HSEs are shown in Figure 5.6. The representative bioprinted dermal equivalent displayed in Figure 5.6a shows a good distribution of cells throughout the scaffold. A consistent layer of dermal fibroblasts could be seen lining the top surface of the scaffold. Within the scaffold clusters of cells could be seen near the upper surface of the Alvetex®. The number of cells within scaffold increased towards the bottom of the scaffold. Underneath the scaffold a thick layer fibroblast was visible. Fibres of eosin stained ECM produced by the fibroblasts were also observed with the scaffold. The representative H&E stained full-thickness HSE can be seen in Figure 5.6B. The dermis of the full-thickness HSE was well populated with thick layers of fibroblasts above and

beneath the scaffold. A dense and even distribution of dermal fibroblasts could be seen within the scaffold. The epidermis of the HSE contained visible basal, spinous, granular and a very thin stratum corneum. The basal layer was located directly above the dermal-epidermal junction indicated by the dotted line, although this layer was inconsistent. The differentiating and superficially migrating keratinocytes formed a spinous layer. The layer of granular cells indicated by the darker and slightly speckled haematoxylin stained nuclei which separated during sectioning was located above the spinous keratinocytes.

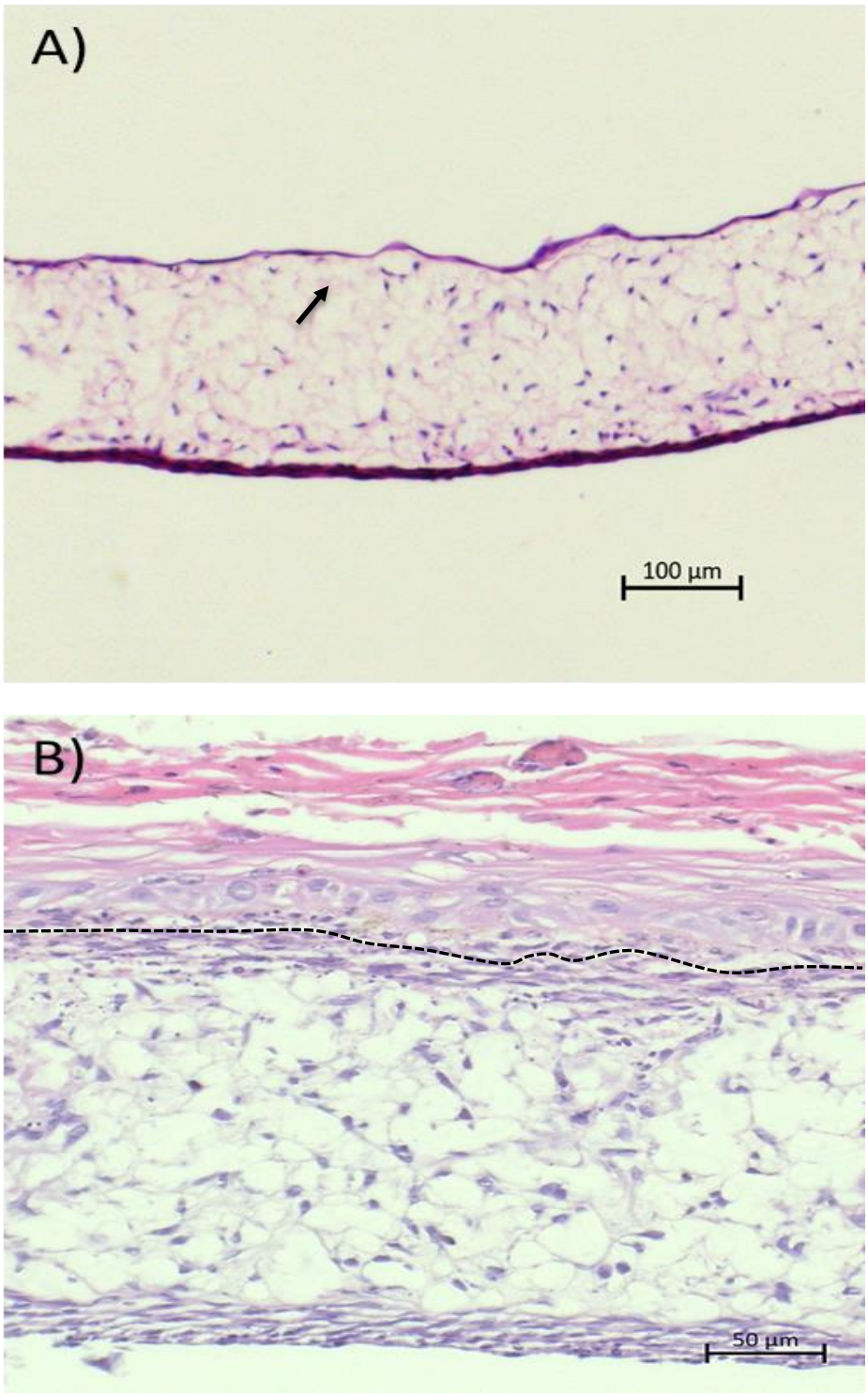

Figure 5.6. Representative images of haematoxylin and eosin stained bioprinted dermal and full-thickness HSEs. *A) Representative image of a bioprinted dermal equivalent, black arrow indicates ECM. B) Representative image of a H&E stained full-thickness skin equivalent. Dotted line indicates dermal-epidermal junction. Scale bar: 50 µm.*

5.2.5 Structural validation of human skin equivalents

In addition to H&E staining bioprinted full-thickness HSEs were also stained with Picro-Sirius red to detect dermal collagen, periodic acidic-Schiff (PAS) to stain muco-substances found in basement membranes and Verhoeff-van Gieson staining to distinguish any elastin fibres from collagen. The representative images of bioprinted 96-well HSEs are presented in Figure 5.7. Picro-Sirius red staining of bioprinted full-thickness skin equivalents showed that the dermis was heavily loaded with collagen as expected (Figure 5.7A). Large thick cross-linked collagen layers could be seen directly beneath the epidermis at the dermal epidermal junction. This layer of collagen could be seen across the dermis, supporting the formation of an epidermis. Collagen within the scaffold was stained with less intensity and visually appeared smaller within the dermis much like physiological human skin (Ueda et al. 2019). The cell nuclei and cytoplasm were stained dark orange rather than yellow due to over exposure to ethanol during stain differentiation and section dehydration. A sheet of cross-linked collagen was also visible at the bottom of the scaffold. Verhoeff–Van Gieson staining of bioprinted full-thickness HSEs (Figure 5.7B) did not reveal any elastin fibres or precursors which would have stained grey/black present in the dermis. The PAS detected glycoproteins (black arrows) however this was not representative of a uniform basement membrane at the dermal-epidermal junction (Figure 5.7C).

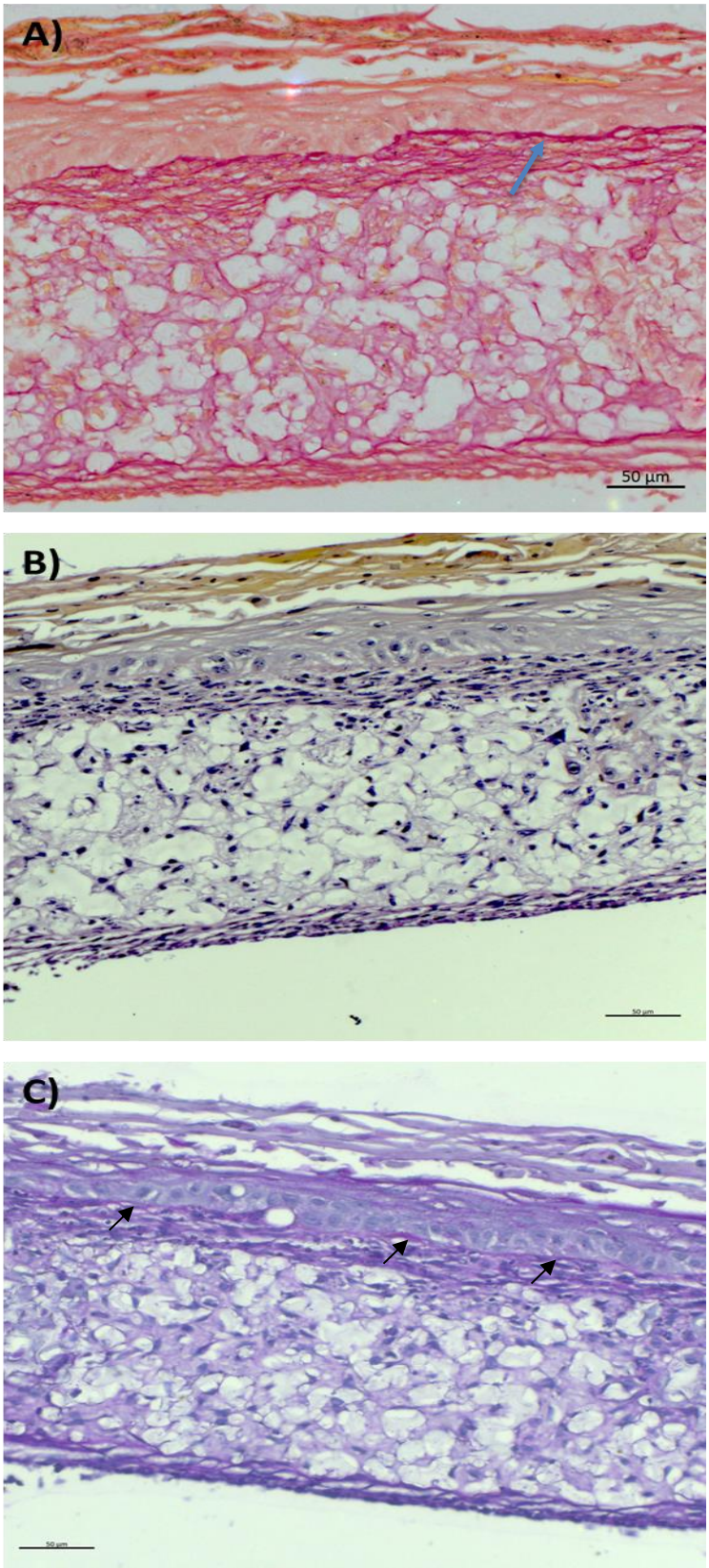

Figure 5.7. Representative images of bioprinted HSEs stained with Picro-Sirius red, periodic acidic-Schiff, and Verhoeff-van Geison staining. *A) Picro-Sirius red staining, blue arrow indicates cross-linked collagen mesh at dermal-epidermal junction. B) Verhoeff-van Geison staining. C) Periodic acidic-Schiff staining. Black arrows indicate glycoproteins. Scale bars: 50µm*

Immunofluorescence staining was used to stain different markers present throughout the different layers in the epidermis of bioprinted full-thickness HSEs (Figure 5.8). The negative control is shown in Figure 5.9. Cytokeratin 14 (CK14) was detected directly above the dermal-epidermal junction (white dotted line) indicating the presence of basal keratinocytes at the dermal epidermal junction. Basal keratinocytes begin superficially migrate, stratify and express cytokeratin 10 (CK10) when undergoing differentiation. CK10 was positively detected above basal keratinocytes indicating stratification and the formation of a spinous strata. Involucrin which is expressed in the same regions as CK10 was also detected above the basal strata. Loricrin which is present in the corneal envelope of the epidermis was also detected in the bioprinted HSEs. Overall, the bioprinted full-thickness HSEs featured the relevant epidermal differentiation markers within the correct regions of the epidermis showing that the HSE's comparable to handmade 96-well HSEs.

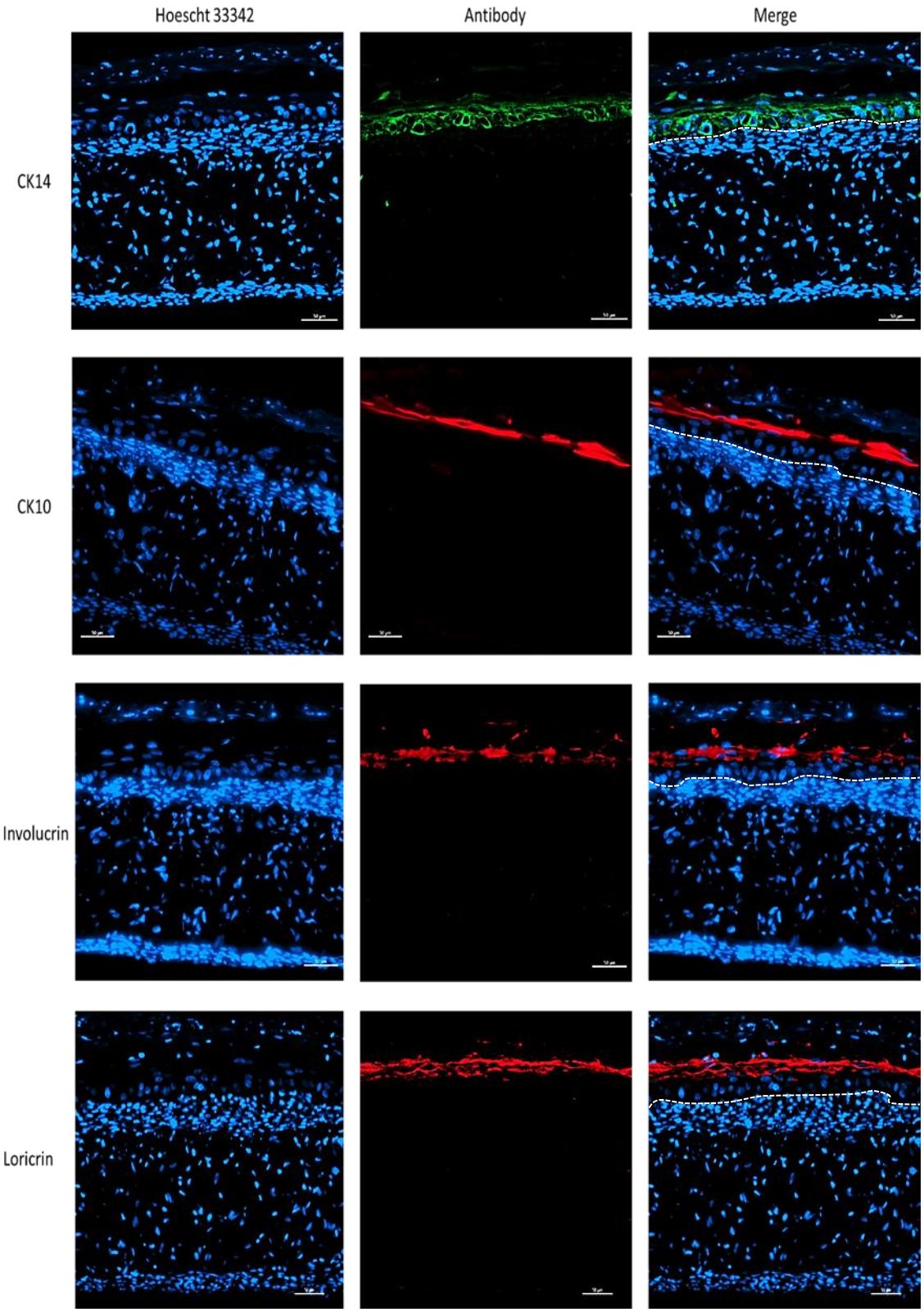

Figure 5.8. Representative images of immunofluorescent stained bioprinted full-thickness HSEs. *HSEs stained for CK14 (green), CK10 (red), involucrin (red) and loricrin (red). Cell nuclei were stained blue with Hoechst 33342. Scale bars: 50µm.*

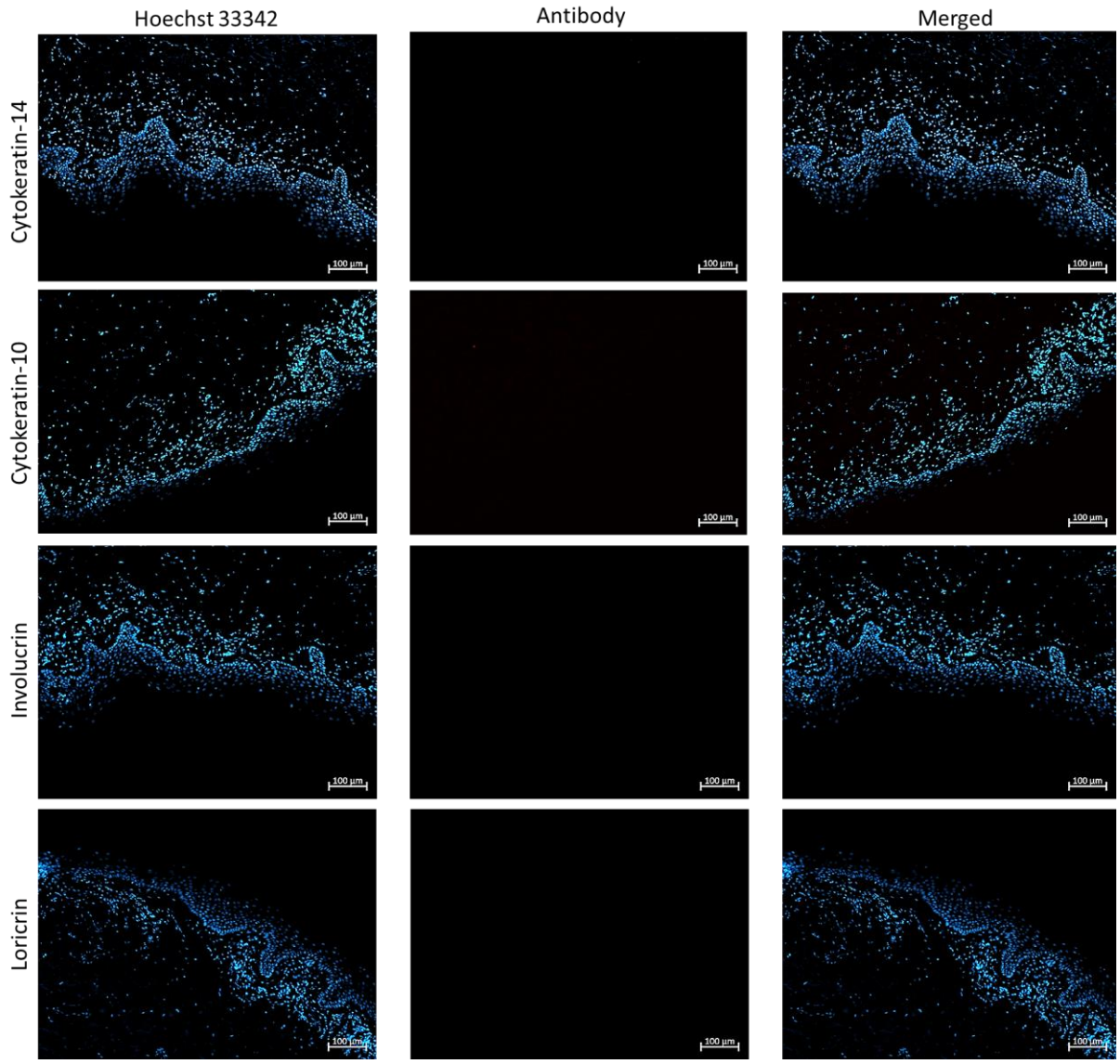

Figure 5.9. Null primary (negative control) images for immunofluorescent staining of bioprinted HSEs. *Blue nuclear staining shown using Hoechst 33342. Scale bars: 100µm.*

5.2.6 Functional in-vitro validation of human skin equivalents

Once the relevant epidermal markers were detected and the development of a human full-thickness HSE confirmed, it was necessary to demonstrate the feasibility for *in-vitro* applications of the bioprinted full-thickness Skimune3D® HSE. This required the bioprinting of fully autologous HSEs using the parameters identified earlier in this chapter. The bioprinted HSEs were co-cultured with autologous peripheral blood monocytes (PBMCs) which were isolated from donor whole blood as described in section 2.5. The methodology for establishing the co-culture was described in section 2.9. The aim of this study was to establish an *in-vitro* platform which could be used to test therapeutic antibodies. As discussed in chapter 4, qualitative histological analysis of HSEs to identify proinflammatory immunotoxic reactions would not be feasible. For this reason, the levels of proinflammatory cytokines present within the supernatants of the co-cultures were quantified across three biological donors. Proinflammatory cytokines were quantified as expression of the cytokines would be elevated during an immune response, allowing the immunotoxicity of the monoclonal antibodies to be compared. The mean concentrations of the proinflammatory cytokines are presented in Figure 5.10. Analysis of supernatants for interferon gamma (IFN-γ) revealed elevated IFN-γ levels in co-cultures treated with Muromonab-CD3 (OKT3). Levels of IFN-γ secretion from OKT3 treated co-cultures were significantly increased ($p<0.0001$) when compared to controls and Tysabri. The detected levels of interleukin-10 (IL-10) were also elevated in OKT3 treated co-cultures. This level of secretion was significant ($p<0.01$) when compared to the media control. Secretion of interleukin-12 p70 (IL-12p70) and interleukin-13 (IL-13) were consistent across all co-cultures and no statistical significance was observed. Interestingly analysis of interleukin-1 beta (IL-1β) secretion showed very little secretion from media control cultures while the other conditions showed high variability, no significance between conditions was observed. Secretion of interleukin-2 (IL-2) was shown to be increased in OKT3 co-cultures. This level of secretion was significant ($p<0.01$) when compared to the media and isotype controls. Interleukin-4 (IL-4) levels were found to be relatively steady across conditions with no statistical significance. Secretion of interleukin-6 (IL-6) was elevated in all co-cultures with little variation between conditions. Tumour necrosis factor alpha (TNF-α) levels of OKT3 treated co-cultures were significantly increased ($p<0.01$) when compared to the media control.

The production of and application of each cytokine quantified from the supernatant of the autologous co-cultures is summarised in table 5.3. The elevated IL-2 levels in OKT3 (Muromonab) treated levels were significant when compared to the media and isotype controls, suggesting an OKT3 induced T cell response. This links to IFN-γ expression in OKT3 treated co-cultures, where T cells activated by IL-2 could then increase expression of IFN-γ. Interestingly, there was no statistical significance in secretion of both IL-4 and IL-13. IL-4 and IL-13 are both associated with a Th2 type response (Berger 2000; Swain *et al*. 1990), and the lack of expression of IL-4 and IL-13 suggests that a Th2 immune response was not induced. The elevated expression of TNF-α is comparable to the use of OKT3 *in-vivo* while the levels of TFNα, IFN-γ and IL-2 are similar to cytokine profiles generated in *in-vitro* (Gaston *et al*. 1991; Römer *et al*. 2011). This study indicates that it is feasible to use fully humanised full-thickness bioprinted HSEs to identify the immunotoxicity of monoclonal antibodies *in-vitro* by multiplex quantification of cytokines to create a cytokine profile.

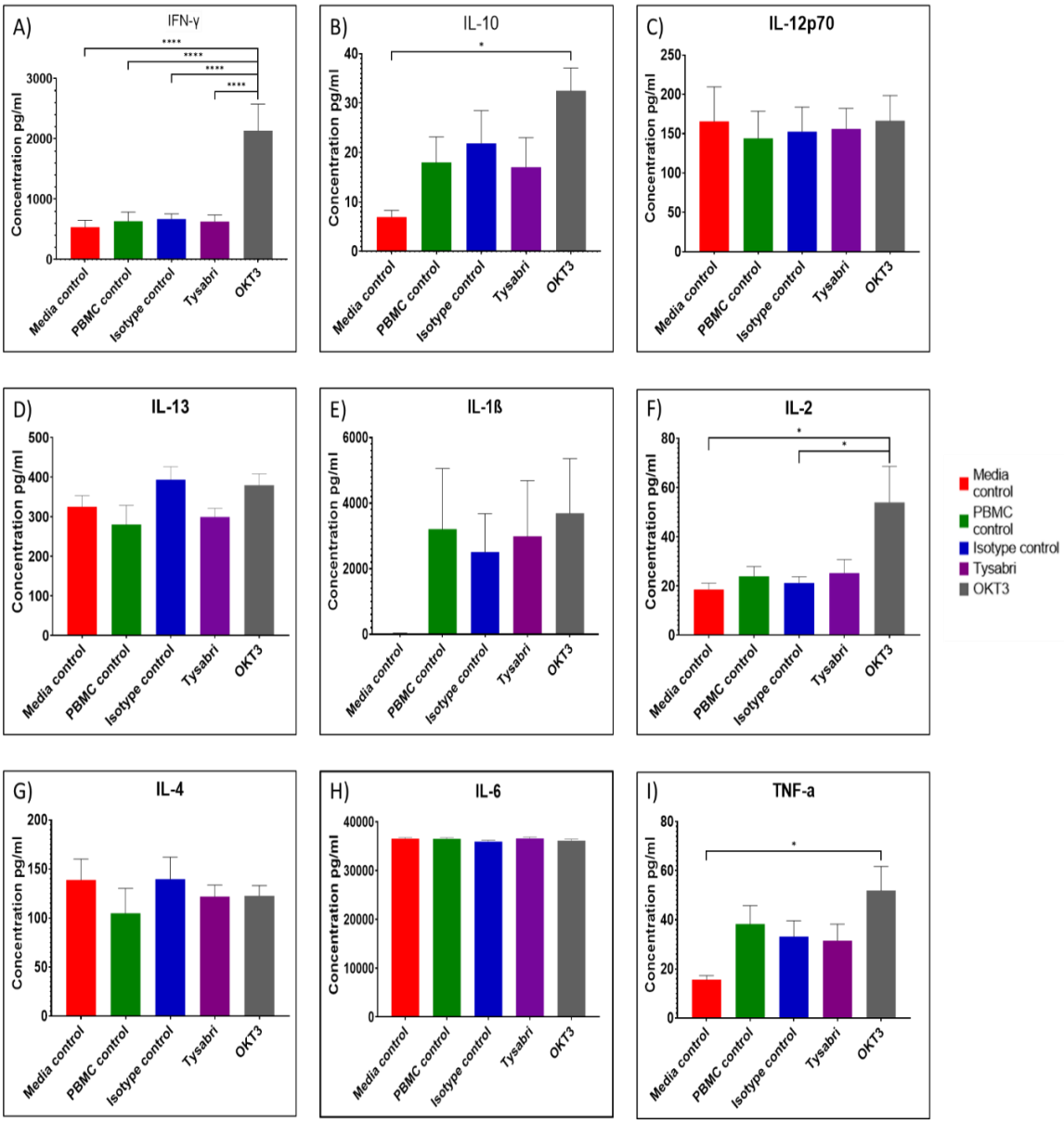

Figure 5.10. Mean proinflammatory cytokine concentrations from autologous co-cultures. *The concentrations of cytokines detected from the supernatants of autologous co-cultures. Detected concentrations of interferon gamma (IFN-γ), interleukin-10 (IL-10), interleukin-12 p 70 (IL-12p70A), interleukin-13 (IL-13), interleukin-1 beta (IL-1β), interleukin-2 (IL-2), interleukin-4 (IL-4), interleukin-6 (IL-6) and tumour necrosis factor alpha (TNFα) are shown in (A),(B) (C), (D), (E), (F), (G), (H), and (I) respectively. Statistically significant differences between conditions are indicated by * and **** which represent p values of $p < 0.05$ and $p < 0.0001$ respectively.*

5.3 Discussion

The bioprinted dermal and full-thickness HSEs were similar in structure to handmade HSE produced in 96-well and 24-well formats (Figure 5.11). The fibroblast ECM layer lining the top of the bioprinted dermal HSEs was not only capable of withstanding the forces of dispensed droplets but also supported the formation of an epidermis without keratinocytes infiltration of the dermis. The arrangement of dermal collagen was identical to handmade dermal equivalents produced in the 96-well and 24-well format. The loose and unorganised arrangement of dermal collagen within the scaffold was similar in nature to the ECM structure of the papillary dermis of physiological human skin as presented in Chapter 3. When comparing the structure of the bioprinted tissue to previously handmade HSEs and physiological human skin (Figure 5.11) is shown that the bioprinted tissue is similar in structure to handmade HSEs and human skin.

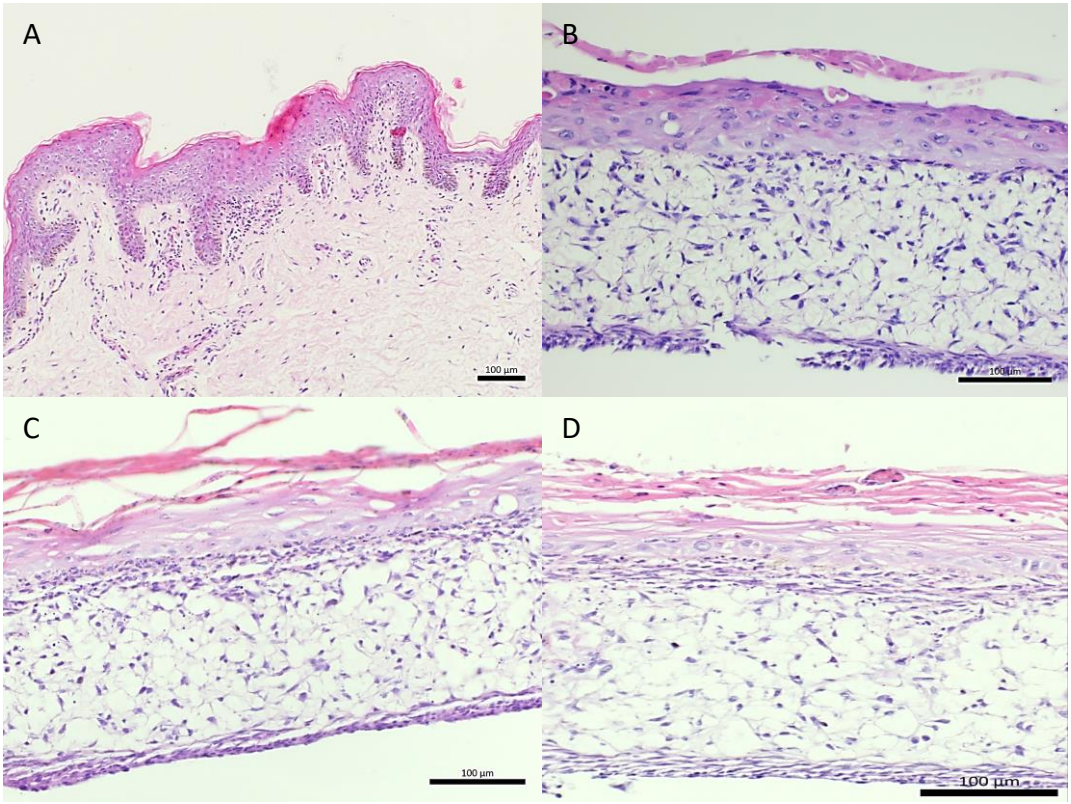

Figure 5.11. Comparison of the bioprinted HSE to other HSEs in this thesis and to human skin. *A) Physiological human skin. B) Handmade 24-well HSE. C) Handmade 96-well HSE. D) Bioprinted 96-well HSE. Scale bars: 100µm.*

Verhoeff–Van Gieson staining of bioprinted HSEs did not reveal any elastin fibres or elastin precursors as expected. Interestingly, PAS did positively detect the presence of glycoproteins in the bioprinted HSEs, however this did not indicate the formation of a full and consistent basement membrane at the dermal-epidermal junction. The basement membrane consists of collagen type IV, collagen type VII, laminins, nidogens and perlecan (Breitkreutz et al. 2013; Morrissey and Sherwood 2015).

Collagens type IV, type VII and perlecan are synthesised by both fibroblasts and keratinocytes and cannot be distinguished from the dermal collagen synthesised by fibroblasts within the HSEs (Morrissey and Sherwood 2015). Nidogens are primarily synthesised by the dermal fibroblasts (Breitkreutz et al. 2013) while keratinocytes are responsible for production of laminin-332 and laminin-551 are produced by the epidermal keratinocytes (Morrissey and Sherwood 2015; Sugawara et al. 2008). The regions of the dermal-epidermal junction in bioprinted HSEs with poor glycoprotein staining also featured an inconstant stratum basale. Additionally, missing components of the basement membrane at the dermal-epidermal junction has been linked to the apoptosis of basal keratinocytes (Sher *et al*. 2006), potentially explaining the formation of vacuoles in the epidermis of the HSEs. Alternatively, such vacuoles may simply be due to the primary keratinocytes undergoing senescence after prolonged culture. Senescent keratinocytes could in turn limit the production of a full basement membrane as healthy basal keratinocytes are necessary to from the structure of a basement membrane (Morrissey and Sherwood 2015; Sugawara et al. 2008). Differentiation and stratification of the epidermis was characterised by positive staining for cytoskeletal keratins, cornified envelope precursors and a marker of a cornified envelope by immunofluorescent staining. Staining for basal CK14 and supra-basal CK10 confirmed the formation of both the basal and spinous strata's confirming epidermal stratification. Staining for involucrin revealed the presence of a precursor marker for the cornified envelope while positive detection of loricrin suggested the formation of a cornified envelop. Overall, this data suggests that the bioprinted HSEs were representative of handmade HSEs and human skin.

The modified Jetlab system retrofitted with solenoid micro dispensing valves demonstrated that droplet volumes could easily be manipulated by influencing the dwell time of the solenoid valve and the backpressure applied to the bio-ink reservoir. With the possibility to create a fold increase in droplet volume of greater than 7 (26.6 µL at 100µs with 100mmHg to 209.8 µL at 1000µs and 500mmHg) this bioprinting platform exhibits some degree of flexibility. The output of the bioprinting system could be further increased as the maximum dwell time achievable with the Jetlab is 3276µs and maximum backpressure achievable 800mmHg. Increasing these parameters increases volume per droplet and decreases the number of droplets required per print, therefore reducing total deposition time which is preferable for a high throughput printing process. However, there may be some disadvantages to increasing the volume

per droplet. As the volume of each droplet increases the droplet also become larger in size resulting in elongation of droplet. This can lead to the formation of ligaments and satellite droplets. The formation of satellite droplets can impact the impact the accuracy of deposited droplets and further reduce printing resolution (Jang, Kim, and Moon 2009). The capability of the retrofitted Jetlab platform to dispense droplets in the range of nanolitres is comparable to other studies investigating the use of solenoid microvalves for bioprinting (Faulkner-Jones *et al*. 2013; Keriquel *et al*. 2017; Okubo *et al*. 2019). As expected microvalve based deposition produced a larger volume per drop than other typical drop-on-demand (DOD) processes such as inkjet and laser assisted bioprinting (LABP) which offer picolitre level resolution (Sekitani *et al*. 2008; Singh *et al*. 2010). This lower resolution per droplet is necessary for high through put deposition of cells at the concentrations required to create a bioprinted HSE.

The inclusion of an agitation system to the bio-ink reservoirs allowed the Jetlab to reliably dispense cell laden bio-inks over a 60-minute period. The large number of cells printed initially with bio-inks containing $20x10^6$ cells/mL and $40x10^6$ cells/mL was largely attributed to the settling of cells within the reservoir into the valve inlet immediately after loading inks into the reservoir cartridge and before activation of the agitation system. The reproducibility of the number of cells dispensed at $20x10^6$ cells/mL was ideal but was not achieved with the bio-ink containing $40x10^6$ cells/mL. However, this reproducibility may also be achieved when printing cells at higher concentrations. For applications which require a greater output reproducibility at larger cell concentrations could be improved by increasing the voltage applied to the agitator motor or by using a motor which can accommodate a higher rpm. This was not further investigated as bio-ink concentrations of $20x10^6$ cells/mL and $25x10^6$ cells/mL proved adequate for the biofabrication of HSEs. Overall, the modified Jetlab platform was shown to be capable of handling a variety of cell concentrations. The data presented in this chapter shows that this bioprinting platform could dispense cells at higher concentrations than DOD inkjet systems which typically use bio-inks containing $<10^6$ cells/mL (Murphy and Atala 2014). However, it is yet to be investigated if the modified Jetlab printer could print cells at concentrations of up to 10^8 cells/mL as reported by LABP processes (Ackermann *et al*. 2010; Guillotin *et al*. 2010; Murphy and Atala 2014). The loss in fibroblast viability over time can be associated with maintaining adherent cells in suspension at suboptimal temperatures. Furthermore, testing of cell viability immediately post printing for both primary fibroblasts and keratinocytes yielded results

that were comparable to the microvalve based work of Lee *et al,* where fibroblast and keratinocyte viability where reported to be 95±2.3% and 85.5± 5.7% (Lee *et al*. 2009). This data suggested that cell loss immediately post printing using the solenoid fitted Jetlab platform was in line with data for microvalve based printing of skin cells established in literature.

The rational for scaling down to a 96-well transwell platform was to increase the number of models that could be manufactured per donor and to potentially reduce development costs. In terms of development costs, the cost to isolate and bulk up cells for the previous 24-well format and the 96-well format was unchanged, was the lead for bulking of cells and HSE culture. However, cost per well of culture for skin equivalents from the 24-well format to 96-well format were reduced by a factor of 8 for submerged dermal and basal strata incubation, and a reduction by a factor of 10 for air-liquid interphase (ALI) incubation of HSEs. These reduction in costs were attributed to the reduction in the volume of media required from the 24-well format (1.6-1mL per HSE) to the 96-well (200µL-100 µL). As established in chapter 4 the overall number of cells required to produce a single HSE in the 96-well format was reduced from the 24-well format. This reduction in cells per HSE improved the scalability of the HSE by allowing over a three-fold increase in the number of HSE to be produced per donor (Figure 5.12). This three-fold increase could be further expanded should the issues regarding keratinocyte culture and replicative capacity highlighted in this thesis be addressed in future work. As for reproducibility, the bioprinting platform proved to be reliable and printed HSEs performed in a similar manner to the handmade HSEs during characterisation.

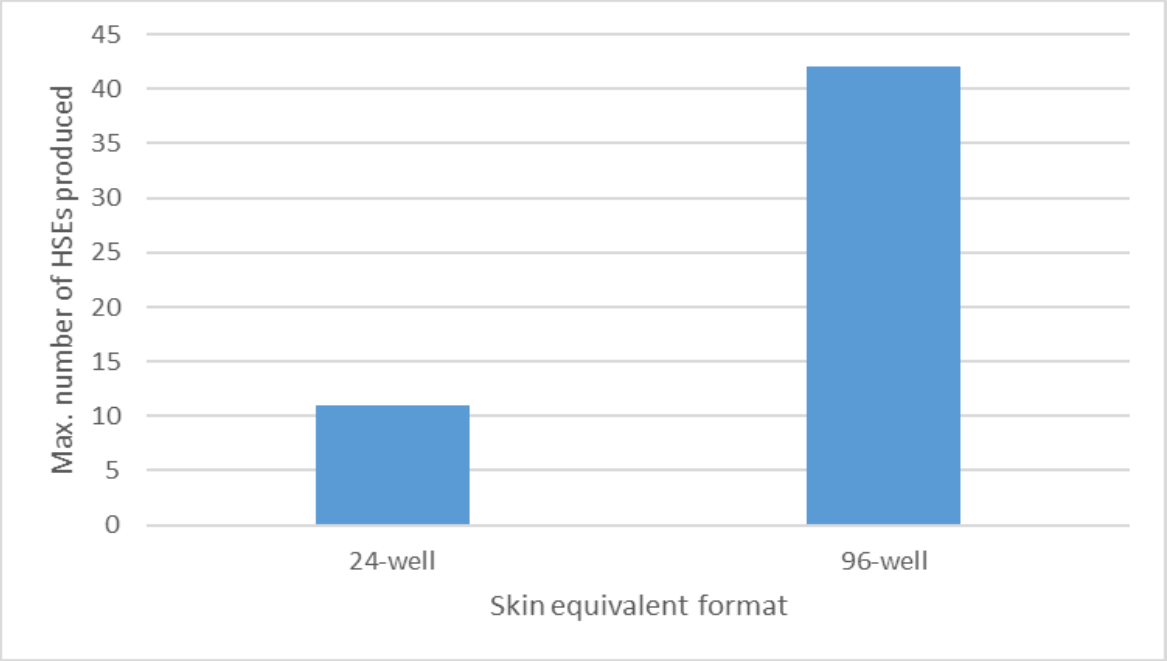

Figure 5.12. Comparing the maximum number of full-thickness HSEs manufactured from a single donor. *24-well information provided by Alcyomics.*

Cytokine	Produced by	Function	Reference
IFN- γ	CD4 T cells, CD8 T cells and natural killer (NK) cells	• Promotes antigen presentation to CD4 T cells	Billiau and Va-ndenbroeck 2001
IL-10	Macrophages, monocytes, T cells, B cells and keratinocytes	• Inhibits expression of IL-1 and TNF-α, attenuating cell mediated immune response	(Mehrotra *et al*. 1998)
IL-12p70	Activated monocytes/ macrophages	• Induces production of Th1 cells • Induces IFN-γ production	(Gately *et al*. 1993; Hsieh *et al*. 1993; Zheng *et al*. 2016)

		• Restricts IL-4 mediated IFN-γ suppression	
IL-13	Th2 cells and NK cells	• Inhibits expression of IL-1β, IL-6, IL-8, and TNF-α	Mckenzie and Matthews 2001
IL-1β	Monocytes and dendritic cells	• B cell maturation and proliferation	Dinarello 1989
IL-2	T cells	• T cell proliferation • Proliferation and differentiation of B cells, NK cells monocytes and macrophages.	(Smith 1988)
IL-4	Mast cells, T cells and mesenchymal stromal cells	• Regulates CD4 T cells differentiation into Th2 cells	(Chen *et al*. 2004)
IL-6	T cells, monocytes, fibroblasts, and keratinocytes	• Stimulates B cell differentiation and cytokine production	(Paquet and Pierard 1996)
TNF-α	Activated monocytes, macrophages, B	• Induces inflammation	(Idriss and Naismith 2000)

	cells, T cells and fibroblasts		

Table 5.3. Summary of pro-inflammatory cytokine panel. *The production and function of the cytokines quantified from the supernatants of autologous co-cultures.*

Chapter 6 General Discussion and Conclusions

6.1 Achievement of Objectives

This thesis aimed to develop handmade and bioprinted Skimune3D® human skin equivalents (HSEs) which would be comparable to human skin and to evaluate the use of the bioprinted HSEs to assess therapeutic antibodies in-vitro. As presented in this thesis the handmade Skimune3D® HSE established in the 6-well format by Hill *et al* (Hill *et al*. 2015) was successfully optimised manually to a 24-well format, manually scaled down further to a 96-well format and replicated using solenoid microvalve bioprinting (Figure 6.1).

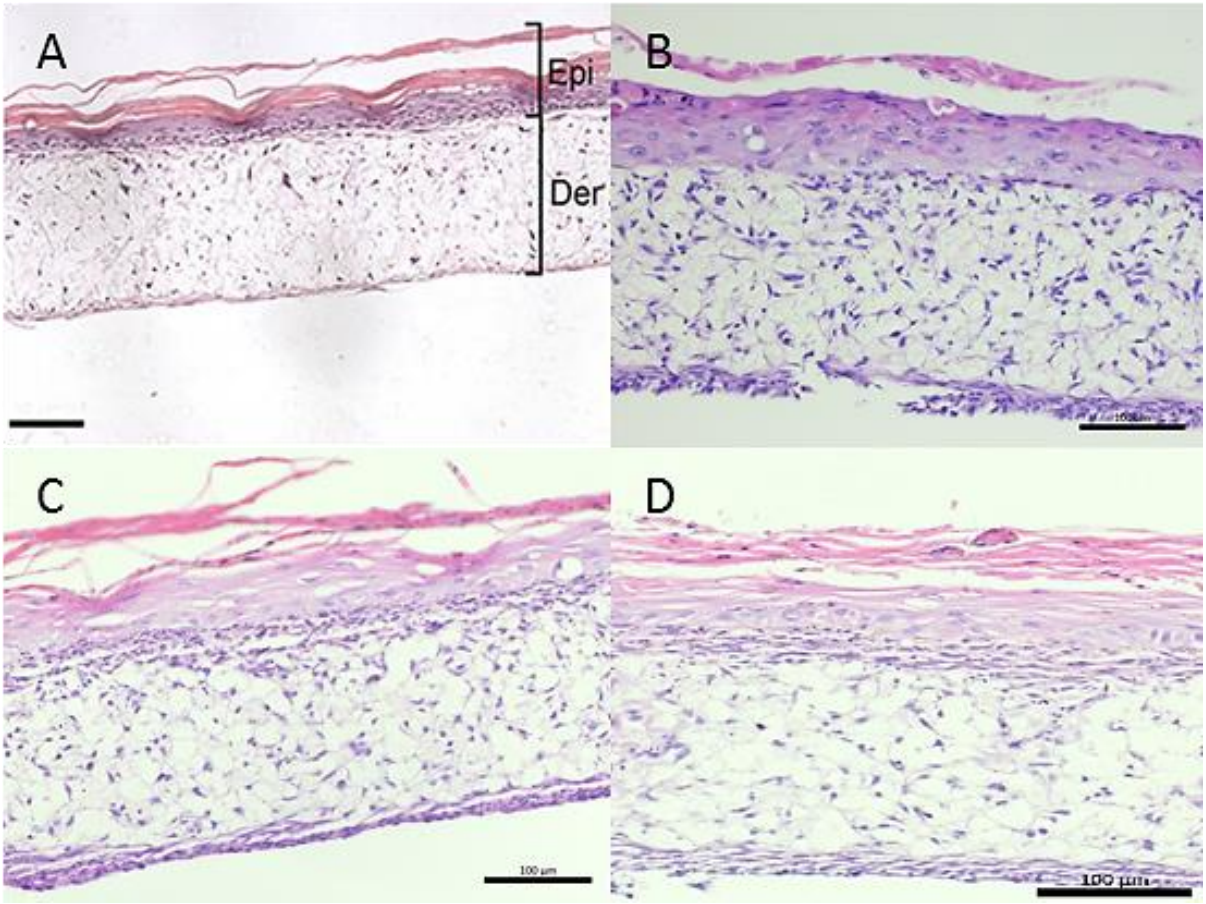

Figure 6.1. Histology of HSEs across all formats. *A) Original 6-well HSE developed by Hill et al (adapted from Hill et al 2015), Scale bar: 100µm. B) Handmade 24-well HSE, scale bar: 100µm. C) Handmade 96-well HSE, scale bar: 100µm. D) Bioprinted HSE, scale bar: 100µm.*

The structure of the handmade HSEs in both the 24-well and 96-well formats and bioprinted HSEs were compared to human skin. The dermal extra-cellular matrix ECM within the HSEs was shown to be synthesised by primary human fibroblasts. This collagen matrix was reported to be essential for the creation of a separate dermis and

epidermis (Hill *et al*. 2015). The Picro-Sirius red staining of collagen in handmade and bioprinted HSEs revealed a saturated network of collagen, largely consisting of less stained collagen, similar in nature to the papillary dermis of physiological human skin. The staining of epidermal markers such as cytokeratin-14, cytokeratin-10, involucrin and loricrin were detected in the epidermis of both the handmade and bioprinted constructs. This suggested that the epidermis of both the handmade and bioprinted HSEs were representative of human skin. This was particularly true for the handmade 24-well HSEs where the well organised epidermal strata were highly representative of physiological human skin. The scaling from a 24-well format to 96-well HSE allowed HSEs to be constructed with fewer cells whilst still being physiologically representative of physiological human skin. The number of dermal fibroblasts needed per scaffold was reduced from $2x10^6$ in the 24-well format to $0.5x10^6$ in the 96-well format, while the number of epidermal keratinocytes was reduced from $1x10^6$ in the 24-well format to $0.4x10^6$ in the 96-well format. This reduction in the number of cells per scaffold translated to an increase in the number of full-thickness equivalents that could be manufactured per donor. The bioprinted HSEs were used to determine the immunotoxicity of therapeutic antibodies *in-vitro* with the antibody Muromonab (OKT3) resulting in statistically significant expression of proinflammatory cytokines. By comparison, the therapeutic antibody Tysabri which is clinically used as an immunosuppressant did not elicit an immune response. This expression of proinflammatory cytokines revealed that it could be feasible to use bioprinted HSEs for *in-vitro* pre-clinical testing of therapeutic antibodies.

6.2 Novelty

There is an increasing interest in the development of bioprinted tissue for the *in-vitro* assessment of therapeutics although, to date, there is no bioprinted HSE which are commercially available or otherwise available in a 96-well format (Ma *et al*. 2018; Mazzocchi, Soker, and Skardal 2019). The successful bioprinting of Skimune3D® in a 96-well format as reported in this thesis provides a foundation for future work to manufacture HSEs on an industrial scale. To the best of our knowledge this thesis describes the first example of *in-vitro* testing of therapeutic antibodies using a 96-well bioprinted, fully human, full-thickness HSE. To date there have been many attempts to bioprint human skin however there have been no published studies which demonstrate that printed skin could be used for *in-vitro* testing of therapeutic antibodies (Mazzocchi, Soker, and Skardal 2019). The novel application of a fully human bioprinted tissue

suitable for *in-vitro* testing of therapeutic antibodies may be highly beneficial to the drug development process of the pharmaceutical industry (Mazzocchi, Soker, and Skardal 2019). This proof of concept demonstrated in this thesis could be potentially utilised during the different stages of the drug development pipeline for safety testing of drug candidates allowing early elimination or modification of problem candidates, as well as at the preclinical stage to prevent 'late failure' prior the clinical testing phase.

6.3 Long Term Implications of the Research

To date there have been many publications in the field of biofabrication exploring the use of drop-on-demand printing processes such as ink jetting, solenoid microvalves, and laser assisted bioprinting (LABP) (Arai *et al*. 2011; Faulkner-Jones *et al*. 2013; Koch *et al*. 2012). Such studies focus on the biofabrication of constructs using the deposition of high viscosity bio-inks consisting of cell laden cross-linked gels or gel precursors (Lee *et al*. 2014; Michael *et al*. 2013). As a result, few studies investigate the use of cell laden low viscosity bio-inks, therefore, little information is reported on the barriers associated with the deposition of cell laden low viscosity bio-inks. The work outlined in this thesis investigated the impact of cell concentrations within low viscosity bio-inks and continuous agitation of cell-laden bio-inks within the printer reservoirs on the quantitative output of bioprinting cells suspensions over time in addition to the application of bio-ink purges before construction of HSEs. As reported, such factors required implementation and optimisation to utilise cell laden low viscosity bio-inks to successfully construct HSEs that are both physiologically representative and functional. By demonstrating the impact of such factors on printing output and reproducibility, this research may serve as a reference for future studies that aim to improve the printing performance of drop-on-demand (DOD) processes dispensing low viscosity bio-inks for tissue engineering applications.

Currently all commercial HSEs are manufactured using traditional top-down tissue engineering techniques. Therefore such HSEs typically rely on non-human ECM, as is the case for many studies which have bioprinted HSEs (Hill *et al*. 2015; Koch *et al*. 2012; Lee *et al*. 2014; Rasmussen *et al*. 2010). Therefore, commercially available HSEs are not compatible with assays that require fully autologous systems. This thesis has demonstrated a hybridised approach to tissue engineering, combining top-down and bottom-up methodologies to create a fully human HSE which are compatible with fully autologous assays. As reported, the biologically inert scaffold-based approach allows the formation of a fully human HSE. The bioprinting of viable and functional

human cells using solenoid microvalves circumvents the labour-intensive aspect of creating 96-well tissue constructs on a large scale. This unique approach enables the production of biologically representative and functional HSEs that may be developed on a scale suitable for industrial demand.

The approach described in this thesis could be a possible alternative to currently established methods to bioprint HSE's which successfully represent human tissue. This approach could potentially be applied to wider applications such as disease modelling and modelling of wound healing. However, it is acknowledged that these applications may be only achievable in the long-term as the technology is further developed and validated.

In terms of development and use of human HSE's, Skimune3D® offers the benefit of the availability of tests which offer non-animal testing and provide the added benefit of avoiding cross species reactivity which can impact data interpretation.

6.4 Conclusions

- The successful solenoid microvalve based bioprinting of Skimune3D® in a 96-well format as reported in this thesis provides a foundation for future work to manufacture HSEs on an industrial scale.
- Primary human skin cells were shown to be viable post printing and were shown to retain the functional capabilities required of the cells to generate HSEs.
- The co-culture of autologous bioprinted HSEs with autologous peripheral blood monocytes (PBMCs) successfully identified positively and negatively immunotoxic therapeutic antibodies.

Overall, this thesis demonstrates that bioprinted human tissue can bridge the gap between preclinical testing of drugs and first in man studies by identifying adverse immune response *in-vitro* triggered by therapeutic antibodies.

6.5 Recommendations for Future Work

The main limitation for scalable manufacturing of the bioprinted skimune3D® presented in this research is the *in-vitro* replicative capacity of isolated primary human keratinocytes. In this thesis, it was reported that replicative senescence and terminal differentiation in the later passages of keratinocyte culture could adversely affect the formation of the epidermal layer (Lundberg *et al*. 2000; Rheinwald and Green 1975). Therefore, future research should investigate keratinocyte propagation and

maintenance of the healthy basal phenotype; this could be achieved through three possible methodologies. Firstly, keratinocytes could be cultured with the Rho kinase inhibitor Y-27632 to boost proliferative capacity of the epidermal keratinocytes while limiting premature differentiation (Anderson *et al*. 2018; Chapman *et al*. 2010; Chapman *et al*. 2014; Strudwick *et al*. 2015). Secondly, the use of autologous feeder cells could increase the yield of keratinocytes per passage. The extra-cellular secretions of autologous dermal fibroblast feeder cells could boost proliferation, allowing lower inoculation densities for keratinocytes (Llames *et al*. 2015). Thirdly, the use of hydrophobic tissue culture plastic may increase keratinocyte population doubling times and, therefore, should be investigated (Hasskarl *et al*. 2005). By investigating each of the mentioned methodologies it may be feasible to increase the overall number of keratinocytes available to be printed, therefore increasing the potential number of full thickness HSEs developed per donor. Consequently, future studies should also explore the scalability of the Skimune3D® HSE by investigating how many HSEs can be printed per donor by means of incorporating improvements to keratinocyte culture. It should be investigated whether Skimune® could be scaled up beyond its current capacity of testing 12-13 molecule/drugs per donor to match the capacity of current 2D high-throughput screening which is routinely used by drug developers (Stebbings *et al*. 2013).

Furthermore, the proof of concept for immunotoxicity testing of therapeutics using bioprinted tissue demonstrated in this thesis should be further validated. Further validation will require a larger donor cohort (n=10) to account for any variations in immune response between individuals and would necessitate testing of a wider range of therapeutic antibodies. For a true comparison of the HSEs functional use *in-vitro* this data could be compared back to an equivalent assay using physiological human skin (Skimune®). This would provide a direct side by side comparison between the *in-vitro* functionality of the Skimune3D® HSE against physiological human skin.

Future work should also explore methods of reducing the overall lead-time of HSE development. This could involve alteration of the basal incubation time for keratinocytes seeded onto HSEs and potential changes in culture time at air-liquid interface (ALI). To further reduce development lead-time while maintaining an autologous system, future work could investigate the sequential printing of a cell laden dermis and an epidermis by using rapid bioprinting of dermal compartment *in-situ.* This could be achieved by isolating human fibrin from donor matched whole blood

(Mazlyzam *et al*. 2007) to dispense both layers of a full-thickness HSE within a single printing session.

References

Ackermann, K., S. Lombardi Borgia, H. C. Korting, K. R. Mewes, and M. Schäfer-Korting. 2010. 'The Phenion® Full-Thickness Skin Model for Percutaneous Absorption Testing', *Skin Pharmacology and Physiology*, 23: 105-12.

Ahmed, S. S., X. N. Wang, M. Fielding, A. Kerry, I. Dickinson, R. Munuswamy, I. Kimber, and A. M. Dickinson. 2016. 'An in vitro human skin test for assessing sensitization potential', *J Appl Toxicol*, 36: 669-84.

Ali, N., M. Hosseini, S. Vainio, A. Taieb, M. Cario-Andre, and H. R. Rezvani. 2015. 'Skin equivalents: skin from reconstructions as models to study skin development and diseases', *Br J Dermatol*, 173: 391-403.

Anderson, Erik D., Inka Sastalla, Noah J. Earland, Minai Mahnaz, Ian N. Moore, Francisco Otaizo-Carrasquero, Timothy G. Myers, Christopher A. Myles, Sandip K. Datta, and Ian A. Myles. 2018. 'Prolonging culture of primary human keratinocytes isolated from suction blisters with the Rho kinase inhibitor Y-27632', *PLoS One*, 13: e0198862.

Andres, E., M. Barry, A. Hundt, C. Dini, E. Corsini, S. Gibbs, E. L. Roggen, and P. J. Ferret. 2017. 'Preliminary performance data of the RHE/IL-18 assay performed on SkinEthic™ RHE for the identification of contact sensitizers', *International Journal of Cosmetic Science*, 39: 121-32.

Arai, K., S. Iwanaga, H. Toda, C. Genci, Y. Nishiyama, and M. Nakamura. 2011. 'Three-dimensional inkjet biofabrication based on designed images', *Biofabrication*, 3: 034113.

Attarwala, H. 2010. 'TGN1412: From Discovery to Disaster', *Journal of young pharmacists : JYP*, 2: 332-36.

Barlow, Y., and R. J. Pye. 1990. 'Keratinocyte culture', *Methods Mol Biol*, 5: 83-97.

Basketter, D. A., N. Alepee, T. Ashikaga, J. Barroso, N. Gilmour, C. Goebel, J. Hibatallah, S. Hoffmann, P. Kern, S. Martinozzi-Teissier, G. Maxwell, K. Reisinger, H. Sakaguchi, A. Schepky, M. Tailhardat, and M. Templier. 2014. 'Categorization of chemicals according to their relative human skin sensitizing potency', *Dermatitis*, 25: 11-21.

Baumann, Andreas, Kelly Flagella, Roy Forster, Lolke de Haan, Sven Kronenberg, Mathias Locher, Wolfgang F. Richter, Frank-Peter Theil, and Marque Todd. 2014. 'New challenges and opportunities in nonclinical safety testing of biologics', *Regulatory Toxicology and Pharmacology*, 69: 226-33.

Behrens, D. T., D. Villone, M. Koch, G. Brunner, L. Sorokin, H. Robenek, L. Bruckner-Tuderman, P. Bruckner, and U. Hansen. 2012. 'The epidermal basement membrane is a composite of separate laminin- or collagen IV-containing networks connected by aggregated perlecan, but not by nidogens', *J Biol Chem*, 287: 18700-9.

Berger, A. 2000. 'Th1 and Th2 responses: what are they?', *BMJ (Clinical research ed.)*, 321: 424-24.

Blaeser, A., D. F. Duarte Campos, U. Puster, W. Richtering, M. M. Stevens, and H. Fischer. 2016. 'Controlling Shear Stress in 3D Bioprinting is a Key Factor to Balance Printing Resolution and Stem Cell Integrity', *Adv Healthc Mater*, 5: 326-33.

Blaich, Guenter, Andreas Baumann, Sven Kronenberg, Lolke de Haan, Peter Ulrich, Wolfgang F. Richter, Jay Tibbitts, Simon Chivers, Edit Tarcsa, Robert Caldwell, and Flavio Crameri. 2016. 'Non-clinical Safety Evaluation of Biotherapeutics – Challenges, Opportunities and new Insights', *Regulatory Toxicology and Pharmacology*, 80: S1-S14.

Bode, Gerd, Peter Clausing, Frederic Gervais, Jeanet Loegsted, Jörg Luft, Vicente Nogues, and Jennifer Sims. 2010. 'The utility of the minipig as an animal model in regulatory toxicology', *Journal of Pharmacological and Toxicological Methods*, 62: 196-220.

Bode, Gerd, and Petra Starck-Lantova. 2018. 'Future of Regulatory Safety Assessments.' in Franz J. Hock and Michael R. Gralinski (eds.), *Drug Discovery and Evaluation: Methods in Clinical Pharmacology* (Springer International Publishing: Cham).

Bokhari, M., R. J. Carnachan, N. R. Cameron, and S. A. Przyborski. 2007. 'Novel cell culture device enabling three-dimensional cell growth and improved cell function', *Biochem Biophys Res Commun*, 354: 1095-100.

Breitkreutz, D., I. Koxholt, K. Thiemann, and R. Nischt. 2013. 'Skin basement membrane: the foundation of epidermal integrity--BM functions and diverse roles of bridging molecules nidogen and perlecan', *Biomed Res Int*, 2013: 179784.

Bruckner, P. 2010. 'Suprastructures of extracellular matrices: paradigms of functions controlled by aggregates rather than molecules', *Cell Tissue Res*, 339: 7-18.

Candi, E., R. Schmidt, and G. Melino. 2005. 'The cornified envelope: a model of cell death in the skin', *Nat Rev Mol Cell Biol*, 6: 328-40.

Chapman, S., X. Liu, C. Meyers, R. Schlegel, and A. A. McBride. 2010. 'Human keratinocytes are efficiently immortalized by a Rho kinase inhibitor', *J Clin Invest*, 120: 2619-26.

Chapman, S., D. H. McDermott, K. Shen, M. K. Jang, and A. A. McBride. 2014. 'The effect of Rho kinase inhibition on long-term keratinocyte proliferation is rapid and conditional', *Stem Cell Res Ther*, 5: 60.

Chen, Luqiu, Kristy A. Grabowski, Jun-ping Xin, John Coleman, Zan Huang, Baltazar Espiritu, Serhan Alkan, H. Bill Xie, Yuechun Zhu, Fletcher A. White, John Clancy, and Hua Huang. 2004. 'IL-4 Induces Differentiation and Expansion of Th2 Cytokine-Producing Eosinophils', *The Journal of Immunology*, 172: 2059.

Chen, X., and S. L. Thibeault. 2012. 'Response of fibroblasts to transforming growth factor-β1 on two-dimensional and in three-dimensional hyaluronan hydrogels', *Tissue Eng Part A*, 18: 2528-38.

Cottrez, Françoise, Elodie Boitel, Claude Auriault, Pierre Aeby, and Hervé Groux. 2015. 'Genes specifically modulated in sensitized skins allow the detection of sensitizers in a reconstructed human skin model. Development of the SENS-IS assay', *Toxicology in Vitro*, 29: 787-802.

Cottrez, Françoise, Elodie Boitel, Jean-Claude Ourlin, Jean-Luc Peiffer, Isabelle Fabre, Imène-Sarah Henaoui, Bernard Mari, Ambre Vallauri, Agnes Paquet, Pascal Barbry, Claude Auriault, Pierre Aeby, and Hervé Groux. 2016. 'SENS-IS, a 3D reconstituted epidermis based model for quantifying chemical

sensitization potency: Reproducibility and predictivity results from an inter-laboratory study', *Toxicology in Vitro*, 32: 248-60.

Cubo, N., M. Garcia, J. F. Del Canizo, D. Velasco, and J. L. Jorcano. 2016. '3D bioprinting of functional human skin: production and in vivo analysis', *Biofabrication*, 9: 015006.

Cui, X., K. Breitenkamp, M. G. Finn, M. Lotz, and D. D. D'Lima. 2012. 'Direct human cartilage repair using three-dimensional bioprinting technology', *Tissue Eng Part A*, 18: 1304-12.

Derby, Brian. 2010. 'Inkjet Printing of Functional and Structural Materials: Fluid Property Requirements, Feature Stability, and Resolution', *Annual Review of Materials Research*, 40: 395-414.

DiMasi, Joseph A., Henry G. Grabowski, and Ronald W. Hansen. 2016. 'Innovation in the pharmaceutical industry: New estimates of R&D costs', *Journal of Health Economics*, 47: 20-33.

el-Ghalbzouri, A., S. Gibbs, E. Lamme, C. A. Van Blitterswijk, and M. Ponec. 2002. 'Effect of fibroblasts on epidermal regeneration', *Br J Dermatol*, 147: 230-43.

Fang, Y., J. P. Frampton, S. Raghavan, R. Sabahi-Kaviani, G. Luker, C. X. Deng, and S. Takayama. 2012. 'Rapid generation of multiplexed cell cocultures using acoustic droplet ejection followed by aqueous two-phase exclusion patterning', *Tissue Eng Part C Methods*, 18: 647-57.

Faulkner-Jones, A., C. Fyfe, D. J. Cornelissen, J. Gardner, J. King, A. Courtney, and W. Shu. 2015. 'Bioprinting of human pluripotent stem cells and their directed differentiation into hepatocyte-like cells for the generation of mini-livers in 3D', *Biofabrication*, 7: 044102.

Faulkner-Jones, A., S. Greenhough, J. A. King, J. Gardner, A. Courtney, and W. Shu. 2013. 'Development of a valve-based cell printer for the formation of human embryonic stem cell spheroid aggregates', *Biofabrication*, 5: 015013.

Fletcher, E. A. K., M. Eltahir, F. Lindqvist, J. Rieth, G. Tornqvist, J. Leja-Jarblad, and S. M. Mangsbo. 2018. 'Extracorporeal human whole blood in motion, as a tool

to predict first-infusion reactions and mechanism-of-action of immunotherapeutics', *Int Immunopharmacol*, 54: 1-11.

Freeman, A. E., H. J. Igel, B. J. Herrman, and K. L. Kleinfeld. 1976. 'Growth and characterization of human skin epithelial cell cultures', *In Vitro*, 12: 352-62.

Ganderup, Niels Christian, Warren Harvey, Jens Thing Mortensen, and Wafa Harrouk. 2012. 'The Minipig as Nonrodent Species in Toxicology—Where Are We Now?', *International Journal of Toxicology*, 31: 507-28.

Gaston, R. S., M. H. Deierhoi, T. Patterson, E. Prasthofer, B. A. Julian, W. H. Barber, D. A. Laskow, A. G. Diethelm, and J. J. Curtis. 1991. 'OKT3 first-dose reaction: association with T cell subsets and cytokine release', *Kidney Int*, 39: 141-8.

Gately, Maurice K., Aimee G. Wolitzky, Phyllis M. Quinn, and Richard Chizzonite. 1993. 'IL-2-Independent Activation of LAK Cells by a Heterodimeric Cytokine, Interleukin-12.' in Michail V. Sitkovsky and Pierre A. Henkart (eds.), *Cytotoxic Cells: Recognition, Effector Function, Generation, and Methods* (Birkhäuser Boston: Boston, MA).

Gibbs, Susan, Emanuela Corsini, Sander W. Spiekstra, Valentina Galbiati, Horst W. Fuchs, George DeGeorge, Matthew Troese, Patrick Hayden, Wei Deng, and Erwin Roggen. 2013. 'An epidermal equivalent assay for identification and ranking potency of contact sensitizers', *Toxicology and Applied Pharmacology*, 272: 529-41.

Grouf, J. L., A. M. Throm, J. L. Balestrini, K. A. Bush, and K. L. Billiar. 2007. 'Differential effects of EGF and TGF-beta1 on fibroblast activity in fibrin-based tissue equivalents', *Tissue Eng*, 13: 799-807.

Guillotin, B., A. Souquet, S. Catros, M. Duocastella, B. Pippenger, S. Bellance, R. Bareille, M. Remy, L. Bordenave, J. Amedee, and F. Guillemot. 2010. 'Laser assisted bioprinting of engineered tissue with high cell density and microscale organization', *Biomaterials*, 31: 7250-6.

Hasskarl, Jens, Palanivel Velupillai, Siribang-on Piboonniyom, Miranda Grace, and Karl Münger. 2005. 'Long-Term Maintenance of Human Keratinocytes In Vitro', *Journal of Investigative Dermatology*, 124: 475-78.

Hata, Ryu-ichiro, Hironobu Sunada, Katsuhiko Arai, Toshiaki Sato, Yoshifumi Ninomiya, Yutaka Nagai, and Haruki Senoo. 1988. 'Regulation of collagen metabolism and cell growth by epidermal growth factor and ascorbate in cultured human skin fibroblasts', *European Journal of Biochemistry*, 173: 261-67.

Hay, M., D. W. Thomas, J. L. Craighead, C. Economides, and J. Rosenthal. 2014. 'Clinical development success rates for investigational drugs', *Nat Biotechnol*, 32: 40-51.

Hayman, M. W., K. H. Smith, N. R. Cameron, and S. A. Przyborski. 2004. 'Enhanced neurite outgrowth by human neurons grown on solid three-dimensional scaffolds', *Biochem Biophys Res Commun*, 314: 483-8.

———. 2005. 'Growth of human stem cell-derived neurons on solid three-dimensional polymers', *J Biochem Biophys Methods*, 62: 231-40.

Hill, D. S., N. D. Robinson, M. P. Caley, M. Chen, E. A. O'Toole, J. L. Armstrong, S. Przyborski, and P. E. Lovat. 2015. 'A Novel Fully Humanized 3D Skin Equivalent to Model Early Melanoma Invasion', *Mol Cancer Ther*, 14: 2665-73.

Hoffman, R. M. 1991. 'Three-dimensional histoculture: origins and applications in cancer research', *Cancer Cells*, 3: 86-92.

Hsieh, C. S., S. E. Macatonia, C. S. Tripp, S. F. Wolf, A. O'Garra, and K. M. Murphy. 1993. 'Development of TH1 CD4+ T cells through IL-12 produced by Listeria-induced macrophages', *Science*, 260: 547-9.

Hull, B. E., S. E. Sher, S. Rosen, D. Church, and E. Bell. 1983. 'Fibroblasts in isogeneic skin equivalents persist for long periods after grafting', *J Invest Dermatol*, 81: 436-8.

Idriss, H. T., and J. H. Naismith. 2000. 'TNF alpha and the TNF receptor superfamily: structure-function relationship(s)', *Microsc Res Tech*, 50: 184-95.

Jang, Daehwan, Dongjo Kim, and Jooho Moon. 2009. 'Influence of Fluid Physical Properties on Ink-Jet Printability', *Langmuir*, 25: 2629-35.

Kanitakis, J. 2002. 'Anatomy, histology and immunohistochemistry of normal human skin', *Eur J Dermatol*, 12: 390-9; quiz 400-1.

Keriquel, Virginie, Hugo Oliveira, Murielle Rémy, Sophia Ziane, Samantha Delmond, Benoit Rousseau, Sylvie Rey, Sylvain Catros, Joelle Amédée, Fabien Guillemot, and Jean-Christophe Fricain. 2017. 'In situ printing of mesenchymal stromal cells, by laser-assisted bioprinting, for in vivo bone regeneration applications', *Scientific Reports*, 7: 1778.

Kirschner, Nina, and Johanna M. Brandner. 2012. 'Barriers and more: functions of tight junction proteins in the skin', *Annals of the New York Academy of Sciences*, 1257: 158-66.

Koch, L., A. Deiwick, S. Schlie, S. Michael, M. Gruene, V. Coger, D. Zychlinski, A. Schambach, K. Reimers, P. M. Vogt, and B. Chichkov. 2012. 'Skin tissue generation by laser cell printing', *Biotechnol Bioeng*, 109: 1855-63.

Koch, L., S. Kuhn, H. Sorg, M. Gruene, S. Schlie, R. Gaebel, B. Polchow, K. Reimers, S. Stoelting, N. Ma, P. M. Vogt, G. Steinhoff, and B. Chichkov. 2010. 'Laser printing of skin cells and human stem cells', *Tissue Eng Part C Methods*, 16: 847-54.

Krieg, Thomas, and Monique Aumailley. 2011. 'The extracellular matrix of the dermis: flexible structures with dynamic functions', *Exp Dermatol*, 20: 689-95.

Kuhn, C., and H. L. Weiner. 2016. 'Therapeutic anti-CD3 monoclonal antibodies: from bench to bedside', *Immunotherapy*, 8: 889-906.

Lee, V., G. Singh, J. P. Trasatti, C. Bjornsson, X. Xu, T. N. Tran, S. S. Yoo, G. Dai, and P. Karande. 2014. 'Design and fabrication of human skin by three-dimensional bioprinting', *Tissue Eng Part C Methods*, 20: 473-84.

Lee, W., J. C. Debasitis, V. K. Lee, J. H. Lee, K. Fischer, K. Edminster, J. K. Park, and S. S. Yoo. 2009. 'Multi-layered culture of human skin fibroblasts and keratinocytes through three-dimensional freeform fabrication', *Biomaterials*, 30: 1587-95.

Li, L. N., L. B. Margolis, and R. M. Hoffman. 1991. 'Skin toxicity determined in vitro by three-dimensional, native-state histoculture', *Proc Natl Acad Sci U S A*, 88: 1908-12.

Li, L., R. Paus, A. Slominski, and R. M. Hoffman. 1992. 'Skin histoculture assay for studying the hair cycle', *In Vitro Cell Dev Biol*, 28a: 695-8.

Lillie, J. H., D. K. MacCallum, and A. Jepsen. 1980. 'Fine structure of subcultivated stratified squamous epithelium grown on collagen rafts', *Exp Cell Res*, 125: 153-65.

Lippens, S., G. Denecker, P. Ovaere, P. Vandenabeele, and W. Declercq. 2005. 'Death penalty for keratinocytes: apoptosis versus cornification', *Cell Death & Differentiation*, 12: 1497-508.

Liu, Ying, Yue Li, Ning Li, Wen Teng, Min Wang, Yingbo Zhang, and Zhibo Xiao. 2016. 'TGF-β1 promotes scar fibroblasts proliferation and transdifferentiation via up-regulating MicroRNA-21', *Scientific Reports*, 6: 32231.

Llames, Sara, Eva García-Pérez, Álvaro Meana, Fernando Larcher, and Marcela del Río. 2015. 'Feeder Layer Cell Actions and Applications', *Tissue engineering. Part B, Reviews*, 21: 345-53.

Lundberg, A. S., W. C. Hahn, P. Gupta, and R. A. Weinberg. 2000. 'Genes involved in senescence and immortalization', *Curr Opin Cell Biol*, 12: 705-9.

Ma, Xuanyi, Justin Liu, Wei Zhu, Min Tang, Natalie Lawrence, Claire Yu, Maling Gou, and Shaochen Chen. 2018. '3D bioprinting of functional tissue models for personalized drug screening and in vitro disease modeling', *Advanced Drug Delivery Reviews*, 132: 235-51.

Mallampati, Ramya, Ram R. Patlolla, Saurab Agarwal, R. Jayachandra Babu, Patrick Hayden, Mitchell Klausner, and Mandip S. Singh. 2010. 'Evaluation of EpiDerm full thickness-300 (EFT-300) as an in vitro model for skin irritation: studies on aliphatic hydrocarbons', *Toxicology in vitro : an international journal published in association with BIBRA*, 24: 669-76.

Marga, F., K. Jakab, C. Khatiwala, B. Shepherd, S. Dorfman, B. Hubbard, S. Colbert, and F. Gabor. 2012. 'Toward engineering functional organ modules by additive manufacturing', *Biofabrication*, 4: 022001.

Mazlyzam, A. L., B. S. Aminuddin, N. H. Fuzina, M. M. Norhayati, O. Fauziah, M. R. Isa, L. Saim, and B. H. Ruszymah. 2007. 'Reconstruction of living bilayer human skin equivalent utilizing human fibrin as a scaffold', *Burns*, 33: 355-63.

Mazzocchi, Andrea, Shay Soker, and Aleksander Skardal. 2019. '3D bioprinting for high-throughput screening: Drug screening, disease modeling, and precision medicine applications', *Applied Physics Reviews*, 6: 011302.

McMillan, J. R., M. Akiyama, and H. Shimizu. 2003. 'Epidermal basement membrane zone components: ultrastructural distribution and molecular interactions', *J Dermatol Sci*, 31: 169-77.

Mehrotra, P. T., R. P. Donnelly, S. Wong, H. Kanegane, A. Geremew, H. S. Mostowski, K. Furuke, J. P. Siegel, and E. T. Bloom. 1998. 'Production of IL-10 by human natural killer cells stimulated with IL-2 and/or IL-12', *J Immunol*, 160: 2637-44.

Michael, S., H. Sorg, C. T. Peck, L. Koch, A. Deiwick, B. Chichkov, P. M. Vogt, and K. Reimers. 2013. 'Tissue engineered skin substitutes created by laser-assisted bioprinting form skin-like structures in the dorsal skin fold chamber in mice', *PLoS One*, 8: e57741.

Midgley, A. C., M. Rogers, M. B. Hallett, A. Clayton, T. Bowen, A. O. Phillips, and R. Steadman. 2013. 'Transforming growth factor-beta1 (TGF-beta1)-stimulated fibroblast to myofibroblast differentiation is mediated by hyaluronan (HA)-facilitated epidermal growth factor receptor (EGFR) and CD44 co-localization in lipid rafts', *J Biol Chem*, 288: 14824-38.

Mikos, A. G., G. Sarakinos, S. M. Leite, J. P. Vacanti, and R. Langer. 1993. 'Laminated three-dimensional biodegradable foams for use in tissue engineering', *Biomaterials*, 14: 323-30.

Moll, R., M. Divo, and L. Langbein. 2008. 'The human keratins: biology and pathology', *Histochem Cell Biol*, 129: 705-33.

Morrissey, Meghan A., and David R. Sherwood. 2015. 'An active role for basement membrane assembly and modification in tissue sculpting', *Journal of Cell Science*, 128: 1661.

Murphy, S. V., and A. Atala. 2014. '3D bioprinting of tissues and organs', *Nat Biotechnol*, 32: 773-85.

Negro, Andrea, Thibaud Cherbuin, and Matthias P. Lutolf. 2018. '3D Inkjet Printing of Complex, Cell-Laden Hydrogel Structures', *Scientific Reports*, 8: 17099.

Nemes, Z., and P. M. Steinert. 1999. 'Bricks and mortar of the epidermal barrier', *Exp Mol Med*, 31: 5-19.

Ng, W. L., J. M. Lee, W. Y. Yeong, and M. Win Naing. 2017. 'Microvalve-based bioprinting - process, bio-inks and applications', *Biomater Sci*, 5: 632-47.

Ng, W. L., J. T. Z. Qi, W. Y. Yeong, and M. W. Naing. 2018. 'Proof-of-concept: 3D bioprinting of pigmented human skin constructs', *Biofabrication*, 10: 025005.

Ng, Wei Long, Wai Yee Yeong, and May Win Naing. 2017. 'Polyvinylpyrrolidone-Based Bio-Ink Improves Cell Viability and Homogeneity during Drop-On-Demand Printing', *Materials (Basel, Switzerland)*, 10: 190.

Okubo, Nami, A. J. Qureshi, Kenny Dalgarno, Kheng L. Goh, and Suchitra Derebail. 2019. 'Cost-effective microvalve-assisted bioprinter for tissue engineering', *Bioprinting*, 13: e00043.

Pammolli, Fabio, Laura Magazzini, and Massimo Riccaboni. 2011. 'The productivity crisis in pharmaceutical R&D', *Nature Reviews Drug Discovery*, 10: 428.

Panwar, A., and L. P. Tan. 2016. 'Current Status of Bioinks for Micro-Extrusion-Based 3D Bioprinting', *Molecules*, 21.

Paquet, P., and G. E. Pierard. 1996. 'Interleukin-6 and the skin', *Int Arch Allergy Immunol*, 109: 308-17.

Park, Y., M. Sugimoto, A. Watrin, M. Chiquet, and E. B. Hunziker. 2005. 'BMP-2 induces the expression of chondrocyte-specific genes in bovine synovium-

derived progenitor cells cultured in three-dimensional alginate hydrogel', *Osteoarthritis Cartilage*, 13: 527-36.

Pedrosa, Tatiana do Nascimento, Carolina Motter Catarino, Paula Comune Pennacchi, Sílvia Romano de Assis, Fabrícia Gimenes, Márcia Edilaine Lopes Consolaro, Silvia Berlanga de Moraes Barros, and Silvya Stuchi Maria-Engler. 2017. 'A new reconstructed human epidermis for in vitro skin irritation testing', *Toxicology in Vitro*, 42: 31-37.

Phillips, C. L., S. B. Combs, and S. R. Pinnell. 1994. 'Effects of ascorbic acid on proliferation and collagen synthesis in relation to the donor age of human dermal fibroblasts', *J Invest Dermatol*, 103: 228-32.

Pranay, Tanwar, Arora Sandeep Kumar, and Seema Chhabra. 2013. 'Civatte bodies: a diagnostic clue', *Indian journal of dermatology*, 58: 327-27.

Prior, Helen, Fiona Sewell, and Jane Stewart. 2017. 'Overview of 3Rs opportunities in drug discovery and development using non-human primates', *Drug Discovery Today: Disease Models*, 23: 11-16.

Proksch, E., J. M. Brandner, and J. M. Jensen. 2008. 'The skin: an indispensable barrier', *Exp Dermatol*, 17: 1063-72.

Prunieras, M., M. Regnier, and D. Woodley. 1983. 'Methods for cultivation of keratinocytes with an air-liquid interface', *J Invest Dermatol*, 81: 28s-33s.

Rasmussen, Cathy, Ken Gratz, Frank Liebel, Michael Southall, Michelle Garay, Surjya Bhattacharyya, Nick Simon, Marie Vander Zanden, Kelly Van Winkle, John Pirnstill, Sara Pirnstill, Allen Comer, and B. Lynn Allen-Hoffmann. 2010. 'The StrataTest® human skin model, a consistent in vitro alternative for toxicological testing', *Toxicology in Vitro*, 24: 2021-29.

Regnier, M., A. Patwardhan, A. Scheynius, and R. Schmidt. 1998. 'Reconstructed human epidermis composed of keratinocytes, melanocytes and Langerhans cells', *Med Biol Eng Comput*, 36: 821-4.

Regnier, M., M. J. Staquet, D. Schmitt, and R. Schmidt. 1997. 'Integration of Langerhans cells into a pigmented reconstructed human epidermis', *J Invest Dermatol*, 109: 510-2.

Rheinwald, J. G., and H. Green. 1975. 'Serial cultivation of strains of human epidermal keratinocytes: the formation of keratinizing colonies from single cells', *Cell*, 6: 331-43.

Ribeiro, R. D. C., D. Pal, D. Jamieson, K. S. Rankin, M. Benning, K. W. Dalgarno, and A. M. Ferreira. 2017. 'Temporary Single-Cell Coating for Bioprocessing with a Cationic Polymer', *ACS Appl Mater Interfaces*, 9: 12967-74.

Rognoni, E., and F. M. Watt. 2018. 'Skin Cell Heterogeneity in Development, Wound Healing, and Cancer', *Trends Cell Biol*, 28: 709-22.

Römer, Paula S., Susanne Berr, Elita Avota, Shin-Young Na, Manuela Battaglia, Ineke ten Berge, Hermann Einsele, and Thomas Hünig. 2011. 'Preculture of PBMCs at high cell density increases sensitivity of T-cell responses, revealing cytokine release by CD28 superagonist TGN1412', *Blood*, 118: 6772-82.

Rosdy, M., and L. C. Clauss. 1990. 'Terminal epidermal differentiation of human keratinocytes grown in chemically defined medium on inert filter substrates at the air-liquid interface', *J Invest Dermatol*, 95: 409-14.

Saito, Kazutoshi, Yuko Nukada, Osamu Takenouchi, Masaaki Miyazawa, Hitoshi Sakaguchi, and Naohiro Nishiyama. 2013. 'Development of a new in vitro skin sensitization assay (Epidermal Sensitization Assay; EpiSensA) using reconstructed human epidermis', *Toxicology in Vitro*, 27: 2213-24.

Saito, Kazutoshi, Osamu Takenouchi, Yuko Nukada, Masaaki Miyazawa, and Hitoshi Sakaguchi. 2017. 'An in vitro skin sensitization assay termed EpiSensA for broad sets of chemicals including lipophilic chemicals and pre/pro-haptens', *Toxicology in Vitro*, 40: 11-25.

Schafer-Korting, M., U. Bock, W. Diembeck, H. J. Dusing, A. Gamer, E. Haltner-Ukomadu, C. Hoffmann, M. Kaca, H. Kamp, S. Kersen, M. Kietzmann, H. C. Korting, H. U. Krachter, C. M. Lehr, M. Liebsch, A. Mehling, C. Muller-Goymann, F. Netzlaff, F. Niedorf, M. K. Rubbelke, U. Schafer, E. Schmidt, S. Schreiber, H. Spielmann, A. Vuia, and M. Weimer. 2008. 'The use of reconstructed human epidermis for skin absorption testing: Results of the validation study', *Altern Lab Anim*, 36: 161-87.

Schimek, Katharina, Hao-Hsiang Hsu, Moritz Boehme, Jacob Jan Kornet, Uwe Marx, Roland Lauster, Ralf Pörtner, and Gerd Lindner. 2018. 'Bioengineering of a Full-Thickness Skin Equivalent in a 96-Well Insert Format for Substance Permeation Studies and Organ-On-A-Chip Applications', *Bioengineering (Basel, Switzerland)*, 5: 43.

Sekitani, Tsuyoshi, Yoshiaki Noguchi, Ute Zschieschang, Hagen Klauk, and Takao Someya. 2008. 'Organic transistors manufactured using inkjet technology with subfemtoliter accuracy', *Proceedings of the National Academy of Sciences*, 105: 4976.

Sher, I., S. Zisman-Rozen, L. Eliahu, J. M. Whitelock, N. Maas-Szabowski, Y. Yamada, D. Breitkreutz, N. E. Fusenig, E. Arikawa-Hirasawa, R. V. Iozzo, R. Bergman, and D. Ron. 2006. 'Targeting perlecan in human keratinocytes reveals novel roles for perlecan in epidermal formation', *J Biol Chem*, 281: 5178-87.

Sims, C. D., P. E. Butler, Y. L. Cao, R. Casanova, M. A. Randolph, A. Black, C. A. Vacanti, and M. J. Yaremchuk. 1998. 'Tissue engineered neocartilage using plasma derived polymer substrates and chondrocytes', *Plast Reconstr Surg*, 101: 1580-5.

Singh, M., H. M. Haverinen, P. Dhagat, and G. E. Jabbour. 2010. 'Inkjet printing-process and its applications', *Adv Mater*, 22: 673-85.

Smietana, K., M. Siatkowski, and M. Moller. 2016. 'Trends in clinical success rates', *Nat Rev Drug Discov*, 15: 379-80.

Smith, K. A. 1988. 'Interleukin-2: inception, impact, and implications', *Science*, 240: 1169-76.

Smith, L. T., K. A. Holbrook, and J. A. Madri. 1986. 'Collagen types I, III, and V in human embryonic and fetal skin', *Am J Anat*, 175: 507-21.

Spiekstra, S. W., M. J. Toebak, S. Sampat-Sardjoepersad, P. J. van Beek, D. M. Boorsma, T. J. Stoof, B. M. von Blomberg, R. J. Scheper, D. P. Bruynzeel, T. Rustemeyer, and S. Gibbs. 2005. 'Induction of cytokine (interleukin-1alpha and tumor necrosis factor-alpha) and chemokine (CCL20, CCL27, and CXCL8) alarm signals after allergen and irritant exposure', *Exp Dermatol*, 14: 109-16.

Spiekstra, Sander W., Melanie Breetveld, Thomas Rustemeyer, Rik J. Scheper, and Susan Gibbs. 2007. 'Wound-healing factors secreted by epidermal keratinocytes and dermal fibroblasts in skin substitutes', *Wound Repair and Regeneration*, 15: 708-17.

Stebbings, R., D. Eastwood, S. Poole, and R. Thorpe. 2013. 'After TGN1412: recent developments in cytokine release assays', *Journal of immunotoxicology*, 10: 75-82.

Stebbings, Richard, Lucy Findlay, Cherry Edwards, David Eastwood, Chris Bird, David North, Yogesh Mistry, Paula Dilger, Emily Liefooghe, Isabelle Cludts, Bernard Fox, Gill Tarrant, Jane Robinson, Tony Meager, Carl Dolman, Susan J. Thorpe, Adrian Bristow, Meenu Wadhwa, Robin Thorpe, and Stephen Poole. 2007. '"Cytokine Storm" in the Phase I Trial of Monoclonal Antibody TGN1412: Better Understanding the Causes to Improve PreClinical Testing of Immunotherapeutics', *The Journal of Immunology*, 179: 3325.

Strober, W. 2015. 'Trypan Blue Exclusion Test of Cell Viability', *Curr Protoc Immunol*, 111: A3.B.1-a3.B.3.

Strudwick, Xanthe L., Debbie L. Lang, Louise E. Smith, and Allison J. Cowin. 2015. 'Combination of Low Calcium with Y-27632 Rock Inhibitor Increases the Proliferative Capacity, Expansion Potential and Lifespan of Primary Human Keratinocytes while Retaining Their Capacity to Differentiate into Stratified Epidermis in a 3D Skin Model', *PLoS One*, 10: e0123651.

Sugawara, Koji, Daisuke Tsuruta, Masamitsu Ishii, Jonathan C.R. Jones, and Hiromi Kobayashi. 2008. 'Laminin-332 and -511 in skin', *Exp Dermatol*, 17: 473-80.

Sun, T., P. McMinn, M. Holcombe, R. Smallwood, and S. MacNeil. 2008. 'Agent based modelling helps in understanding the rules by which fibroblasts support keratinocyte colony formation', *PLoS One*, 3: e2129.

Swain, S. L., A. D. Weinberg, M. English, and G. Huston. 1990. 'IL-4 directs the development of Th2-like helper effectors', *J Immunol*, 145: 3796-806.

Tabatabaei Shafiei, Mahdieh, Catalina M. Carvajal Gonczi, Mohammed Samiur Rahman, Ashley East, Jonathan François, and Peter J. Darlington. 2014.

'Detecting glycogen in peripheral blood mononuclear cells with periodic acid schiff staining', *Journal of visualized experiments : JoVE*: 52199.

Ueda, Maho, Susumu Saito, Teruasa Murata, Tomoko Hirano, Ryoma Bise, Kenji Kabashima, and Shigehiko Suzuki. 2019. 'Combined multiphoton imaging and biaxial tissue extension for quantitative analysis of geometric fiber organization in human reticular dermis', *Scientific Reports*, 9: 10644.

van Meer, Peter J. K., Marlous Kooijman, Vera Brinks, Christine C. Gispen-de Wied, Beatriz Silva-Lima, Ellen H. M. Moors, and Huub Schellekens. 2013. 'Immunogenicity of mAbs in non-human primates during nonclinical safety assessment', *mAbs*, 5: 810-16.

Villone, D., A. Fritsch, M. Koch, L. Bruckner-Tuderman, U. Hansen, and P. Bruckner. 2008. 'Supramolecular interactions in the dermo-epidermal junction zone: anchoring fibril-collagen VII tightly binds to banded collagen fibrils', *J Biol Chem*, 283: 24506-13.

Visk, DeeAnn. 2015. 'Will Advances in Preclinical In Vitro Models Lower the Costs of Drug Development?', *Applied In Vitro Toxicology*, 1: 79-82.

Wang, Zhenxiang, Ying Wang, Farhang Farhangfar, Monica Zimmer, and Yongxin Zhang. 2012. 'Enhanced Keratinocyte Proliferation and Migration in Co-culture with Fibroblasts', *PLoS One*, 7: e40951.

Wilson, W. C., Jr., and T. Boland. 2003. 'Cell and organ printing 1: protein and cell printers', *Anat Rec A Discov Mol Cell Evol Biol*, 272: 491-6.

Wong, Chi Heem, Kien Wei Siah, and Andrew W. Lo. 2018. 'Estimation of clinical trial success rates and related parameters', *Biostatistics*, 20: 273-86.

Wong, R., S. Geyer, W. Weninger, J. C. Guimberteau, and J. K. Wong. 2016. 'The dynamic anatomy and patterning of skin', *Exp Dermatol*, 25: 92-8.

Wong, T., J. A. McGrath, and H. Navsaria. 2007. 'The role of fibroblasts in tissue engineering and regeneration', *Br J Dermatol*, 156: 1149-55.

Xu, T., C. A. Gregory, P. Molnar, X. Cui, S. Jalota, S. B. Bhaduri, and T. Boland. 2006. 'Viability and electrophysiology of neural cell structures generated by the inkjet printing method', *Biomaterials*, 27: 3580-8.

Xu, T., J. Jin, C. Gregory, J. J. Hickman, and T. Boland. 2005. 'Inkjet printing of viable mammalian cells', *Biomaterials*, 26: 93-9.

Yeo, C., N. Saunders, D. Locca, A. Flett, M. Preston, P. Brookman, B. Davy, A. Mathur, and S. Agrawal. 2009. 'Ficoll-Paque versus Lymphoprep: a comparative study of two density gradient media for therapeutic bone marrow mononuclear cell preparations', *Regen Med*, 4: 689-96.

Yu, X., G. P. Dillon, and R. B. Bellamkonda. 1999. 'A laminin and nerve growth factor-laden three-dimensional scaffold for enhanced neurite extension', *Tissue Eng*, 5: 291-304.

Zheng, H., Y. Ban, F. Wei, and X. Ma. 2016. 'Regulation of Interleukin-12 Production in Antigen-Presenting Cells', *Adv Exp Med Biol*, 941: 117-38.

Zopf, D. A., S. J. Hollister, M. E. Nelson, R. G. Ohye, and G. E. Green. 2013. 'Bioresorbable airway splint created with a three-dimensional printer', *N Engl J Med*, 368: 2043-5.

Appendices

Appendix A - Ethical Approval

Now that you have completed the application process please visit the National Research Ethics Service website > After Review

You are invited to give your view of the service that you have received from the National Research Ethics Service and the application procedure. If you wish to make your views known please use the feedback form available on the website.

The attached document *"After ethical review – guidance for researchers"* gives detailed guidance on reporting requirements for studies with a favourable opinion, including:

- Notifying substantial amendments
- Adding new sites and investigators
- Progress and safety reports
- Notifying the end of the study

The NRES website also provides guidance on these topics, which is updated in the light of changes in reporting requirements or procedures.

We would also like to inform you that we consult regularly with stakeholders to improve our service. If you would like to join our Reference Group please email referencegroup@nres.npsa.nhs.uk.

10/H0906/58	**Please quote this number on all correspondence**

Yours sincerely

pp. L. Kirkbride

Mr Chris Turnock
Chair

Email: laura.kirkbride@sotw.nhs.uk

Enclosures: "After ethical review – guidance for researchers"

Copy to: *Newcastle upon Tyne Hospitals NHS Foundation Trust*

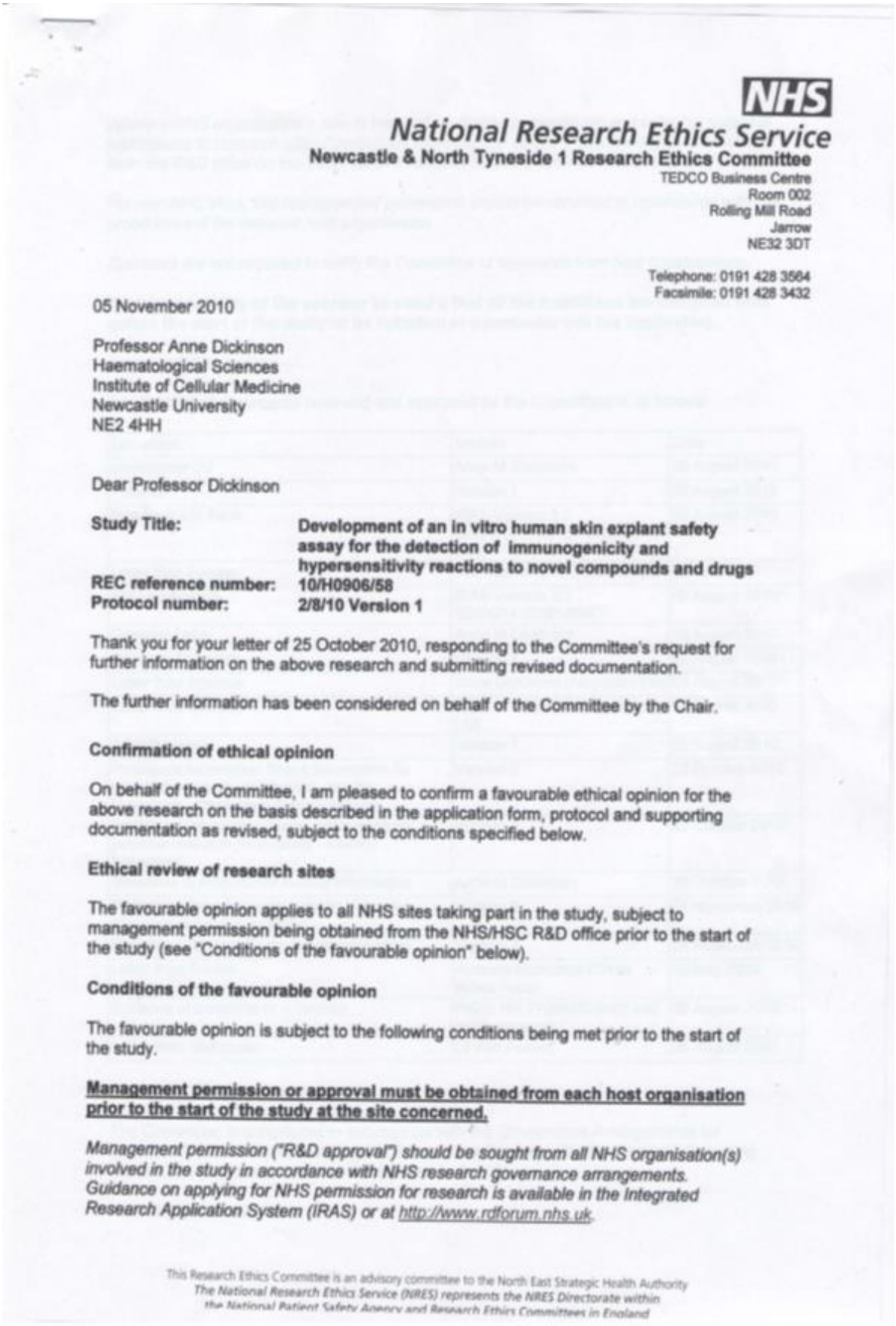

NHS

National Research Ethics Service

Newcastle & North Tyneside 1 Research Ethics Committee

TEDCO Business Centre
Room 002
Rolling Mill Road
Jarrow
NE32 3DT

Telephone: 0191 428 3564
Facsimile: 0191 428 3432

05 November 2010

Professor Anne Dickinson
Haematological Sciences
Institute of Cellular Medicine
Newcastle University
NE2 4HH

Dear Professor Dickinson

Study Title: **Development of an in vitro human skin explant safety assay for the detection of immunogenicity and hypersensitivity reactions to novel compounds and drugs**

REC reference number: **10/H0906/58**

Protocol number: **2/8/10 Version 1**

Thank you for your letter of 25 October 2010, responding to the Committee's request for further information on the above research and submitting revised documentation.

The further information has been considered on behalf of the Committee by the Chair.

Confirmation of ethical opinion

On behalf of the Committee, I am pleased to confirm a favourable ethical opinion for the above research on the basis described in the application form, protocol and supporting documentation as revised, subject to the conditions specified below.

Ethical review of research sites

The favourable opinion applies to all NHS sites taking part in the study, subject to management permission being obtained from the NHS/HSC R&D office prior to the start of the study (see "Conditions of the favourable opinion" below).

Conditions of the favourable opinion

The favourable opinion is subject to the following conditions being met prior to the start of the study.

Management permission or approval must be obtained from each host organisation prior to the start of the study at the site concerned.

Management permission ("R&D approval") should be sought from all NHS organisation(s) involved in the study in accordance with NHS research governance arrangements. Guidance on applying for NHS permission for research is available in the Integrated Research Application System (IRAS) or at http://www.rdforum.nhs.uk.

This Research Ethics Committee is an advisory committee to the North East Strategic Health Authority
The National Research Ethics Service (NRES) represents the NRES Directorate within the National Patient Safety Agency and Research Ethics Committees in England

Figure I. Approval from National Research Ethics Service for collection and use of human samples.

Appendix B – Conference Proceedings and Publications

Conference proceedings

2016 27th Annual Solid Freeform Fabrication Symposium (Austin, Texas, USA). Investigating chocolate as a material for additive manufacturing. **Ahmed MM**, Birchall L, Dimitrov I, Garmendia X, Murray G and Sallstrom N.

2017 Arthritis Research UK/MeDe Research Exhibition (Newcastle University, UK): *Microvalve dispensing of cells in media*. **Ahmed MM**, Benning M, and Dalgarno K.

2018 Biofabrication (Wurzburg, Germany): *Development of 3D Human Skin Equivalents for Toxicity Testing and Bioprinting Fibroblasts*. **Ahmed MM**, Benning M, Dickinson AM, DS Hill, Lovat PE, and Dalgarno KW.

2018 EPSRC Centre for Additive Manufacturing and 3D Printing industry day. (University of Nottingham, UK): *Bioprinting Skin Equivalents for Toxicity Testing*. **Ahmed MM**, Benning M, Dickinson AM, DS Hill, Lovat PE, and Dalgarno KW.

2018 MeDe Innovation 5th Annual Conference (University of Sheffield, UK). *Bioprinting Skin Equivalents for Toxicity Testing*. **Ahmed MM**, Benning M, Dickinson AM, DS Hill, Lovat PE, and Dalgarno KW.

Publications

2019 S.S. Ahmed, J. Whritenour, **M.M. Ahmed,** L. Bibby, L. Darby, X.N. Wang, J. Watson, A.M. Dickinson. 2019. Evaluation of a human in vitro skin test for predicting drug hypersensitivity reactions. Toxicology and Applied Pharmacology, 369

2020 S.S. Ahmed, **M.M. Ahmed**, L. Bibby, L. Darby, X.N. Wang, J. Watson, A.M. Dickinson. 2020. An in vitro human skin test for assessing adverse reactions to biologics. Journal of applied toxicology, submitted.